NAVAL POSTGRADUATE SCHOOL
MONTEREY, CALIFORNIA

THESIS

DEVELOPMENT OF A LOW FREQUENCY
AMBIENT NOISE STORM MODEL
FOR THE ARCTIC OCEAN

by

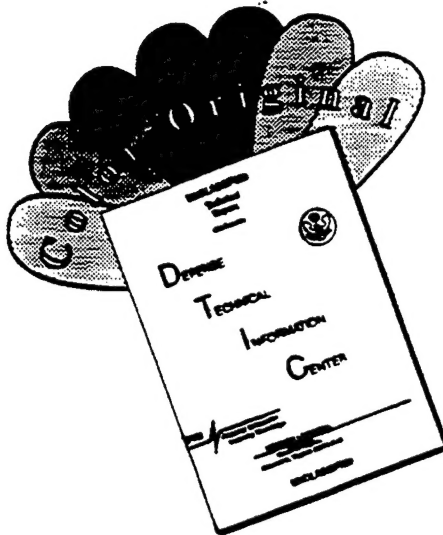David A.Collins

December, 1996

Thesis Advisors: Robert H. Bourke
                                          James H. Wilson

Approved for public release; distribution is unlimited.

DISCLAIMER NOTICE

THIS DOCUMENT IS BEST QUALITY AVAILABLE. THE COPY FURNISHED TO DTIC CONTAINED A SIGNIFICANT NUMBER OF COLOR PAGES WHICH DO NOT REPRODUCE LEGIBLY ON BLACK AND WHITE MICROFICHE.

REPORT DOCUMENTATION PAGE

Form Approved OMB No. 0704-0188

1. AGENCY USE ONLY *(Leave blank)*	2. REPORT DATE December 1996	3. REPORT TYPE AND DATES COVERED Master's Thesis	
4. TITLE AND SUBTITLE DEVELOPMENT OF A LOW FREQUENCY AMBIENT NOISE STORM MODEL FOR THE ARCTIC OCEAN		5. FUNDING NUMBERS	
6. AUTHOR(S) Collins David A.			
7. PERFORMING ORGANIZATION NAME(S) AND ADDRESS(ES) Naval Postgraduate School Monterey CA 93943-5000		8. PERFORMING ORGANIZATION REPORT NUMBER	
9. SPONSORING/MONITORING AGENCY NAME(S) AND ADDRESS(ES)		10. SPONSORING/MONITORING AGENCY REPORT NUMBER	

11. SUPPLEMENTARY NOTES The views expressed in this thesis are those of the author and do not reflect the official policy or position of the Department of Defense or the U.S. Government.

12a. DISTRIBUTION/AVAILABILITY STATEMENT Approved for public release; distribution is unlimited.	12b. DISTRIBUTION CODE

13. ABSTRACT *(maximum 200 words)*

The development of an ambient noise model for use in ice-covered Arctic waters is the primary goal of this research. The generation of ambient noise is considered to originate from large scale deformation of the ice cover (pressure ridge formation) which is caused on a synoptic scale by convergence of the ice cover due to wind stress/speed associated with the passage of Arctic storms.

The Arctic Storm Noise Model (ASNM) has been developed as a dynamic model to predict the occurrence of extreme noise events. The emphasis is on accurately predicting the large increases or decreases in ambient noise, which observations have shown to be in the order of 20 to 30 dB over a matter of hours.

ASNM was adapted from the Ambient Noise Directional Estimation System (ANDES) for use under the Arctic pack ice. ASNM predictions are compared quantitatively to noise measurements made by ice-mounted drifting buoys in the Arctic basin during the early 1990's. Results showed that for extreme events (<5th or >95th percentile) ASNM is accurate in predicting both the level of ambient noise and the large increases in the noise record.

Due to the encouraging results further improvements are recommended to increase the robustness of the model for potential tactical use by submarine units operating under the Arctic pack ice.

14. SUBJECT TERMS Oceanography, Low Frequency Ambient Noise, Arctic, Storm Noise			15. NUMBER OF PAGES 155
			16. PRICE CODE
17. SECURITY CLASSIFICATION OF REPORT Unclassified	18. SECURITY CLASSIFICATION OF THIS PAGE Unclassified	19. SECURITY CLASSIFICATION OF ABSTRACT Unclassified	20. LIMITATION OF ABSTRACT UL

DEVELOPMENT OF A LOW FREQUENCY AMBIENT NOISE STORM MODEL FOR THE ARCTIC OCEAN

David A. Collins
Lieutenant Commander, British Navy
B.Sc., University of Loughborough, England, 1985

Submitted in partial fulfillment
of the requirements for the degree of

MASTER OF SCIENCE IN PHYSICAL OCEANOGRAPHY

from the

NAVAL POSTGRADUATE SCHOOL
December 1996

Author: _____

David A. Collins

Approved by: _____

Robert H. Bourke, Thesis Co-Advisor

_____

James H. Wilson, Thesis Co-Advisor

_____

Robert H. Bourke, Chairman, Department of Oceanography

iii

ABSTRACT

The development of an ambient noise model for use in ice-covered Arctic waters is the primary goal of this research. The generation of ambient noise is considered to originate from large scale deformation of the ice cover (pressure ridge formation) which is caused on a synoptic scale by convergence of the ice cover due to wind stress/speed associated with the passage of Arctic storms.

The Arctic Storm Noise Model (ASNM) has been developed as a dynamic model to predict the occurrence of extreme noise events. The emphasis is on accurately predicting the large increases or decreases in ambient noise, which observations have shown to be in the order of 20 to 30 dB over a matter of hours.

ASNM was adapted from the Ambient Noise Directional Estimation System (ANDES) for use under the Arctic pack ice. ASNM predictions are compared quantitatively to noise measurements made by ice-mounted drifting buoys in the Arctic basin during the early 1990's. Results showed that for extreme events (<5th or >95th percentile) ASNM is accurate in predicting both the level of ambient noise and the large increases in the noise record.

Due to the encouraging results further improvements are recommended to increase the robustness of the model for potential tactical use by submarine units operating under the Arctic pack ice.

TABLE OF CONTENTS

x

LIST OF FIGURES

I. INTRODUCTION

A. POLITICAL/NAVAL CONTEXT

Since the end of the Cold War and the dismantling of
the military might of the former USSR, developed countries,
and NATO countries in particular, have subjected their armed
forces to considerable restructuring and downsizing. Russia
has also downsized all branches of their armed forces,
except the submarine force. The reduction in total number of
submarines reflects only the retirement of many very old,
less capable diesel submarines. New production of Russian
submarines has continued at the pre-cold war schedule. The
recent narrow re-election (July 1996) in Russia of Boris
Yeltsin in the face of a Communist resurgence illustrates
how potentially fragile the democratic process remains
within the former USSR.

The former Soviet Union maintained an impressive
maritime submarine force for power projection at sea, of
which the new Akula attack submarine and Typhoon ballistic
missile submarine in particular are the elite of the
service. In fact, the Akula and Typhoon are possibly the
quietest SSN and SSBN submarines in the world.

Despite the recent turbulent years within the former
USSR, renewed submarine deployments from Russian bases
continue to both the North Atlantic and Arctic Oceans. Since
the end of the cold war, Russia has produced every scheduled

1

new SSN and SSBN on time and most new submarine platforms (e.g., Akulas and Typhoons) have joined the Arctic Fleet. Therefore, the Arctic Ocean and in particular the ice-covered Arctic Seas remain a high priority operational area for both United States and allied NATO submarine forces.

B.   OCEANOGRAPHIC APPLICATIONS

The oceanography of the Arctic Ocean is unique and its acoustic characteristics are of utmost importance to submarine operations. In the submariners tactical scenario of detection and evasion the ability to detect and track the opposing unit whilst avoiding counter-detection is paramount. Contrary to mid-latitude open-ocean operations, where shipping dominates the ambient noise field, the level of background ambient noise (AN) in ice-covered waters is dominated by the ice noise due to pressure ridging at low (<500Hz) frequencies. Moreover, it is the spatial and temporal variation in the level of AN in the Arctic pack ice which can create the potential for a significant tactical advantage to be gained. Changes in AN levels of 20dB to 30dB over a period of several hours is common in the pack ice environment as the arrival (or departure) of Arctic storms induce more (or less) pressure ridging events (Feller, 1994; Fritsch, 1995).

The ability to accurately predict periods when generally low or high values of AN may be expected can be

tactically useful to the submarine commander. Acoustic detection ranges are virtually exclusively a function of the background AN in Arctic waters. The ability to anticipate periods of very low AN levels could provide tactical advantages in detection and tracking during an operational scenario. Predicted periods of higher AN would provide the submarine commander with the opportunity to carry out noisier routine housekeeping chores, which could be masked by the higher background AN.

C. OBJECTIVES

The preceding section illustrates the need for an accurate forecasting tool to predict the level of Arctic pack ice AN. This research concentrates on this objective.

Previous work at the Naval Postgraduate School (Oard, 1987; Parsons, 1992; Feller, 1994; Fritsch, 1995) have concentrated on the analysis of ambient noise data acquired from ice-mounted buoys drifting in the Arctic and its peripheral seas. They correlated AN with environmental parameters to identify the dominant forcing mechanisms and physical processes which caused large changes in AN level. The current research is focused on the development of a predictive, low frequency ambient noise model which can be tested against 'ground truth' - ambient noise values obtained from drifting buoys or directional arrays.

The methodology used to achieve this objective directly relates to the organization and structure of this thesis. The next section reviews the literature associated with the identification and analysis of the forcing mechanisms of ambient noise in ice-covered waters. Chapter II examines the data which has been utilized in this research and the statistical preparation of the data. Chapter III examines the developmental work undertaken to produce a model capable of predicting under-ice AN and the inputs necessary to achieve this. The limitations of the current AN model are discussed in detail in this section. Chapter IV presents the comparison of the predicted ambient noise values and the measured data and analyzes the correlation of these values. These results verify the degree of accuracy of the model as well as its robustness. The final chapter presents conclusions and recommendations relating to the research.

D.   FORCING MECHANISMS AND PHYSICAL PROCESSES

A review of literature reveals extensive work concerning the origins of low frequency noise generated under the ice. Many mechanisms have been identified and all are directly or indirectly related to stressing of the ice cover (Buck and Wilson, 1986; Makris and Dyer, 1986; Oard, 1987).

Oard (1987) relates the stressing of the ice to two main processes. The noise produced is dependent upon the

4

areal extent of the generating force, the wind or current
stress, which initiates or sustains the motion and produces
ice/ice interactions. Secondly, she relates the dependency
of the generated noise associated with the closely packed
ice cover of the central Arctic to high stress mechanisms
such as lead formation, rafting and pressure ridging. Oard
notes that once an external force is applied, subordinate
forcing functions are developed such as ice momentum,
divergence/convergence and vorticity.

It is important to understand the spectral
decomposition of the noise-generating mechanisms. Table 1
relates frequency to primary noise generating mechanisms.

Table 1. Generic Arctic Ambient Noise Spectral Decomposition (adapted from Parsons, 1992).

Frequency band	Primary Noise-Generating Mechanism
1 - 10 Hz	Seismic vibrations
10 - 300 Hz	Pressure ridging
300 - 500 Hz	Ice/ice interactions, pressure ridging, wind

Buck and Wilson (1986) explain in detail the formation
mechanisms and processes associated with pressure ridging.
As an external stress is applied, such as wind force,
thinner refrozen leads in the Arctic ice would generally

5

prove to be the weakest ice and therefore the first to be deformed. This would stimulate further compressional movement, thickening the pressure ridge, and adding more depth to the ice keel. They report acoustic measurements, taken during a period of near-field active pressure ridging, which demonstrated very high levels of ambient noise, of the order of 93-97 dB, with high horizontal spatial coherence.

Buck and Wilson (1986) conclude that active pressure ridges dominate low frequency ambient noise measurements, even if the hydrophone is not in the immediate vicinity of active ridging. Pressure ridge formation from long range contributes to the noise level at low frequencies at any given location because of favourable propagation at low frequencies. Buck and Wilson (1986) calculated that only one active pressure ridge occuring every 25 nm was required to produce median ambient noise levels for April, the month when their nearfield pressure ridge data was recorded. This calculation assumes that the nearby pressure ridge they observed and the noise level it produced was typical of all pressure ridges in the Arctic. Few other, if any, measurements exist of the noise field generated by active pressure ridging. This lack of observed pressure ridging points to the need of making more near field active pressure ridge measurements. Recordings using a submarine towed array or arrays suspended from ice floes would be perfect methods to obtain directional noise characteristics.

The observation that the average spacing of active pressure ridges is large (~25 nm) is an important but preliminary step in selecting the minimum latitude/longitude cell size to model Arctic ice noise due to pressure ridging. A 1 degree by 1 degree latitude/longitude cell was chosen as an active pressure ridging noise source unit area because it is, on average, large enough to contain a few (1 to 10) active pressure ridges but small enough to accurately model the directionality of distant Arctic storm noise. It is emphasized, however, that a submarine operating within any 1 degree by 1 degree cell may experience a large variation in the spatial distribution of AN due to proximity to a specific active pressure ridge. As will be shown in Chapter IV of this research, high variability existed among the noise levels recorded on 3 relatively closely spaced, ice-mounted buoys. This variability is attributed to the spatial inhomogeneous distribution of the active pressure ridges relative to the buoy locations.

The generation of pressure ridges is associated with high levels of ambient noise and Parsons (1992), Feller (1994), and Fritsch (1995) have shown that high ambient noise levels have been measured resulting from the passage of Arctic storms and their associated high wind speed/stress. The vast ambient noise data bases analyzed by these authors supports spatially discrete active pressure ridges as the dominant, low frequency noise source. This

seems to refute the spatially homogenous ice plate flexure speculations of Makris and Dyer (1986).

Many researchers have examined the relationship between measured levels of ambient noise and environmental correlates such as ice speed and wind speed/stress (Pritchard, 1984; Makris and Dyer, 1986; Lewis and Denner, 1988; Feller, 1994). These studies have shown that higher ice drift speeds and wind speeds are well correlated with higher ambient noise levels, but only for relatively short (hours to days) periods of time. Attempts to model ambient noise with local parameters, however, have generally been less successful mainly because the individual or composite correlations are based upon point source measurements of icepack kinematics. This overlooks the fact that distant noise events contribute significantly to the measured time series.

In the mid latitude open-ocean the ambient noise measured by a receiver at a given location is the sum of all the noise contributions from all directions which include both local and distant shipping sources as well as local and distant wind/wave sources (Urick, 1983). Applying this approach to the ice-covered Arctic Ocean, the low frequency, ambient noise at any one particular point should be the sum of the noise from both local and distant noise-generating areas from all directions. Obtaining an accurate estimation of noise sources both in the near and far-field is dependent

8

upon an accurate estimation of the source level and its directivity as well as an accurate estimate of propagation loss from all sources to the single receiver site. Accurately modelling the noise source and its propagation characteristics will result in a more accurate ambient noise prediction.

Lewis and Denner (1988) state that the scale of ice kinematics is comparable to the scale of the atmospheric forcing phenomena. This suggests that the entire Arctic needs to be considered as potential sources of AN at low frequency. Because of the close association of wind speed/stress and the generation of pressure ridge-induced AN, the spatial variation in wind speed/stress and the resulting ice-ice interactions need to be addressed on a synoptic scale.

II DATA

A. DATA REQUIREMENTS

The discussion in Chapter I has identified that the major mechanism in generating AN under the pack ice is wind speed/stress which influences the amount of pressure ridging and ice/ice interactions taking place in an area at any particular time. The scale of the process is synoptic; therefore, the variation and pattern of wind speed/stress need to be considered over the whole of the Arctic. This demands that such data needs to be an input to the low frequency AN prediction model. The output then needs to be compared to 'ground truth' - actual ambient noise values measured from buoys or arrays deployed under the pack ice over a concurrent time period.

Since no method currently exists to directly locate specific active pressure ridges throughout the Arctic basin, the modelling of this noise source is taken as an average source level per square metre, summed over a 1 degree by 1 degree latitude/longitude cell. This is a major model limitation that will be discussed in Chapter III in the context of the observed high spatial variability recorded from three, relatively closely spaced buoys.

B.   BUOY DATA

1.   Background

Three Ambient Noise Meteorological (AMNET) buoys were installed in the central Arctic pack ice in April 1992 and acquired data for 16-20 months. Feller (1994) has undertaken an in-depth examination and analysis of this data and the reader is referred to this publication for any further detailed information not provided in this chapter. It is these analyzed results that are used in this study as "ground truth" against which to test the model results.

The three buoys were designated 12813, 12815 and 12819 but will be referred to as 13, 15 and 19 for brevity. They were originally located 600 km north of Franz Joseph Land in a roughly isosceles triangular pattern with approximately 100 km between buoys 13 and 19 which were 180 km to the south-east of buoy 15. This separation distance remained relatively constant throughout the length of the recorded data. The prevailing wind and currents determined their drift pattern, which was to the south and southwest over the entire period of time that the data was recorded.

2.   Ambient Noise Data

A single hydrophone was suspended beneath each buoy to a depth of 305 m and the noise field was sampled each hour by measuring eleven frequencies utilizing a frequency-dependent sample time that maintained a constant

time/bandwidth product. As explained by Parsons (1992), this information was processed and saved in situ until an ARGOS satellite pass occurred, whereupon it was transmitted to be later downloaded by the Naval Oceanographic Office.

3.   Preparation of Ambient Noise Data

Feller (1994) explains the techniques and methods he used in the preparation and quality control of the raw data. The noise records were edited for bad and missing data. Bad data points were defined as a value less than the buoy self-noise limit or greater than three standard deviations from the mean of the overall record. A cubic spline was used to establish an hourly time series. A moving filter was then applied to remove outliers after which linear interpolation filled any gaps with two final data quality checks removing any unrealistic spikes.

As the aim of this research is to try and predict general changes in the level of AN, a final two hour smoothing filter was applied to the data set. Estimates of AN, determined by the model are calculated every 12 hours (synoptic hours) and thus the two hour smoothing window does not exert any impact on model/data comparisons.

4.   Positional Data

Buoy positional data was only recorded during the ARGOS satellite passes. The positional data preparation is again explained in detail by Feller (1994). The raw positional

13

data was interpolated using a cubic spline to obtain an hourly time series. Non-physical spikes were edited and linear interpolation filled any missing points. A five hour boxcar average was applied to produce the final time series.

C.   METEOROLOGICAL DATA

1.   NOGAPS

To facilitate the synoptic approach to the modelling of Arctic ice-generated AN, a comprehensive, gridded, 12 hourly meteorological data set was necessary. Specifically wind speed and direction were required for the whole Arctic region. The meteorological data source which fitted these requirements was the Naval Operational Global Atmospheric System (NOGAPS). This data has routinely been acquired and stored in the Meteorology Department at the Naval Postgraduate School since late 1992. It is supplied by the Fleet Numerical Meteorology and Oceanography Center (FNMOC).

As a user of the NOGAPS data, it is important to understand how NOGAPS has been developed and understand what physical limitations exist so that the potential applications of the data can be realistically evaluated. Such an in-depth explanation, however, is not relevant here so the reader is referred to Rosmond (1992) which covers the design and testing of NOGAPS, and to Hogan and Rosmond (1991) which gives a detailed technical description of

14

NOGAPS. Understanding of the limitations of the data, which is used as an Arctic storm noise model input, will aid in the interpretation of the final results.

NOGAPS became operational at FNMOC in 1982 with NOGAPS 3.2 being developed in 1989. The major change was that NOGAPS 3.2 became a global spectral model as opposed to the finite differencing versions prior to 1989. NOGAPS is a forecast system that includes sophisticated data quality control programs, parameter validation, optimal interpolation analysis, non-linear normal mode initialization, forecast model and verification components (Hogan and Rosmond 1991).

Spectral models have proven to be accurate and efficient at predicting the general circulation of the atmosphere. Rosmond (1992) states that in terms of verification and accuracy of prediction, NOGAPS is quite competitive with global models such as the European Centre for Medium Range Weather Forecasts (ECMWF) and the National Meteorology Center (NMS) and ranks in the world top 4 or 5.

A problem with using NOGAPS data as an input to a surface forcing model (Rosmond, 1992) is the systematic error or bias associated with NOGAPS heat, moisture and momentum fluxes. The bias error is directly related to NOGAPS's ability to accurately predict the above fluxes and heat/momentum budgets and a great deal of research effort has gone into reducing this bias.

Focusing on our study region, the Arctic Ocean is undoubtably a data sparse area, even more so than other oceanic areas. Data sparsity is identified (Rosmond, 1992) as a problem with verification of NOGAPS data and the performance of NOGAPS in data sparse oceanic areas must be regarded as approximate. Data sparsity will affect NOGAPS's performance and accuracy in the Arctic, particularly during the northern winter. In spite of this limitation, NOGAPS is considered the most accurate and readily accessible source of data for our Arctic storm model.

Because of data paucity, perfect agreement between model estimates and measured ambient noise data, point by point, is not expected. The objective of our model is to estimate ambient noise trends to predict extreme noise events, and NOGAPS is well suited for this task. In addition, the NOGAPS data suits the needs of this research project in that gridded meteorological data is available for the entire Arctic at regular 12 hour intervals.

2. GEMPAK

The NOGAPS gridded data resolution was 2.5 degrees (latitude) by 5 degrees (longitude). The area of interest was 70-90 degrees north latitude and 0-360 degrees longitude. The wind velocity data was calculated using the 1000 mb pressure fields. Data was extracted for the u (N-S) and v (E-W) component of the wind velocity parameter. This

16

was achieved by using the General Meteorology Package (GEMPAK) which is a suite of applications programs for the analysis, display and diagnosis of geo-referenced data. GEMPAK was originally developed by the Severe Storms Laboratory at the Goddard Space Flight Center of NASA starting in the 1980's. It is now distributed and supported by UCAR Unidata Program Center and the version used in this research was 5.2.

GEMPAK extracted the necessary data at a resolution of 2.5 by 5 degrees. For this research a 1 degree by 1 degree latitude/longitude data grid is required so the data was bilinearly interpolated through the use of a MATLAB program to achieve the necessary resolution.

III   DEVELOPMENT OF AMBIENT NOISE PREDICTION MODEL

A.   METHODOLOGY

The purpose of this study is to develop a predictive model of the under-ice AN at low frequency (<500 Hz) by summing the contributions of both local and distant noise sources. The sound sources reflect the amount of pressure ridging and ice-ice interactions taking place as a direct function of wind speed/stress.

The source level per unit area is empirically determined as a function of the wind speed and is spatially decayed by a transmission loss model to estimate the AN at the receiver. The directional ambient noise can be estimated by summing all distant and local unit area sources. The model estimates AN for selected significant (loud or quiet) synoptic meteorological events, for locations where recorded buoy AN values exist. A comparison of the model estimates with AN measurements can then be made.

As has been discussed in Chapter II, acoustic data from three central Arctic drifting AN buoys for the period April 1992 to August 1993 was obtained and analyzed. The NOGAPS wind speed data for the same time scale was also obtained and manipulated into a 1 by 1 degree gridded format.

To develop a model capable of predicting under-ice AN it was decided to take an already existing open-ocean

ambient noise model and adapt it for use under the Arctic pack ice. The model chosen was the Ambient Noise Directionality Estimation System (ANDES). The newly adapted model is designated the Arctic Storm Noise Model (ASNM).

This next section will cover an overview of ANDES, the changes undertaken to adapt ANDES to ASNM, the required inputs to the new model and sample output and display. The last section will examine in some detail the current limitations of ASNM in predicting under-ice AN.

B.   ANDES

1.   Development of ANDES

ANDES was first introduced in 1986 as an upgrade to its predecessor, the Directional Ambient Noise Estimation System (DANES) and was initiated by the ASW Environmental Acoustics Support (AEAS) Program (Renner, 1993). DANES was coupled with the Aseps Transmission Loss Model (ASTRAL) which allowed the model to be used in range dependent environments and, therefore, estimate the directionality of noise over large areas. ANDES provides estimates of both the horizontal and vertical directionality of the noise field. ASTRAL is a US Navy standard transmission loss model. ANDES also incorporates US Navy standard environmental databases.

Renner (1993) summarizes the development of the ANDES model and provides an in-depth system overview and

description of the use of the model. Readers are referred to this document for more in-depth information.

2. System Overview

The ANDES system consists of three major components.

a. Environmental Data Bases

The databases inherent in the ANDES model are:

1. General Digital Environmental Model (GDEM) output. Typical sound speed fields for geographical areas with similar oceanographic characteristics.

2. Bottom depth. Digital Bathymetry Data Base Confidential version (DBDBC) detailing ocean water depths.

3. Low Frequency Bottom Loss (<1kHz).

4. High Frequency Bottom Loss (>1kHz).

5. Historical Temporal Shipping (HITS) describing average distribution of surface ships.

b. Noise Model

ASTRAL computes propagation loss from the noise sources throughout the ocean. The contributions from these sources are incoherently summed to derive the noise field. The distribution of noise sources related to shipping is described by the HITS data base. The noise sources due to wind forcing are derived from local and basin wide fields.

c. User Interface

The user interface consists of the software

21

necessary to run the model and the graphical display of results and outputs.

C.   ADAPTION OF ANDES TO ASNM

1.   Rationale for Model Modifications

ANDES is an open ocean AN model with noise estimated from the shipping densities in distant and local 1 degree by 1 degree latitude/longitude cells. The contribution to the noise field due to wave action (wind generated) is also modelled in 1 degree lat/long cells in ANDES.

Within the ice-covered Arctic neither of these noise sources are present. As described in Section A of this chapter, the shipping noise source inputs to the model are to be replaced by noise from pressure ridging in areas both local and distant to the receiver. Thus, Arctic noise due to pressure ridging is summed over each 1 degree by 1 degree cell and treated as an 'equivalent' shipping density in ASNM. In ASNM the sea state (wind dependent) component, which contributed to AN calculations in ANDES, was not used.

2.   New System Overview

a.   Data Bases

The new/adapted data bases used in ASNM are:

1. Instead of the GDEM fields a series of six sound speed profiles representing various geographic regions of the Arctic basin (Newton, 1990) were input to NASM. Figure 1 shows the six SSP's.

2. Bottom depth. Instead of the classified DBDBC data base an unclassified version, DBDB5, was used.

3. Low Frequency Bottom Loss (LFBL). Because the noise model predictions are designed to represent conditions for the central, deep water Arctic basins, a generic set of LFBL parameters were inputed.

4. High Frequency Bottom Loss (HFBL). The aim of this research was to develop a low frequency model. Therefore a HFBL data set was not incorporated.

5. The HITS data base was not used but replaced with source level values of Arctic pressure ridging noise detailed in Section D.

b.   Noise Model and User Interface

The operation of the ASTRAL model and user interface were generally unchanged. The wind strength parameter which generated the high frequency noise was not utilized. However, the distribution of noise sources used to calculate AN was now generated by the source level values.

D.   INPUTS TO ASNM

1.   Source Level Densities

The important aspect of replacing the shipping density and wind fields, which were integral to the running of the open ocean ANDES model, with pressure ridging source levels is examined in this chapter. The central theme of this

23
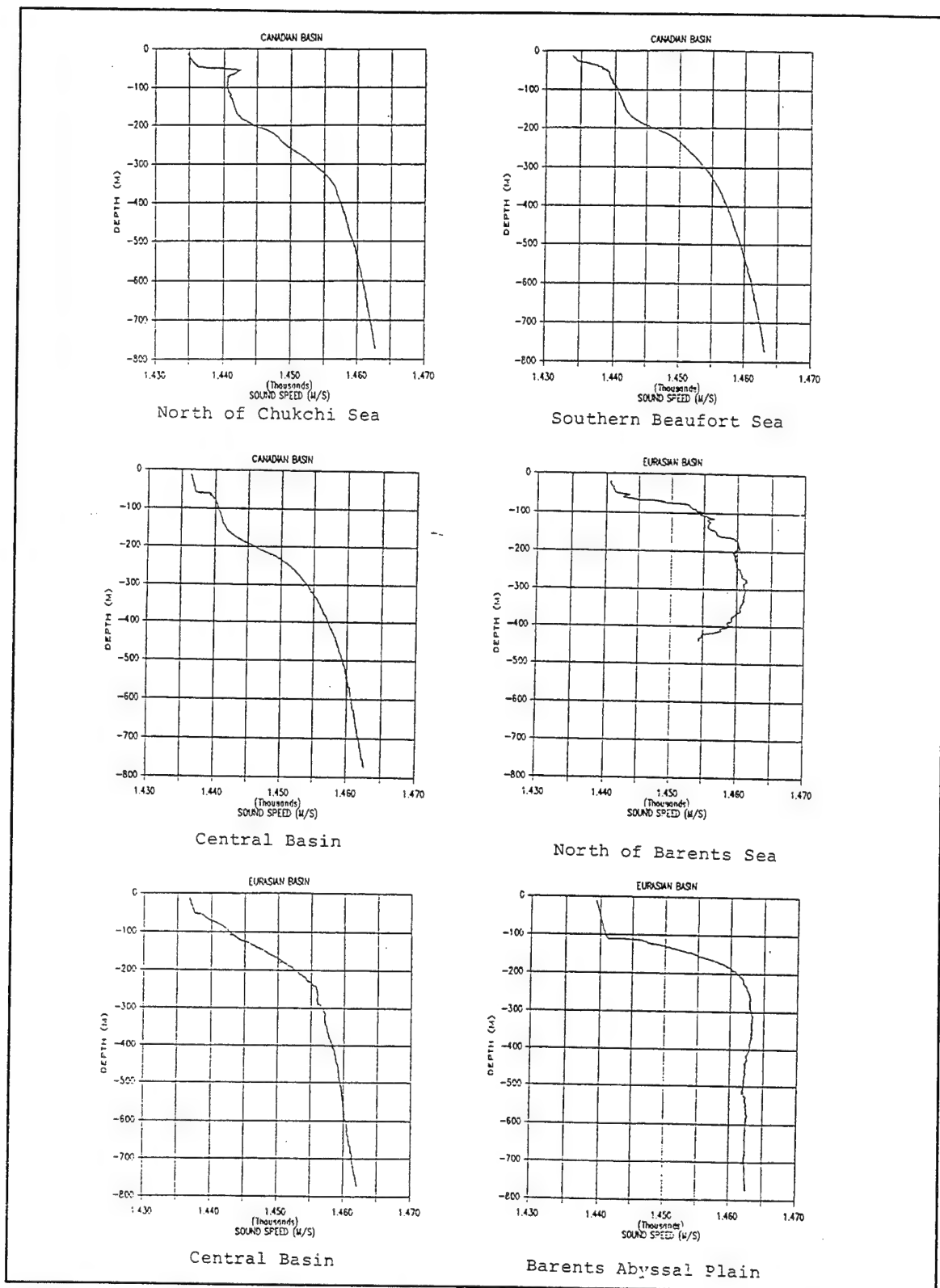
Figure 1   Six sound speed profiles representing various geographic regions of the Arctic basin (from Newton, 1990).

research is the introduction of a set of source level densities (SLD), at selected frequencies, which are wind speed dependent. The methodology was to use an initial set of SLD and then run ASNM for a given synoptic time period and compare the results with the actual measured noise levels. An 'evolutionary' approach was adopted to empirically change the SLD until a 'best-fit' between model estimates and data could be achieved for a particular synoptic event. Running the model for a different synoptic event would then determine the accuracy of the SLD values used and provide an initial verification of the model's accuracy and robustness.

The initial set of SLD values were estimated by Professor Robert H. Bourke and James H. Wilson of the Naval Postgraduate School (NPS). The estimated values were based on several very loud and quiet storm events which passed in the immediate vicinity of the buoy field such that the local noise could be assumed to dominate the distant noise contribution, i.e., the transmission loss could be assumed to be zero. Noise Level (NL) was converted to SLD by an inverse technique developed by Wilson (1983) in converting wind-generated SLD to AN in the open ocean. If straight line propagation is assumed, then $AN = SLD + 10 \log \pi$ in dB (where $10 \log \pi = \sim 5dB$).

The model was initially defined with 30 categories of SLD created as a function of wind speed. From analysis of wind speeds associated with Arctic meteorological synoptic events and several empirical iterations from comparisons of actual and predicted omnidirectional AN values, a frequency-dependent set of SLD values were finalized. These values are shown in Table 2. SLD values are in $dB/uPa/\sqrt{Hz}/m^2$ at 1 m.

Prior to entering these values into the model the SLD was multiplied by the area of its 1 degree by 1 degree latitude/longitude cell to calculate the SL for the cell itself. The SL of any particular 1 degree by 1 degree cell is determined by the average wind speed in the cell and the cell area. The transmission loss from each cell is calculated and will determine the noise source's relative contribution to the total noise field at the receiver. Upon summation of all areas by the model the average noise field and its associated directionality will be obtained for a given receiver location. The source directivity pattern for a submerged monopole, like the ice keel below an active pressure ridge, is mathematically equivalent to a surface dipole (Wilson, 1983). Thus, a surface dipole directivity pattern is assumed for the pressure ridging source.

Table 2 Source Level Density Categories as a Function of Wind Speed (knots) and Frequency.

Cat No	Wind(kts)	50 Hz	100Hz	500Hz
1	0 - 5	53	45	32
2	6 - 7	56	48	36
3	8 - 9	57	49.5	37
4	10 - 11	58	50.5	38.5
5	12 - 13	59	52.5	40
6	14 - 15	60	53.5	41.5
7	16	61	55	43
8	17	62	56	43
9	18	64	57	44
10	19	65	59	45
11	20	67	60	46
12	21	68	61	47
13	22	70	63	47
14	23	72	64	48
15	24	73	65	49
16	25	75	67	50
17	26 - 27	76.5	68.5	51.5
18	28 - 29	78.5	70	53.5
19	30 - 31	80	71.5	55
20	32 - 33	81.5	73	56
21	34 - 35	82.5	74.5	57
22	36 - 37	84	76	58
23	38 - 39	86.5	78	59
24	40 - 42	90	80	60
25	43 - 45	92	82	61.5
26	46 - 48	94	84	63
27	49 - 51	96	87	64.5
28	52 - 55	101	90	66
29	56 - 59	104	93	68
30	>60	107	95	70

2. Land Proximity Effect

Embedded in the program to assign SLD as a function of wind speed is a subroutine to include a land proximity effect that can increase the AN. This increase in noise is experienced in areas where the pack ice interacts with any land surface. In the case of the buoys examined in this research their closest point of approach to land throughout their deployment were the islands in the northern Barents and Kara Seas; those of Severnya Zemlya, Franz Josef Land and, to a lesser degree, Spitsbergen. These islands are generally well encased in the Arctic pack ice during the winter months but, as the ice edge retreats northwards during the summer months, the ice-water boundary becomes more fractured and MIZ-like conditions can be experienced in the general vicinity of these islands, between 79 to 81 degrees North (Joint Ice Center, 1992). It is well recognized that the Marginal Ice Zone (MIZ) is a much noisier environment than either under the pack ice or open ocean. At the MIZ higher noise levels are a result of wave and swell interaction with individual ice flows (Diachok and Winokur, 1974; Makris and Dyer, 1991).

In the winter when pack ice surrounds an island or land mass and the prevailing wind is onshore, the convergence of the ice field would cause a build up in stress causing additional pressure ridging and shearing of

the ice floes resulting in much increased noise levels. If a directional receiver were close to land, its AN values would vastly increase in the direction of the land mass.

To account for this proximity to land effect the SLD wind speed categories (Table 2) were adjusted if a particular 1 degree lat/long cell was near land (defined as less than 200 nm) and, importantly, if the wind was onshore (135T to 235T). If so, the SLD was shifted up one wind speed category for each cell for every 20 nm less than 200 nm.

3.   Changes in Wind Direction

Bourke and Parsons (1993) examined ambient noise records of AMNET buoys in the northern Barents Sea and identified the passage of storm fronts as a direct cause of large rapid increases in the levels of AN as storm fronts passed over individual buoys.

The rapid change in wind direction is important as its effect on ice convergence and ice/ice interactions cause rapid increases in measured AN. Incorporating this effect into ASNM is important. Therefore the SLD wind speed categories (Table 2) were adjusted if a change of wind direction more than 90 degrees occurred over a 12 hour period, but only if the winds were greater than 20 knots. The SLD would be shifted up one wind speed category for every knot of wind speed greater than 20 knots.

In the synoptic events considered in this research the

29

buoy locations were in the central Arctic basin. Very few, if any, frontal features penetrate as far north as this. This was confirmed by analysis of the data which showed no sudden (less than 12 hours) changes in wind direction of greater than 90 degrees. Therefore, this effect was not important in the synoptic events examined here. In other locations where frontal activity is likely the incorporation of this effect is important and must be included.

4.   ASNM Input File

The input file is the primary user input to ASNM. The inputs in the file consist of four logically organized groups: receiver description, noise source description, environmental inputs and output requirements.

A typical input file for a standard run is shown in Figure 2.

```
93020300
MODEL TYPE   MEAN
FREQUENCY         50.00
RCV DEPTH        900.00
POSIT RCV 8454N  8230E
SOURCES     DENSITY
MIN               5.00
ANDMSG      HORIZONTAL   VERTICAL
HORIZ RES        10.00
VERT RES          2.00
FLAGS       ENVIR   SOURCE   TL CZ DB1
MONTH       JUN
TIME          0  0      30  0       4  0
ANDTIM      HORIZONTAL   VERTICAL
HORIZ RES        10.00
VERT RES          5.00
```

Figure 2   Input file for ANDES/ASNM

As the file is formatted for the original ANDES, some parameters are irrelevant for use in ASNM. The relevant parameters are as follows:

1. HEADER; identifying date/time/group of run.

2. MODEL TYPE; 'mean' indicates the model calculates the mean omni-directional noise field.

3. FREQUENCY; select frequency, in Hertz, for run. Model frequencies must be between 20-1200 Hz.

4. RCV DEPTH; receiver depth, in feet. The receiver was placed at 900 ft for all model runs which corresponds with the AMNET buoys' depths.

5. POSIT RCV; latitude and longitude location of receiver.

6. SOURCES; Indicates that the SLD values, given in Section D1, are to be used.

7. MIN; radius, in nautical miles, in which TL is set to zero.

8. ANDMSG; set to determine the horizontal and vertical resolution of the output files.

The FLAGS/MONTH settings are redundant as they invoked the original data sets. The new data sets outlined in Section C2 were "hardwired" so as to be included in the model's calculations.

One important parameter which was also "hardwired" in the program was that of an ice scattering loss model. The Gordon-Bucher (Bucker and Gordon, 1984) ice scattering kernal was chosen because of its close agreement with the empirically derived Buck-Wilson ice scattering kernal (Buck and Wilson, to be published). The inclusion of an under-ice

31

scattering algorithm is necessary because the positive Arctic sound speed gradient results in sound rays refracting upwards to reflect or scatter from the rough under-ice surface. Since scattering loss values under ice are significantly higher than from the sea surface in the open ocean, the addition of an accurate ice scattering kernel to the model was very important. The Oceanographic and Atmospheric Model Library (OAML) approved ice scattering kernal, which includes a theoretical algorithm, based on Burke-Twersky scattering theory, is highly inaccurate and could not be used. The Gordon-Bucher algorithm requires an input of the standard deviation of the mean ice draft to represent the degree of roughness of the underside of the ice canopy. A standard deviation value of 2.0 m was selected based on the data reported in McLaren and Bourke (1992).

5. Meteorological Files

The GEMPAK generated files of wind speeds, outlined in Chapter II, were transformed into matrix data sets based on the 30 SLD categories. This was then used as an input file for the ASNM run. Figure 3 shows an example of a polar view of the distribution of SLD categories for a given synoptic time. This example shows a general area of high wind speed (SLD categories 20-30), located between 70-90 degrees North and 0-60 degrees East (excluding area around Spitsbergen), which analysis later determined to be an area of high AN.
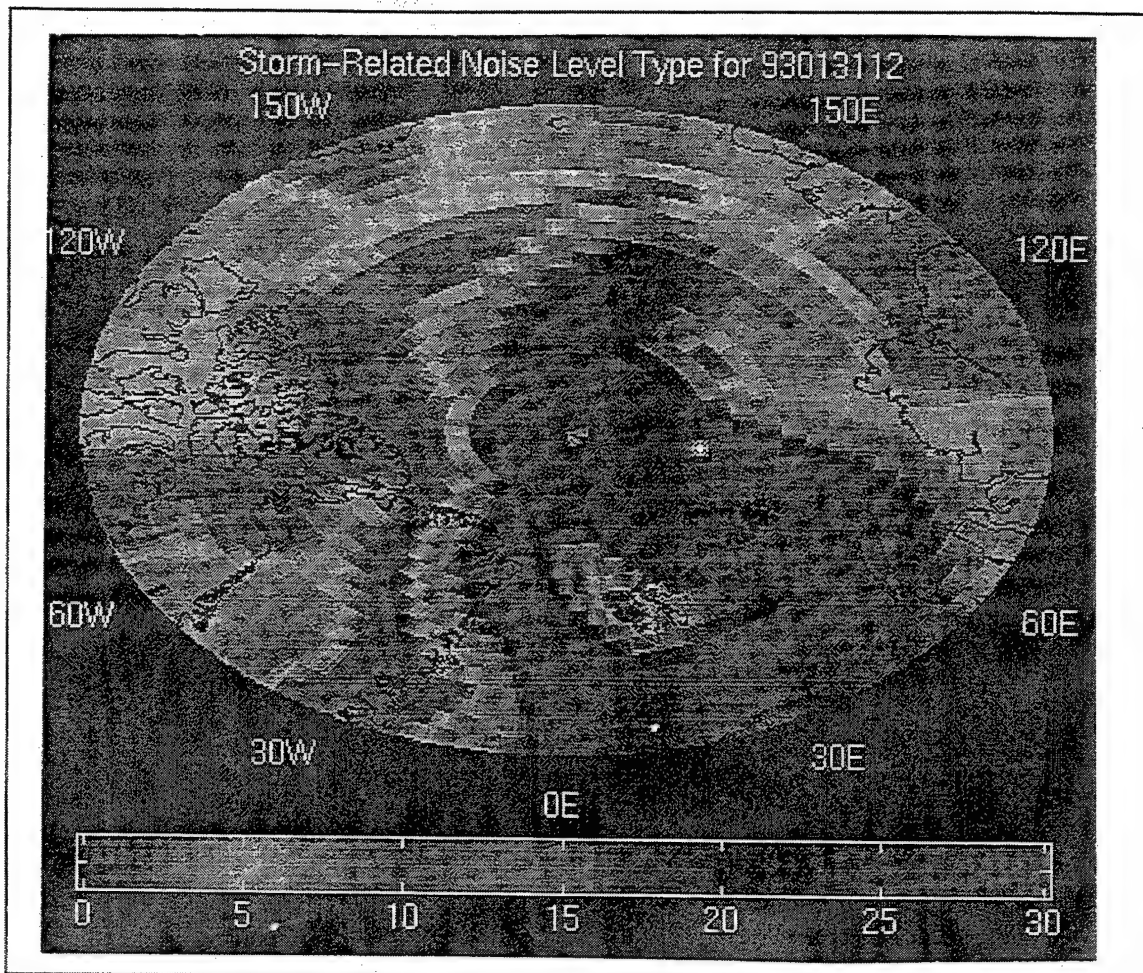
Figure 3   Example of a polar view of the distribution of
Source Level Density Categories (SLD's).

E.   OUTPUTS

An ANDES/NASM model run will produce generally three
main output files. An ASCII file is produced that contains
diagnostic information pertinent to the run, summarizing the
inputs and initialization used. A second ASCII file produced
is the primary noise output file which contains the model
calculations of transmission loss and directional and

omnidirectional values of AN for the given location.

The last file is a binary file that contains detailed noise directionality values in both the horizontal and vertical directions. This is the file which is input into the graphical display section to produce plots of the horizontal and vertical directionality of the received noise and the omnidirectional AN values. Figure 4 and Figure 5 show examples of horizontal and vertical plots of AN

Rcv Lat 84-15-N
Rcv Lon 80-45-E
Receiver Depth 900 ft
Sources:
 TOTAL

Frequency   Omni Noise
  50 Hz   77.0 dB
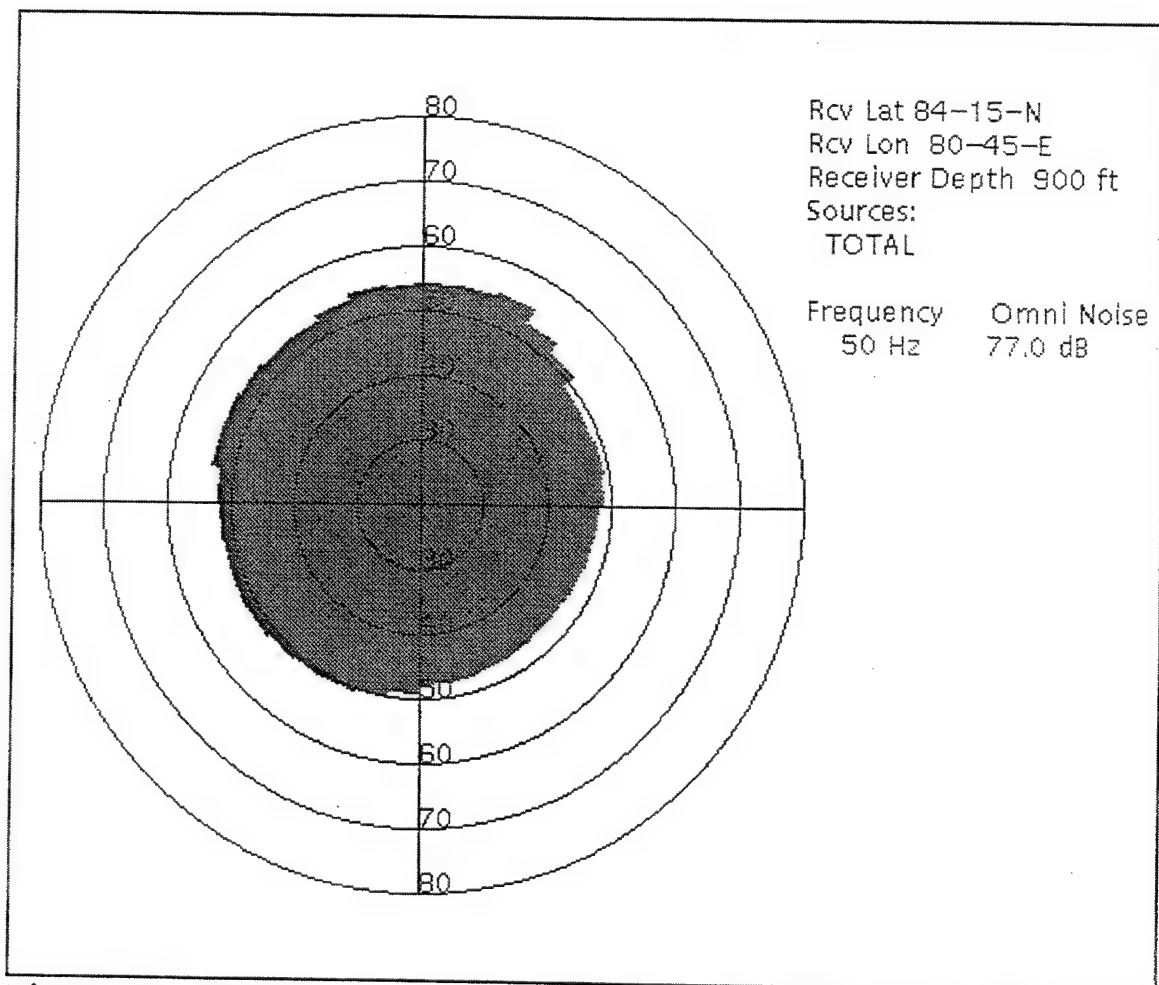
Figure 4 Example of horizontal directionality of ASNM prediction.
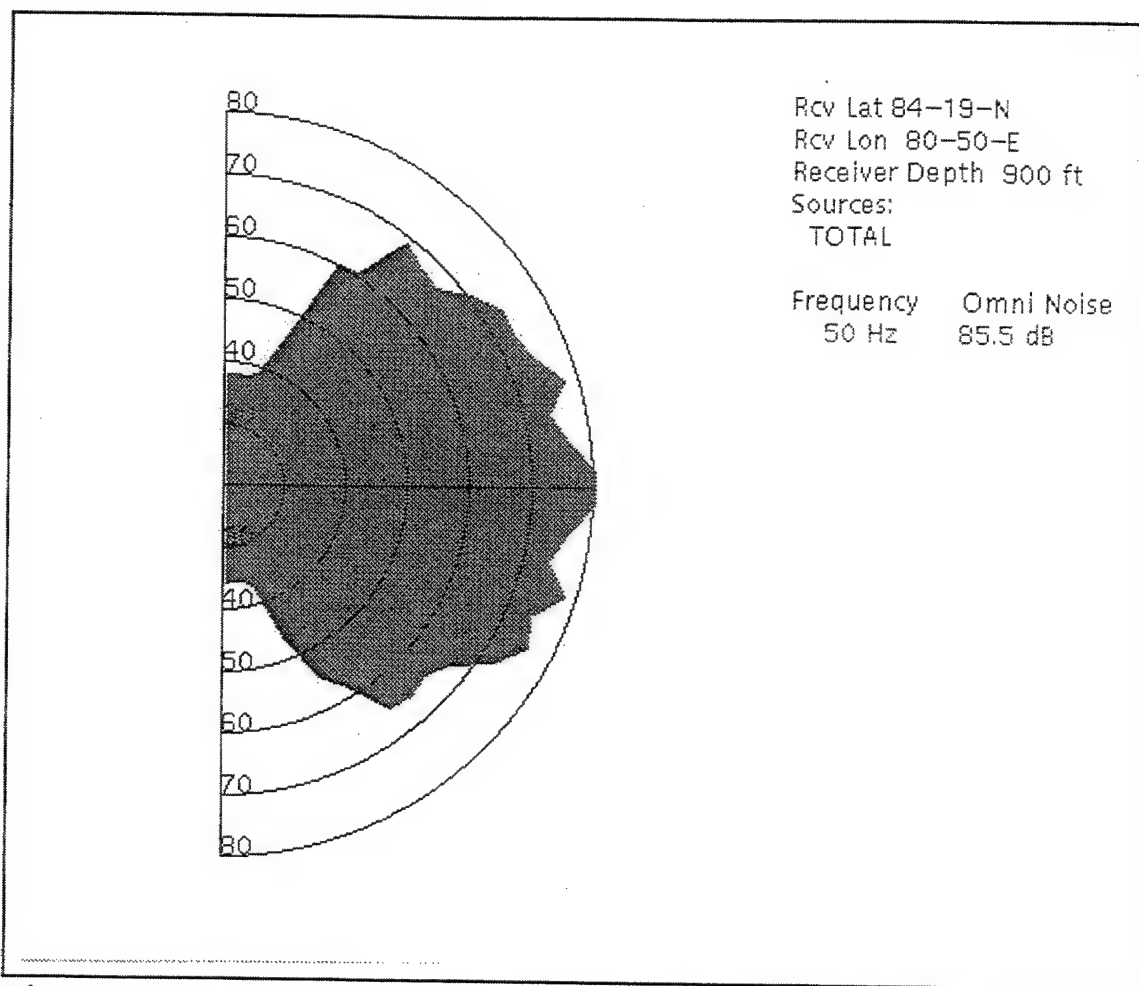
Figure 5 Example of vertical directionality of ASNM prediction.

directionality. Such information was not used in this study because the receivers were omni-directional hydrophones. However, the directional characteristics of the noise field will be important to future studies which will utilize AN data collected by directional towed or moored arrays.

35

F. LIMITATIONS OF THE MODEL

During the development and testing of any model it is
necessary to identify and understand the potential
limitations of the model. Therefore, when interpreting the
results, consideration can be given to these constraints and
limitations and their influence on the results. To determine
the potential limitations of the modified ANDES model it is
necessary to re-examine the nature of the Arctic AN
generating mechanisms and compare this with the model's
methodology to simulate these noise-generating mechanisms.

Chapter I explains the role of wind-generated pressure
ridging in producing low frequency AN under the ice pack.
Figure 6 visually illustrates the nature of the ice surface
in Polar regions. This satellite image shows the numerous
leads, pressure ridges and shear zones present in an ice
covered region. These features represent potential or past
areas of high AN.

Buck and Wilson (1986) emphasize the importance of
identifying the location of all the active pressure ridges
if one is to successfully determine the source of the noise
field observed at a given location. Figure 7a schematically
characterizes the plentiful nature of ice ridges in a
representative area of pack ice in the Arctic. For example
in the Beaufort Sea satellite observations show that there
are approximately ten ice ridges per kilometre. However, it
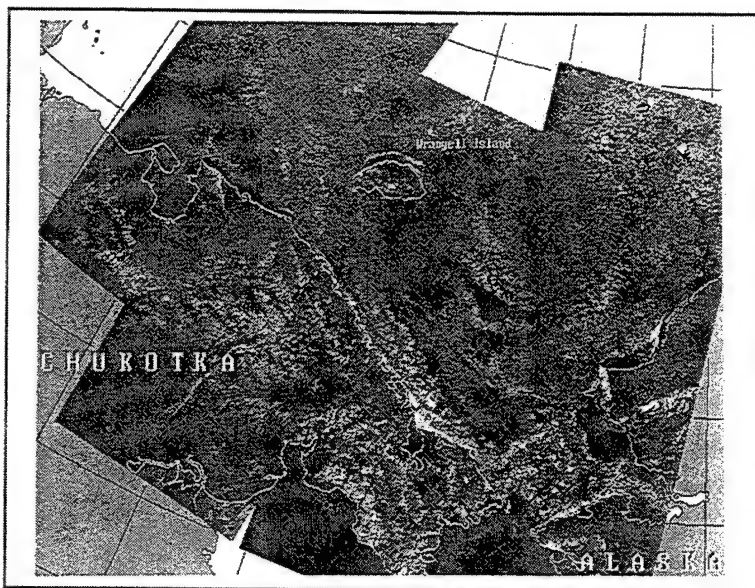
Figure 6 Satellite image showing the nature of the Arctic pack ice surface.

is the active pressure ridges which generate the AN and these are much more difficult, if not impossible, to identify. Buck and Wilson (1986) conclude from their research that, in the month of April, only one in 300-400 ice ridges may be active and that a 20-30 nm spacing is representative of the actual active ice ridge spacing necessary to produce median noise levels. This is illustrated in Figure 7b where the distribution of active pressure ridges becomes spatially much sparser.

The model's methodology to simulate the noise-generating sources is based upon the assumption that the sources are spatially homogeneously distributed within each 1 degree latitude by 1 degree longitude cell, only because

37
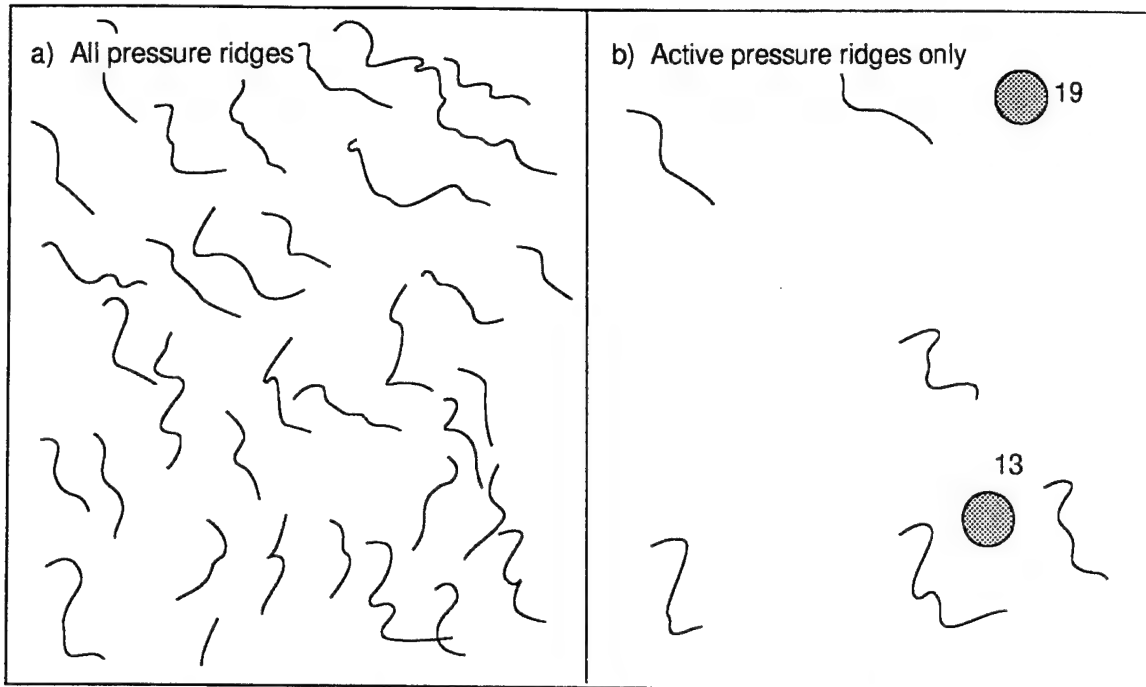
Figure 7   Schematic distribution of pressure ridging showing a) all pressure ridges within an approximate 200 km square area b) only those pressure ridges which are acoustically active. The solid circles denote hypothetical locations of two ambient noise buoys.

there is no current capability to remotely detect the presence of active pressure ridges. Each cell is assigned a source level dependent on the wind speed and its proximity to land, based upon 30 categories of wind speed groupings. This is portrayed schematically in Figure 8a which shows the inclusion of two receiver buoys (13 and 19) at different locations. This scenario shows the two buoys both being affected by similar local and distant wind stress during a synoptic event, and ignoring any land proximity effect, the model would predict similar omnidirectional AN values for both buoys.

The reality of the situation is that the local

a) ASNM places average source of ice noise at center of 1° x 1° cell and AN prediction is independent of buoy position within cell

1° x 1° cell no. 1

19

Source Location

Average 20 kt Winds

1° x 1° cell no. 2

Source Location

Average 20 kt Winds

13

no nearby active pressure ridges

several nearby active pressure ridges

b) Anisotropic real time distribution of active pressure ridges showing that measured noise level can be highly dependent on buoy location within cell

1° x 1° cell no. 1

19

1° x 1° cell no. 2

13

Figure 8 Schematic illustrating a) spatially homogeneous model with wind speed dependent noise source forcing ASNM prediction b) realistic anisotropic spatial distribution of loud active pressure ridging activity. In (a) AN is independent of buoy location; in (b) AN is highly dependent on buoy location.

distribution of pressure ridges are point sources and not homogenous area-wide noise source densities. This widespread contribution of distant pressure ridges, resulting from increased wind speeds, can be accurately modelled, but a

loud active pressure ridge in the nearfield can dominate
distant noise sources making predictions of the measured
noise level at any one location difficult. Relating this to
the preceding scenario, Figure 8b illustrates how a loud
pressure ridge in the vicinity of buoy 13 would increase the
AN levels although the model would have predicted similar
levels for both buoys. These local effects are constantly
observed in the data and are indicative of the spatial
inhomogeneity of active pressure ridges.

Hence, the influence of local pressure ridging is an
important contribution to the noise field and must be
considered when interpreting the results of the model.
Figure 9 illustrates this in relation to the strength of
synoptic storm events. During a period of very low wind
speeds, e.g., less than 10 knots (4.9 m/s), the generation
of pressure ridges is expected to be low over the Arctic
pack ice. However, there is still likely to be some
localized pressure ridging activity due to residual ice
motion. With generally low wind values ASNM will predict low
levels of AN. But if a receiver were in close proximity to
an active pressure ridge, the recorded levels would be
significantly higher than the ASNM predictions. The local
pressure ridging environment would be important. This
situation is illustrated in Figure 9a for which the model is
expected to predict AN levels accurately unless the receiver
happened to be close to an active pressure ridge, which are
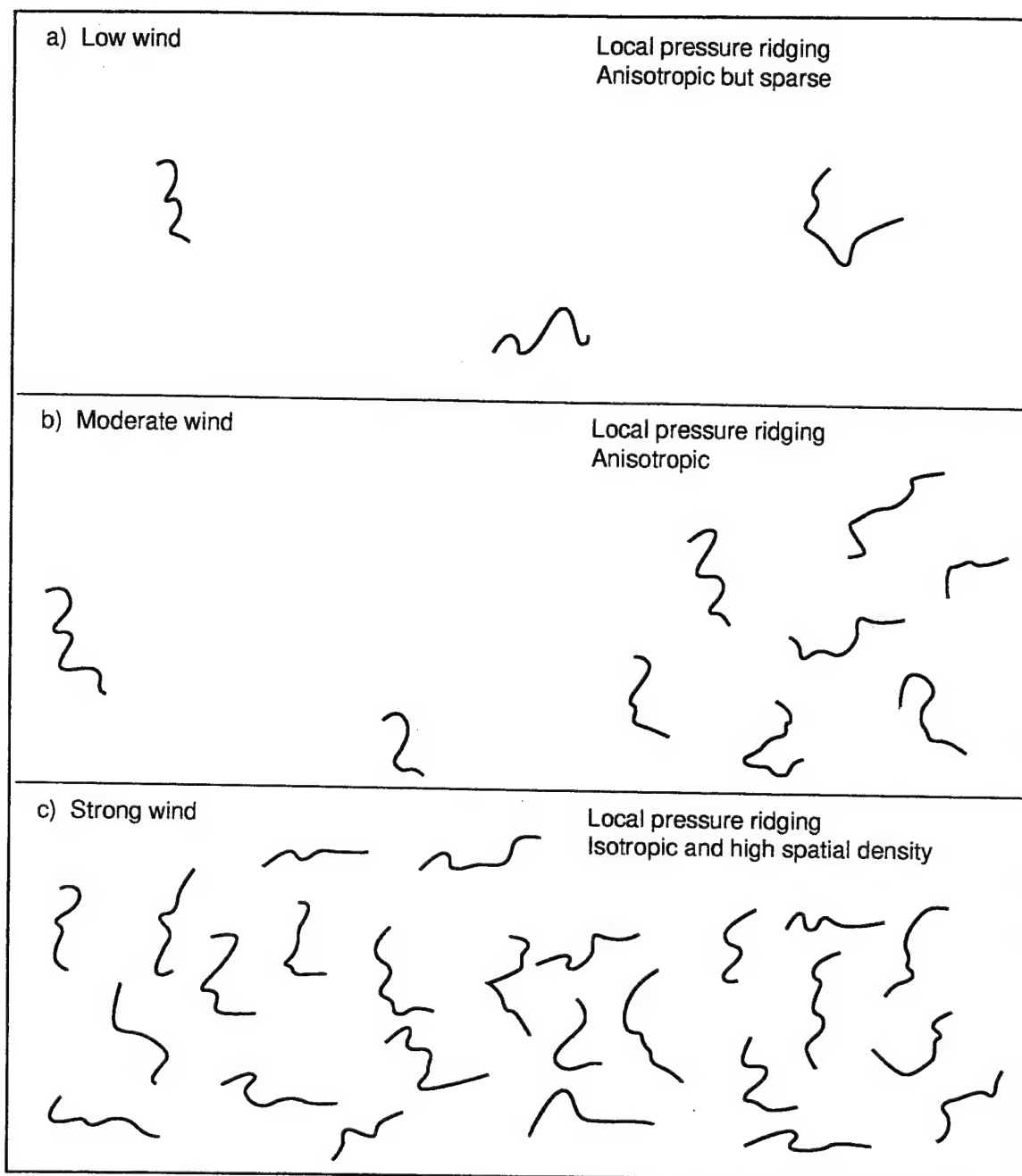
Figure 9   Influence of pressure ridging at a) low wind
speeds where local pressure ridging is anisotropic but
sparse. b) moderate winds where local pressure ridging is
anisotropic and c) strong winds where local pressure ridging
is isotropic and high in spatial density.

41

few in number at this time and location.

During periods of intense synoptic activity affecting large areas of the Arctic basin, when high wind speeds are present in the general vicinity of a receiver, the predicted noise levels are likely to be accurate. This occurs because the increased wind forcing will create a more spatially homogenous distribution of active pressure ridges and the model can be expected to accurately sum the contributions of both near and distant noise sources. This scenario is portrayed in Figure 9c.

At a time of moderate synoptic activity in the vicinity of a receiver the moderate wind speeds are likely to accurately determine the AN contribution of pressure ridges generated at comparatively distant locations. However, any local pressure ridging activity would still affect the accuracy of the model's predicted values. It is at these times of moderate wind strengths where our model predictions are likely to be less accurate. This is illustrated in Figure 9b where the local pressure ridging activity is very important.

The importance of the presence of near-by active pressure ridging is clearly stated above and such information would prove to be an invaluable input to the model. This idea will discussed in greater detail in the recommendations in Chapter V.

IV ANALYSIS AND COMPARISON OF ASNM RESULTS

The preceding chapter has dealt with the development of ASNM and its inputs, outputs and limitations. This chapter examines in detail model predictions of AN and compares them to measured buoy levels of AN. The emphasis is on predicting trends and major changes in AN from quiet periods to very loud periods, as opposed to small scale fluctuations over short temporal periods. Therefore synoptic events were selected where there were large changes in wind speed, i.e., storm events, which would be expected to produce large changes in AN values. One of the synoptic events previously identified by Feller (1994) is used to compare measured AN levels against model predictions. This first synoptic event, during which strong winds were experienced, is analyzed in section A and a second synoptic event, experiencing more moderate winds, is analyzed in section B. A third synoptic event producing a quiet period in the central Arctic basin, identified by Fritsch (1995), is examined in Section C.

A. SYNOPTIC EVENT I

1. Overview

The first synoptic time period analyzed was from 28 Jan 1993 (Julian date 28) to 6 Feb 1993 (Julian date 37). The measured buoy data for this time period has been analyzed by Feller (1994), to which readers are referred for more in-

depth statistical analysis of the AN data. This synoptic
period was chosen as measured AN values varied from
extremely quiet, 5th percentiles levels, to very loud, 95th
percentile levels. The percentiles were calculated by
Feller (1994) and were based on the seasonal record length
of the buoys for the winter months, Nov 1992 to Mar 1993. At
the start of the time series, all buoys recorded levels
close to the 5th percentile level, then increased to the
95th percentile levels over a period of 2-4 days. These high
levels were maintained for 4-5 days until levels decreased
to the 5th percentile values once again.

The location of the buoys at this time was in the
central European Basin. Buoys 13 and 19 were approximately
220-240 nm N-NW of Sveryna Zemlya and buoy 15 was 160-180 nm
north of Franz Josef Land.

The meteorological charts for synoptic periods which
resulted in significant changes in wind speed conditions are
shown in Appendix A (Figures 30 to 35). The general
progression of the weather and associated wind speeds can be
determined by closer examination of these charts. At the
start of the period, 28-29 Jan, a high pressure centre,
(1024 mb), was located in the central Canadian basin and
dominated the Arctic. This maintained relatively weak
pressure gradients in the general vicinity of the buoy
positions. During the same period a deep low moved
northwards along the East Greenland coast and steadily

44

tightened the pressure gradient to the west of the buoy positions. By midday on the 31 Jan, a deep low (947 mb) centred over Spitsbergen produced a very tight pressure gradient in the vicinity of the buoys. Winds in excess of 40 kts (20 m/s) were experienced and over buoy 15, due to its more westerly position, wind speeds were 5-10 kts stronger throughout. These high winds were maintained until the low moved south into the southern Barents Sea and relaxed the pressure gradient, so that wind speeds decreased to below 15 kts near the buoy locations on 4-5 Feb. Throughout this synoptic event the buoys were much further than 200 nm from land and/or the ice-edge. Also the prevailing wind throughout tended to be SE/SW. Therefore the proximity to land effect did not change the SLD category from Table 2 in this synoptic event.

Based upon these meteorological synoptic charts, a corresponding series of charts showing the distribution of SLD categories throughout the Arctic basin were prepared (Appendix A, Figures 36 to 41). Using the SLD data as an input, the model predicts the omnidirectional value of AN at a particular receiver location. Displays of the horizontal directionality of the received AN for buoy 13 (at 50 Hz) are shown in Appendix A (Figures 42 to 47).

As previously stated, an in-depth analysis of the individual noise data sets is not undertaken but rather a comparison of predicted versus measured AN is the objective

of this research. These results are compared in the next section for each buoy, at three frequencies, 50, 100 and 500 Hz.

2. Results

A cross correlation coefficient was calculated between each predicted AN value and its associated measured AN value, over the length of the time series to assess the accuracy of the prediction. This value was normalized so that the correlation coefficient was between -1 and 1. The coefficient was calculated at zero time lag between the two sets of values and at other time lags to determine if a higher correlation coefficient could be achieved if a time lag were superimposed on the two sets of data.

During this research most effort was concentrated on the SLD calculation and model runs at 50 Hz because low frequencies are the most operationally relevant considering the submarine threat. This will be reflected in the discussion of results.

a. 50 Hz

The 50 Hz time series of measured ambient noise versus the 12 hourly ASNM predictions are shown for buoy 13 (Figure 10), buoy 15 (Figure 11) and buoy 19 (Figure 12). Table 3 gives the correlation coefficient for each time. All three buoys have correlation coefficients greater than 0.7, which indicates good correlation between the predicted and
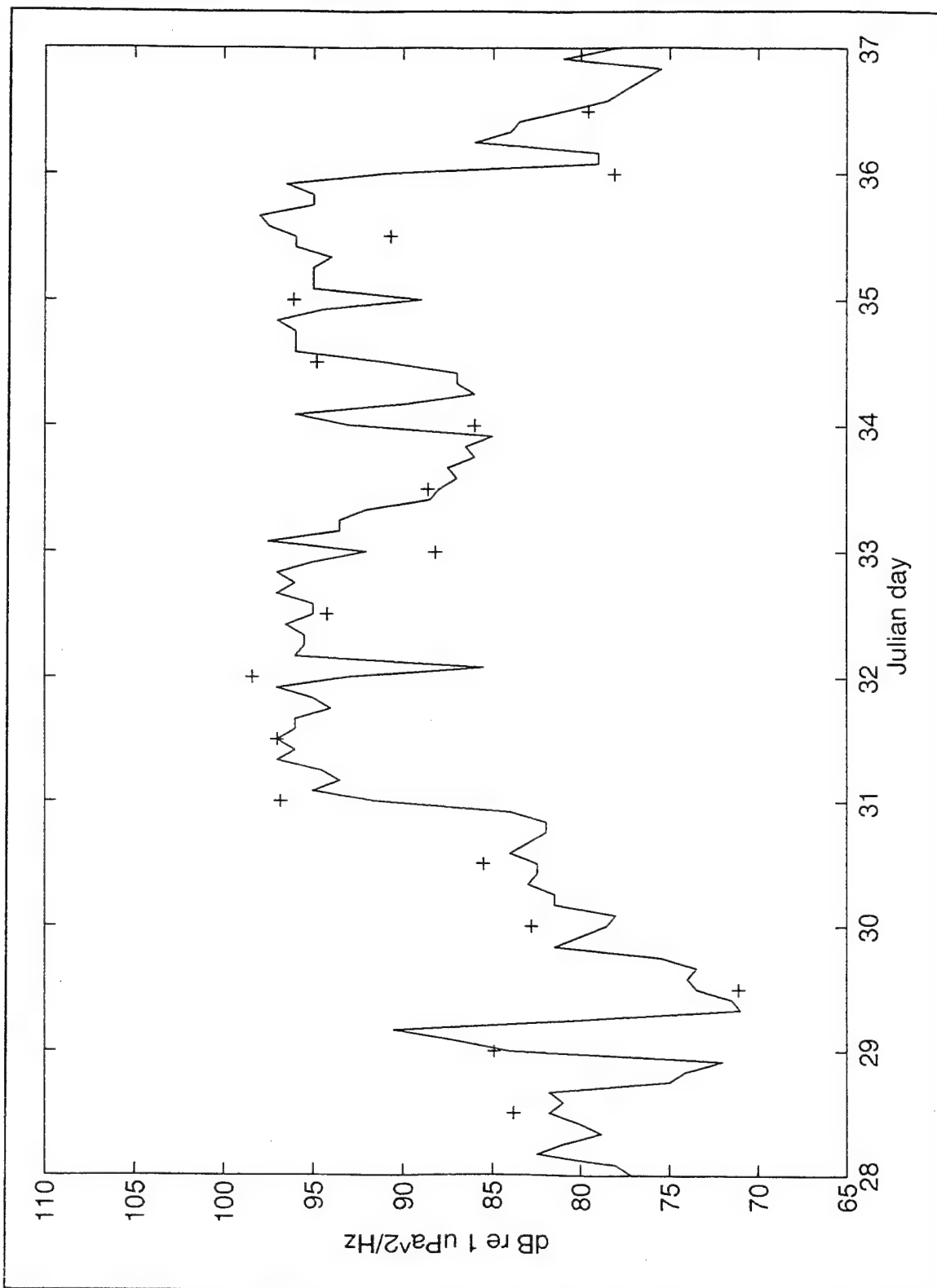
46

Figure 10   Time-series of measured AN levels (line) and ASNM
predictions (crosses) for buoy 13 at 50 Hz, event I
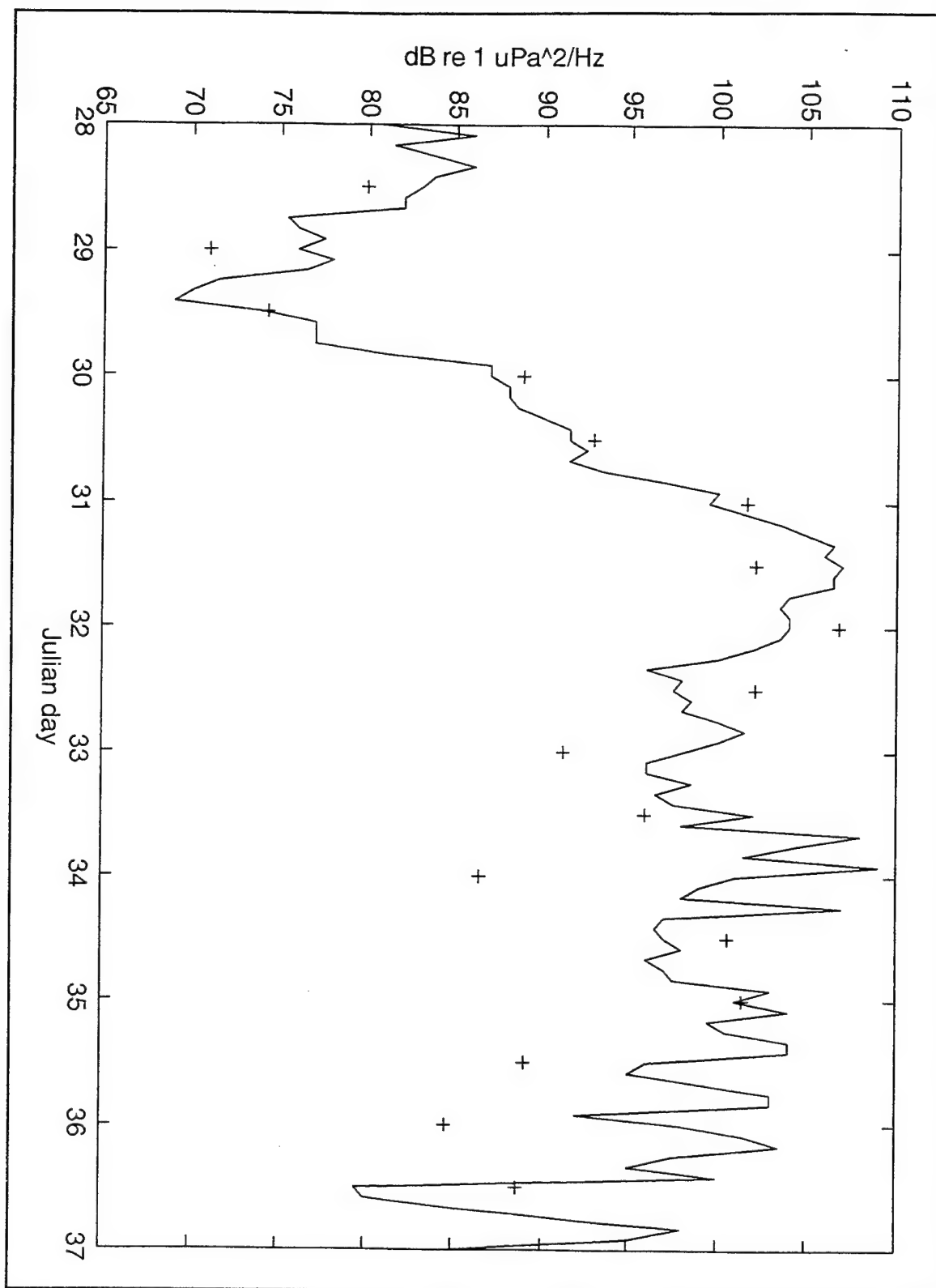
47

Figure 11   Time-series of measured AN levels (line) and ASNM predictions (crosses) for buoy 15 at 50 Hz, event I.
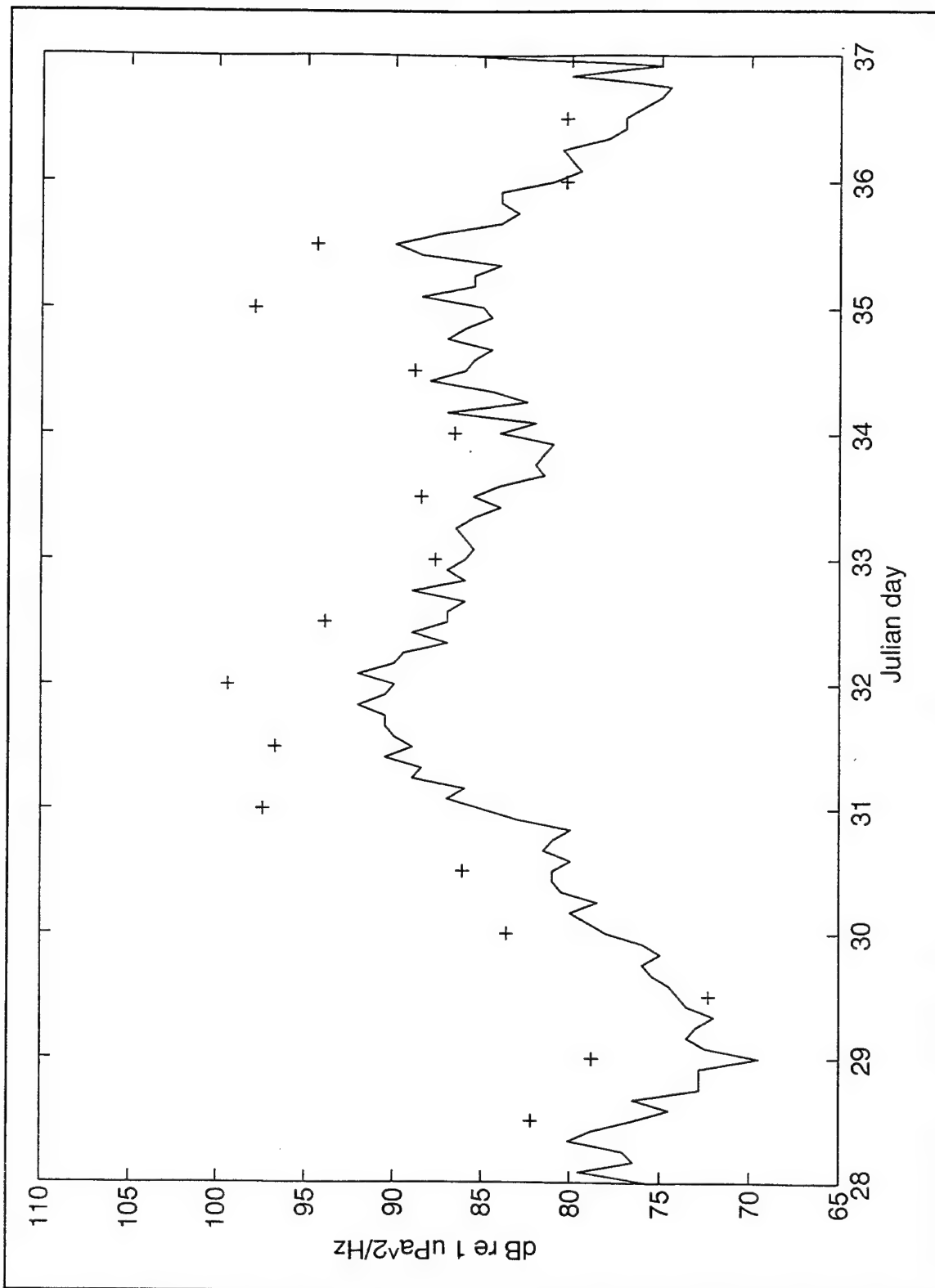
48

Figure 12 Time-series of measured AN levels (line) and ASNM predictions (crosses) for buoy 19 at 50 Hz, event I

49

Table 3. Cross correlation coefficients between predicted and measured levels of AN for 50 Hz, event I. Negative time lags indicate predicted levels lead the measured levels.

50 Hz	Cross	Correlation	Coefficient
Buoy	Zero lag	Max coeff	Lag (Hr)
13	0.754	0.81	-12
15	0.807	0.807	0
19	0.856	0.856	0

measured AN values at 50 Hz.

An important aspect in the development of the ASNM model is the ability to accurately predict those occasions when the AN field changes from quiet periods to loud periods due to strong wind forcing events. Therefore it is the rise in measured AN levels from the 5th percentile value on 29 Jan to peak values greater than the 95th percentile on 31 Jan which needs to be simulated accurately. Table 4 shows the increase in measured noise values from the lowest AN level before the synoptic event began to the first large peak in the noise level. These large increases (23-38 dB) occur over about a 48 hour period. They are compared to the model predicted values over the same (or as similar as possible) time period as the measured values. These values indicate that the predicted increase in AN is in good agreement with that measured at each of the individual buoys.

Table 4. Summary of noise level increases from both measured and predicted values at 50 Hz. Increases in both values are calculated from before the event began to the first large peak in the noise level (adapted from Feller,1994).

Buoys	Noise Increase (dB)	
	Measured	Predicted
13	26.9	26.0
15	38.3	35.8
19	23.4	27.1

A close examination of the measured AN time-series highlights the differences in absolute levels of AN between nearby receiver locations. Buoys 13 and 19 are approximately 60 nm apart, and both exceeded their 95th percentile levels during the storm event. However, while buoy 13 attains maximum values of 95-97 dB, buoy 19's maximum values are 88-90 dB. In terms of model prediction the two buoys are likely to have the same or similar predicted values. In Chapter III this discrepancy has been postulated to be due to the effect of localized pressure ridging. If an active pressure ridge were in the vicinity of buoy 13, it would increase the measured AN levels compared to buoy 19 which would have a more uniform distribution of pressure ridges.

The correlation coefficient for buoy 13 is 0.75. The increase in noise level from the start of the event to the peak value for both measured and predicted values are within 1 dB of each other. From Table 3 it is interesting to note that the maximum correlation for buoy 13 is 0.81 at a time

lag of -12 hours, or one wind speed data time interval. The time lag indicates that the predicted values lead the measured levels of AN by 12 hours. In this case the increase in the correlation coefficient is relatively small. However this provides an insight into the physical processes operating in the ice pack. The model predictions are based on the analyzed wind speeds at a particular synoptic time. There is likely to be a delay between the onset of increased winds, the process of pressure ridging and the generation of AN. Buoys 15 and 19 have maximum correlation coefficients at zero lags. Therefore for Storm 1, characterized by strong winds, at 50 Hz this delay does not seem to be highly significant. Parsons (1992) found a similar rapid response in the noise field due to the passage of a storm front; response times of 1-2 hours were typical.

Buoy 15 (Figure 11) experiences significantly higher levels of measured AN, frequently over 100 dB and peaks at 105-107 dB. Close analysis of the meteorological charts indicate a clear connection between the increased wind speeds which were in excess of 50 kts, experienced by this buoy, and the increased levels of measured AN. The 38.3 dB increase in noise level during the onset of the storm was well forecast by the model which predicted a 35.8 dB increase.

Buoy 19 (Figure 12) has the highest correlation coefficient although ASNM visually appears to over-predict

the noise levels. The trend of the predictions is closely correlated with the measured levels, although the predicted values are between 3-10 dB higher than the measured levels. The noise increase for buoy 19 (Table 4) shows that the model predicts an increase of 27 dB with a measured increase of 23.5 dB. It is hypothesized that the difference in the measured noise levels between buoys 13 and 19 is most likely due to differences in the local pressure ridging environment.

b. 100 Hz

The 100 Hz time-series of measured AN versus the 12 hourly ASNM predictions are shown for buoy 13 (Figure 13), buoy 15 (Figure 14) and buoy 19 (Figure 15). Table 5 gives the correlation coefficients for each time series comparison. The 100 Hz noise record exhibits similar characteristics as at 50 Hz for all three buoys. In terms of absolute values the 100 Hz levels are 4-8 dB less than the 50 Hz values which would be expected with the increase in frequency from 50 to 100 Hz, i.e., negative spectral slope.

Buoy 13 has a correlation coefficient of 0.455, although visually (Figure 13) the general comparison appears to be better. The three AN levels predicted near the end of the data set (Julian day 35 at 1200Z to Julian day 36 at 1200Z) are much lower than the measured AN levels. This large difference lowers the cross correlation coefficient at
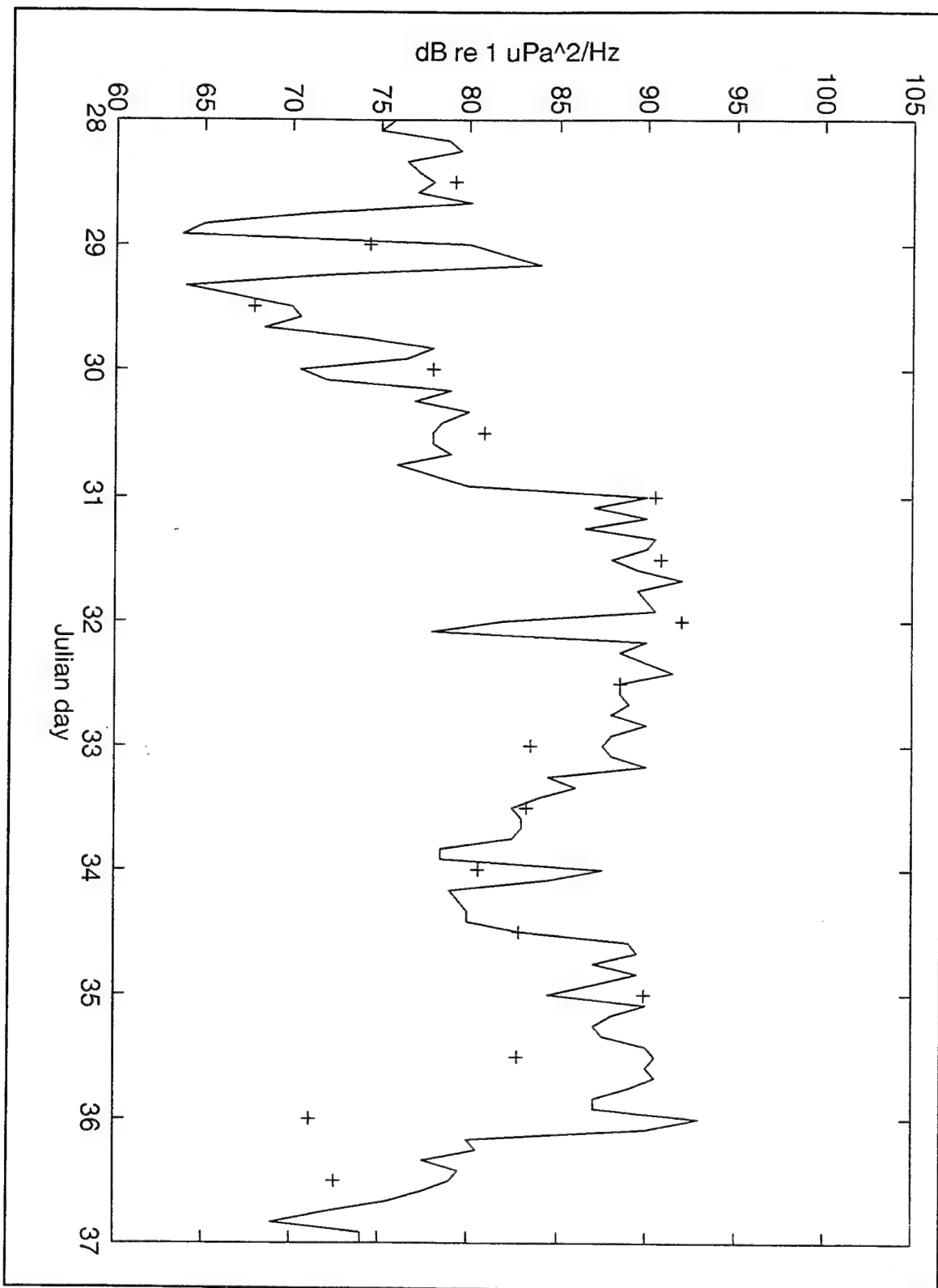
Figure 13   Time-series of measured AN levels (line) and ASNM predictions (crosses) for buoy 13 at 100 Hz, event I.
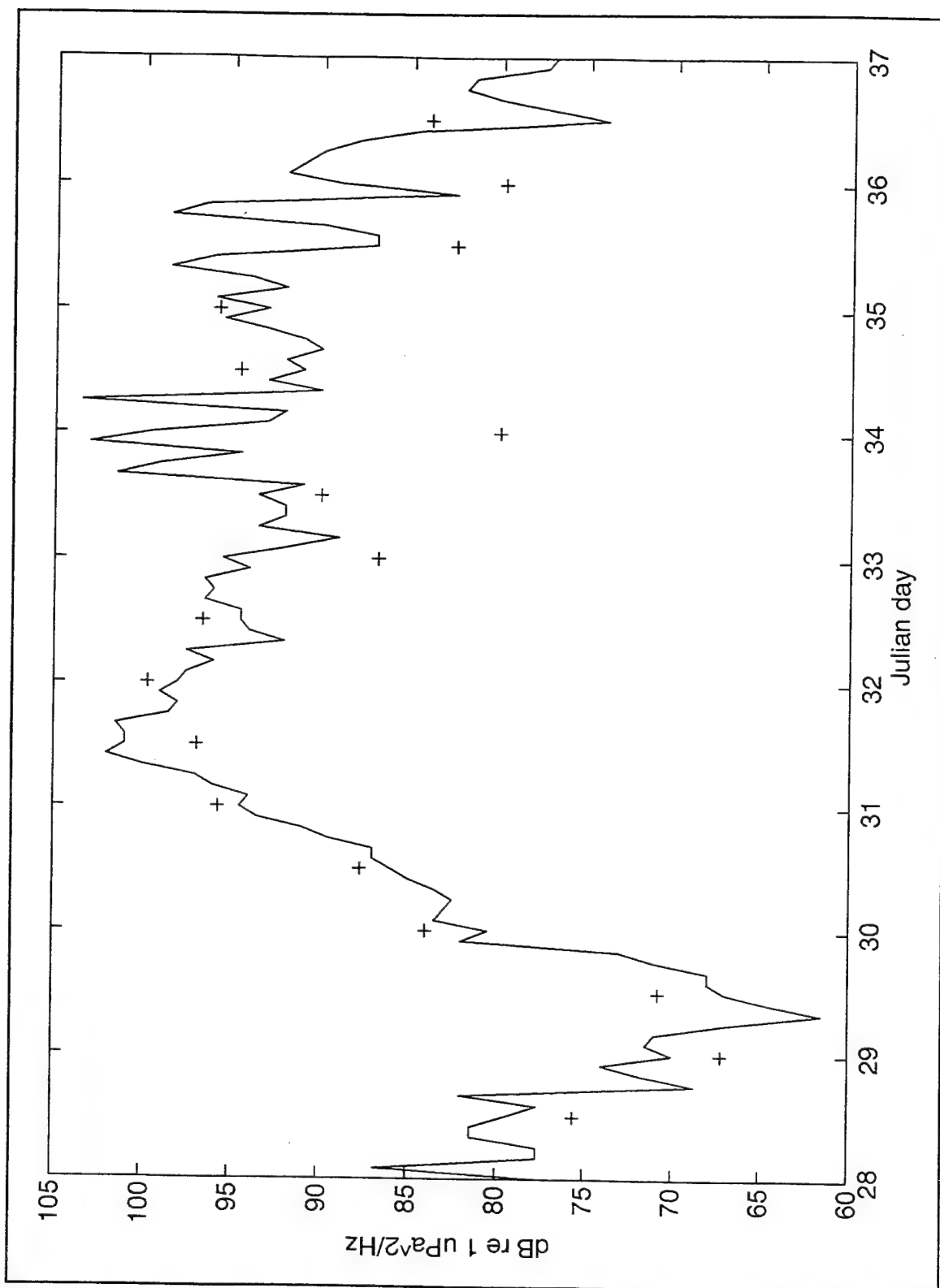
Figure 14   Time series of measured AN levels (line) and ASNM
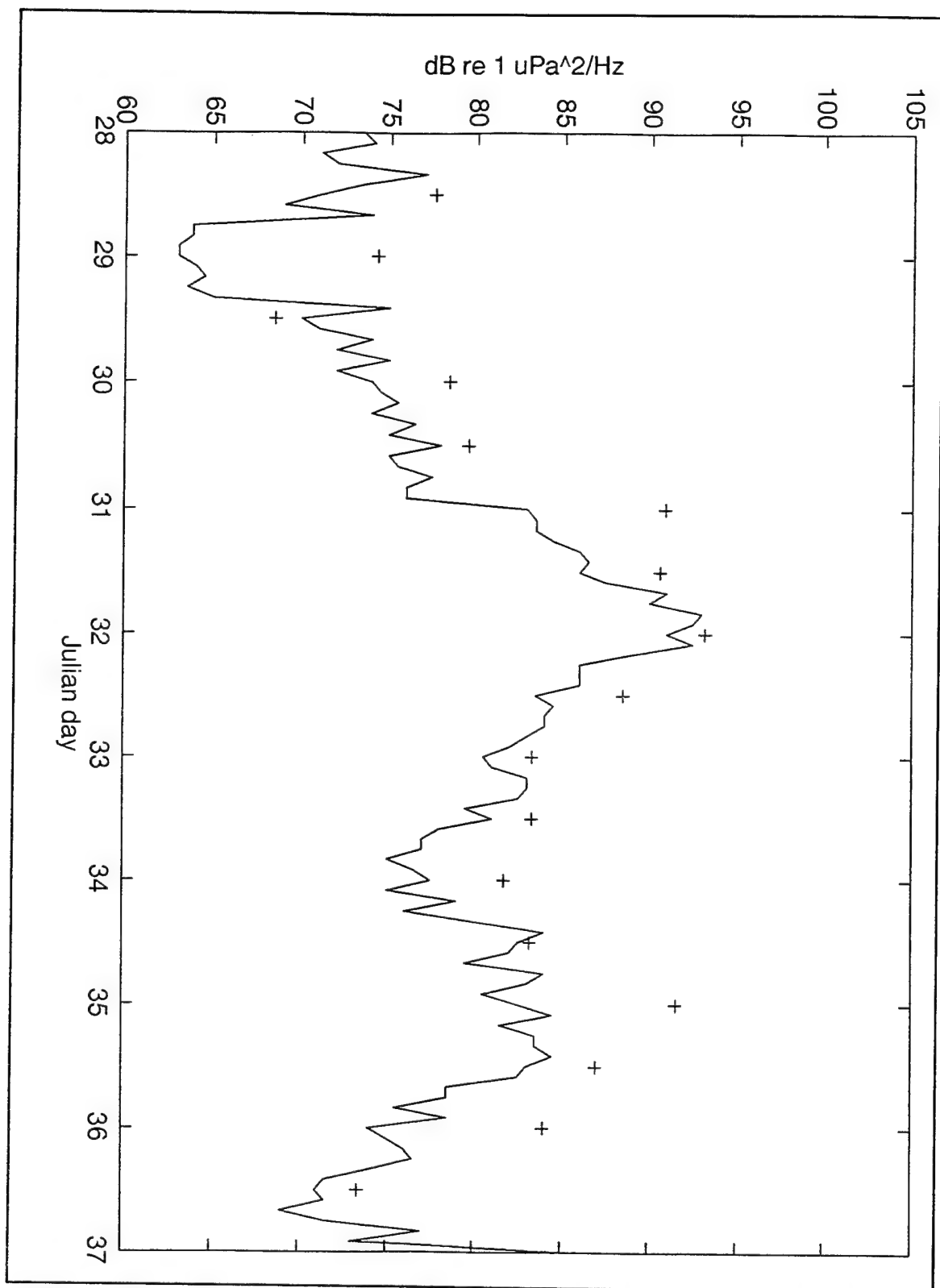predictions (crosses) for buoy 15 at 100 Hz, event I.

55

Figure 15   Time-series of measured AN levels (line) and ASNM
predictions (crosses) for buoy 19 at 100 Hz, event I.

Table 5. Cross correlation coefficients between predicted and measured levels of AN for 100 Hz for event I. Negative time lags indicate predicted values lead the measured levels.

100 Hz	Cross	Correlation	Coefficient
Buoy	(Zero lag)	Max coeff	Lag (Hr)
13	0.455	0.68	-12
15	0.772	0.79	-12
19	0.879	0.879	0

zero lag much more than is indicated visually. A shift of the ASNM predictions ahead 12 hours simply moves the low ASNM levels on Julian day 35 and 36 to be more in line with the low measured AN levels after 1200Z on Julian day 36. Physically the wind field analyses from NOGAPS were most likely in error (early) in predicting the AN level decrease on Julian day 35. A significantly higher correlation, 0.68, is obtained with a 12 hour time lag where the predicted values lead the measured levels. The noise level increases associated with the onset of the stronger winds associated with the storm event are shown in Table 6. For buoy 13, the measured noise level increased by 28 dB and the model predicted a rise of 24.1 dB.

Examining the 100 Hz time series (Figure 14) in more detail, for buoy 15, it can be seen that the peak noise values of 90-92 dB (Julian days 31 - 32) are well predicted by the model. The low AN value, of 64 dB, was experienced

57

Table 6. Summary of noise level increases from both measured and predicted values at 100 Hz. Increases in both values are calculated from before the event began to the first large peak in the noise level (adapted from Feller 1994).

Buoys	Noise Increase (dB)	
	Measured	Predicted
13	28.2	24.1
15	40.8	32.5
19	31.0	24.7

at 290800 (Julian day 29) prior to the onset of the stronger winds associated with the synoptic storm event. The lowest model prediction was 67.9 dB at 291200. Due to the temporal resolution of the meteorological data (12 hourly) some accuracy is lost and, as discussed in Chapter III, the data paucity in the Arctic also introduces inaccuracies which affect the model's predictions.

Buoy 15 has a correlation coefficient of 0.772. The maximum value calculated by the cross covariance, at -12 hour lag, results in a small increase to 0.79. The increase in noise level at buoy 15 is 40.8 dB (Table 6), the largest increase over the 48 hour time period by any buoy. The model predicted a 32.5 dB increase.

Buoy 19 has a high correlation coefficient of 0.879. The measured noise increase of 31 dB is compared to a predicted increase of 24.7 dB. The underpredicted noise levels for buoys 15 and 19 (7-8 dB too low) probably reflect

58

a noise prediction based on mean wind speeds over the synoptic period (12 hrs) compared to an instantaneous AN value measured by the drifting buoy.

c.   500 Hz

The 500 Hz time-series of measured ambient noise versus the 12 hourly ASNM predictions are shown for buoy 13 (Figure 16), buoy 15 (Figure 17) and buoy 19 (Figure 18). Table 7 gives the correlation coefficients for each time series comparison.

At 500 Hz the impact of the storm is less well defined than at either 50 Hz or 100 Hz. Due to the higher transmission loss at 500 Hz the noise field is likely to be dominated by noise sources close to the receiver. Therefore, as opposed to 50 Hz and 100 Hz where the omnidirectional AN is a sum of both local and distant noise sources, at 500 Hz only local noise sources will influence the noise field. Any wind generated pressure ridging in the near field would dominate the noise record. Therefore, at 500 Hz the influence of active pressure ridging activity in the near-field is even more influential than at 50 or 100 Hz.

Examining buoy 13's time-series (Figure 16) it is more difficult to identify the storm event related increase and decrease in AN. The correlation coefficient (0.236) is poor (Table 7) but increases to 0.44 at a 12 hour lag. As before, a few predicted AN levels are much lower than the measured
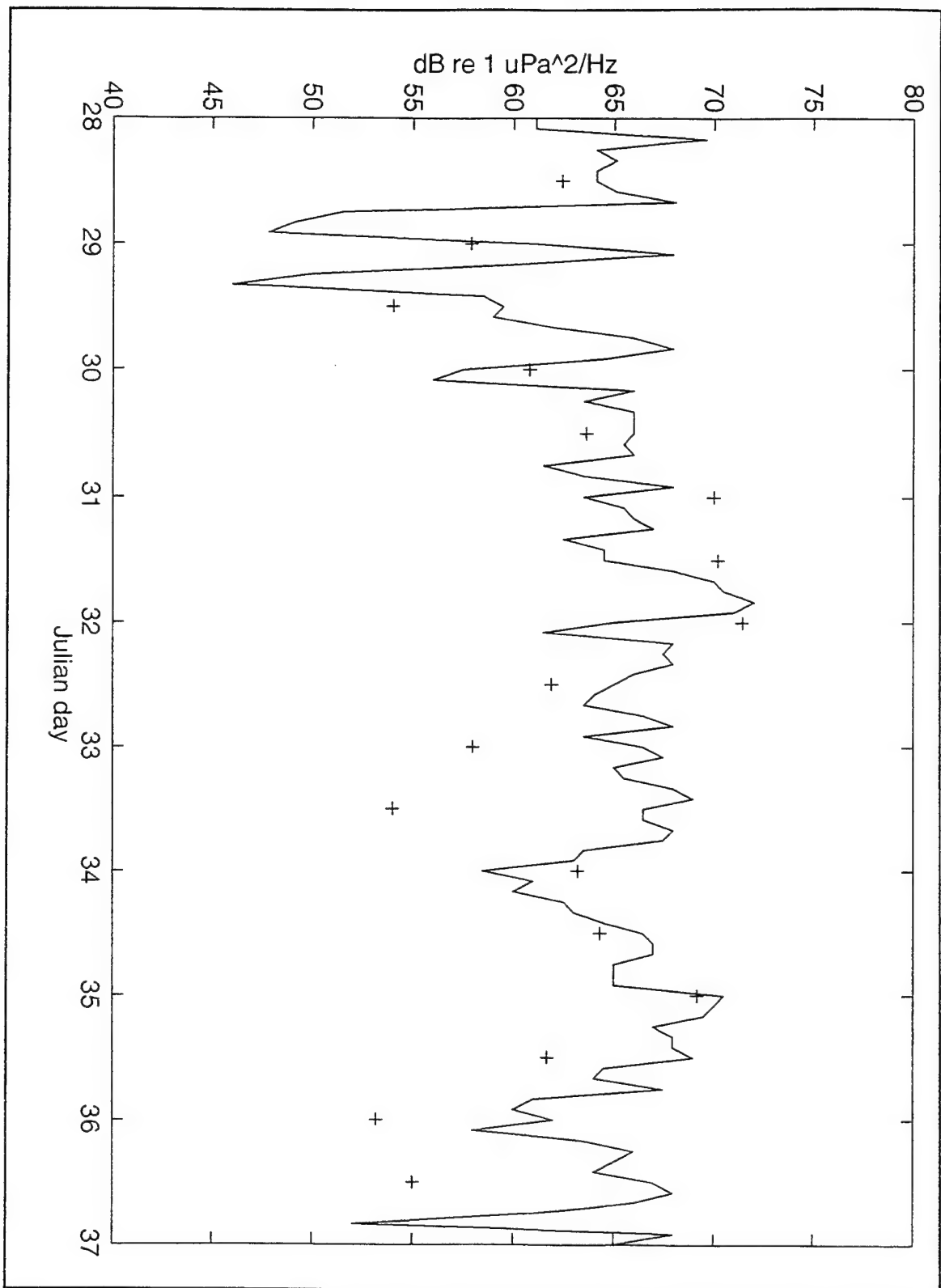
Figure 16   Time-series of measured AN levels (line) and ASNM predictions (crosses) for buoy 13 at 500 Hz, event I.
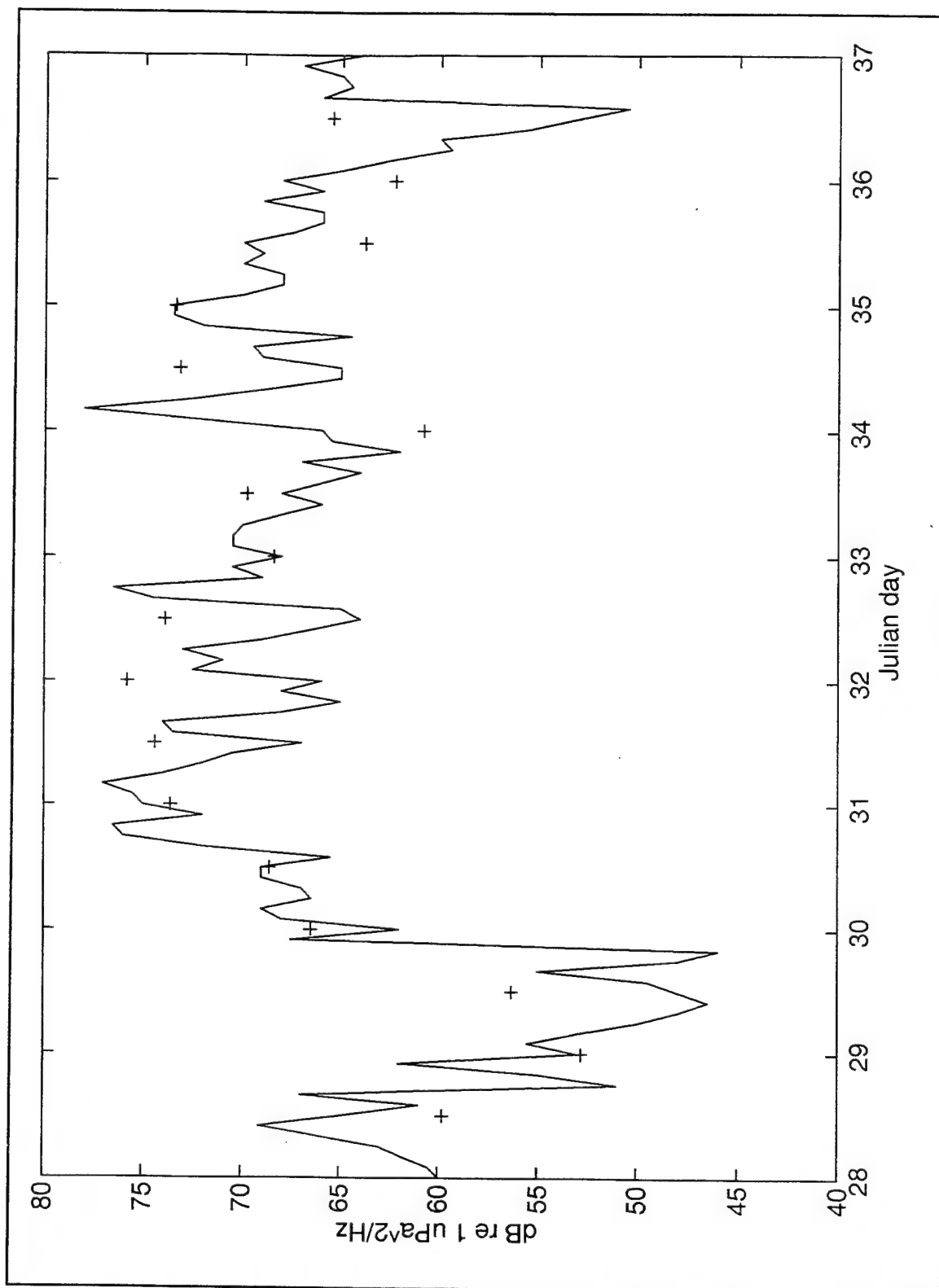
Figure 17   Time-series of measured AN levels (line) and ASNM predictions for buoy 15 at 500 Hz, event I.
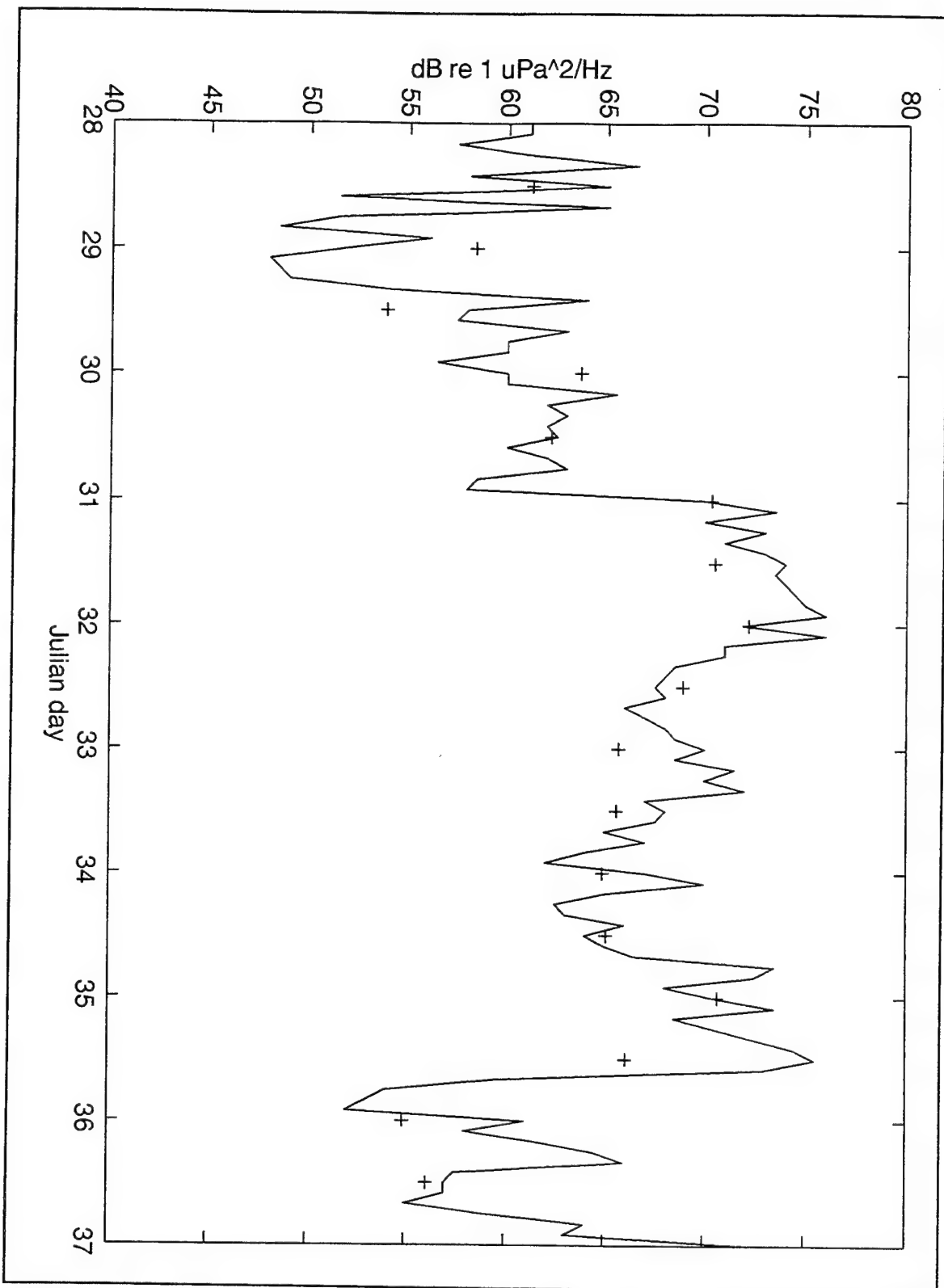
61

Figure 18   Time-series of measured AN levels (line) and ASNM
predictions (crosses) for buoy 19 at 500 Hz, event I.

Table 7. Cross correlation coefficients between predicted and measured levels of AN for 500 Hz, event I. Negative time lags indicate predicted values lead the measured levels.

500 Hz	Cross	Correlation	Coefficient
Buoy	(Zero lag)	Max coeff	Lag (Hr)
13	0.236	0.44	-12
15	0.618	0.68	-12
19	0.847	0.847	0

AN data, hence lowering the cross correlation coefficient. The increase in measured noise level, 26 dB, is the smallest experienced and the model predicts a 17.4 dB rise (Table 8). This is to be expected because the dynamic range of the noise field decreases with increasing frequency.

Buoy 15 (Figure 17) shows a much more identifiable trend with a significant increase of 31 dB and a predicted rise of 23 dB. The noise level exhibits a two step increase from 45-50 dB on 29 Jan to 65-70 dB on 30 Jan to its highest level, 73-77 dB on 31 Jan. These step increases are well predicted by the model. Buoy 15, due to its closer proximity to the area of tightened pressure gradient/higher wind speeds displays the largest values of peak AN. These very high AN levels for buoy 15 have a significant distant as well as local contribution.

Buoy 19 also shows a two-step increase in its noise record from 29 to 31 Jan which is accurately predicted. The

Table 8. Summary of noise level increases from both measured and predicted values at 500 Hz. Increases in both values are calculated from before the event began to the first large peak in the noise level.

Buoys	Noise Increase (dB)	
	Measured	Predicted
13	26.0	17.4
15	31.0	23.0
19	28.0	18.3

overall measured increase in the noise record is 28.1 dB with a predicted value of 18.3 dB (Table 8). The correlation coefficient is 0.847 (Table 7).

3.   Summary

The ASNM predicted values compared favourably with the measured levels of AN, with 66% of the correlation coefficients greater than 0.75. Significantly, the increase in noise levels from before the start of the synoptic event to the first peak in the noise record (normally 48 hours later) has been well predicted by the model. Therefore, on this evidence, the model accurately predicts the large increases in AN.

The differences between the time-series of buoy 13 and 19, at all frequencies, are significant. As previously discussed, despite the close proximity of both receiver locations, changes in the AN time-series differ significantly. A possible explanation is that buoy 13 is

64

closer to an active pressure ridge, hence recording a higher noise level. Alternatively, buoy 19 may have a lack of pressure ridges in its close vicinity and, therefore, displays a relatively quieter noise record. Further research is necessary to determine which level of AN would more accurately represent the contribution of active pressure ridging to the total noise field. Also necessary would be an accurate method of mapping active pressure ridges in the Arctic ice, either by high resolution remote sensing techniques or by acoustic mobile arrays beneath the ice cap.

At 500 Hz the correlation coefficients are less than those at 50 and 100 Hz. This is to be expected as, at 500 Hz, the noise field is dominated by the local wind and, therefore, dominated by events in the near field. The model is geared more to the lower frequencies where a summation of close and distant noise generating events produce the omnidirectional noise field.

Buoy 13's statistical analysis identified a possible trend where higher maximum correlation coefficients were obtained for a 12 hour lag between the time-series data. The predicted values lead the measured levels of AN. This should not be entirely unexpected. Feller (1994) and Fritsch (1995) clearly identify a lag time associated with the relationship between the noise field and local wind speed. Feller (1994) concludes from his analysis that the negative time lag indicates that peak winds occur 7-10 hours before the

corresponding noise peaks. This time difference is due to the time taken by the ice to react to the changing environmental forcing (changes in wind speed).

The resolution of the meteorological data is a constraint. As the data is 12 hourly, identification of time lags less than 12 hours are unresolvable. Meteorological data of shorter temporal resolution would probably result in the identification of a shorter time lag which produces the highest correlation between the data sets.

In conclusion, at the higher wind speeds associated with synoptic event I, there is generally good correlation between the predicted and measured levels of AN. The highest correlations are obtained for zero time lag between the environmental forcing and noise generation.

B.   SYNOPTIC EVENT II

1.   Overview

The second event examined was the passage of a summertime storm from 25 Aug 1992 (Julian day 238) to 30 Aug 1992 (Julian day 243). During this period the noise field varied from extremely quiet (5th percentile levels) at the start of the period (mainly 26 Aug) to very loud (95th percentile levels) during 27 to 29 Aug. These percentiles were calculated by Feller (1994) and were based on the seasonal record lengths for summer (May to Sep). The winter

5th and 95th percentile values are significantly much higher than the summer values. This is because most of the significant storms affecting the Arctic Ocean are in winter and therefore higher 95th percentile values are observed. The wind speeds of Event I ranged between 40-60 kts, while those of event II were between 15-30 kts. These lower wind speeds were strong enough to generate noise levels which periodically exceeded the summer 95% threshold. Therefore, despite the difference in wind speeds between these two events, both were strong enough to produce noise levels great enough to exceed their seasonal threshold levels. However the AN levels for the summer storm examined in this section should be less accurately predicted by ASNM because of the anisotropic nature of local ice ridging spatial distributions associated with moderate storms.

The location of the buoys during this time period was in the central/southern European basin (water depth > 3000 m). Buoys 13 and 19 were approximately 140-180 nm N-NW of Sveryna Zemlya. Buoy 19 was 130-150 nm north of Franz Josef Land.

The meteorological charts for the synoptic periods which resulted in significant changes in wind speed conditions are shown in Appendix B (Figures 48 to 51). The general progression of the synoptic features and associated wind speeds can be ascertained by examination of these charts. At the start of the period, 25 Aug, a weak low

67

(1002 mb) over the New Siberian Islands in the Laptev Sea produced a relatively weak pressure gradient over the buoys and the Arctic Ocean in general. By 27 Aug a deep low (994 mb) developed in the Beaufort Sea and a high (1030 mb) intensified over northern Greenland. This tightened the pressure gradient over the central Arctic and the vicinity of the buoys producing wind speeds of between 20-30 knots. This tighter pressure gradient was maintained as the low tracked NW across the central Arctic. It later tracked into the Laptev Sea such that by 29 Aug the pressure gradient had relaxed in the vicinity of the buoys and the wind speeds were reduced.

The wind direction for this storm was generally from the North (from between NE and NW). At times the buoys were within 200 nm of land. Hence the noise levels appropriately increased during periods of onshore winds (135 degrees to 235 degrees T).

Based upon these meteorological synoptic charts, the corresponding series of SLD distribution charts throughout the Arctic basin for significant synoptic hours (Figures 52 to 55) and the associated directional noise level plots (Figures 56 to 59) were developed and are in Appendix B.

2. Results

a. 50 Hz

The 50 Hz time series of measured ambient noise levels versus the 12 hourly model predictions are shown for buoy 13 (Figure 19), buoy 15 (Figure 20) and buoy 19 (Figure 21). Table 9 gives the correlation coefficients for each of the time series comparisons. As can be seen from the low correlations, the ASNM does not estimate AN levels for moderate (non-extreme) storm events very well, a feature due to the anisotropic distribution of active pressure ridges.

Buoy 15 has the highest correlation coefficient, at 0.462. All three buoys exhibit higher maximum correlation coefficients at 12 hour lags, particularly buoys 13 and 15.

During this period buoys 13 and 19 were within 40-60 nm of each other. Therefore, one may expect a similar noise record at both receiver locations, if the ice stress were spatially homogeneous. On examination of the two noise records, even larger differences are clearly evident than the differences observed between the two buoys during synoptic event I. Peak values during the period of highest winds at buoy 19 are 83-85 dB whilst levels of 91-94 dB are measured at buoy 13. Buoy 13's values are similar to values experienced during the winter storm in synoptic event I. These differences in AN levels and variations are typical of other AN data analyzed over the past decade and point to an
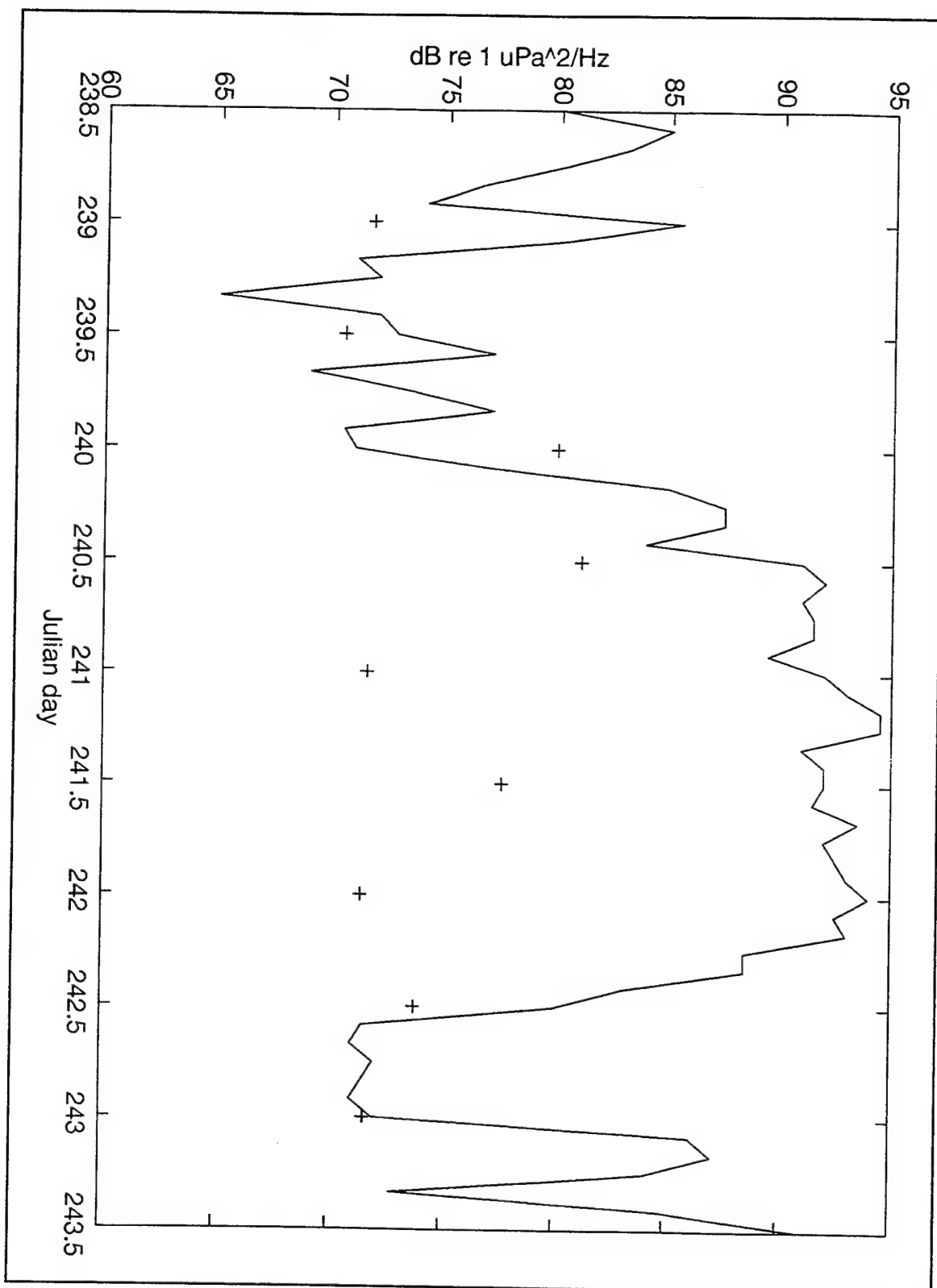
Figure 19   Time-series of measured AN levels (line) and ASNM predictions (crosses) for buoy 13 at 50 Hz, event II.
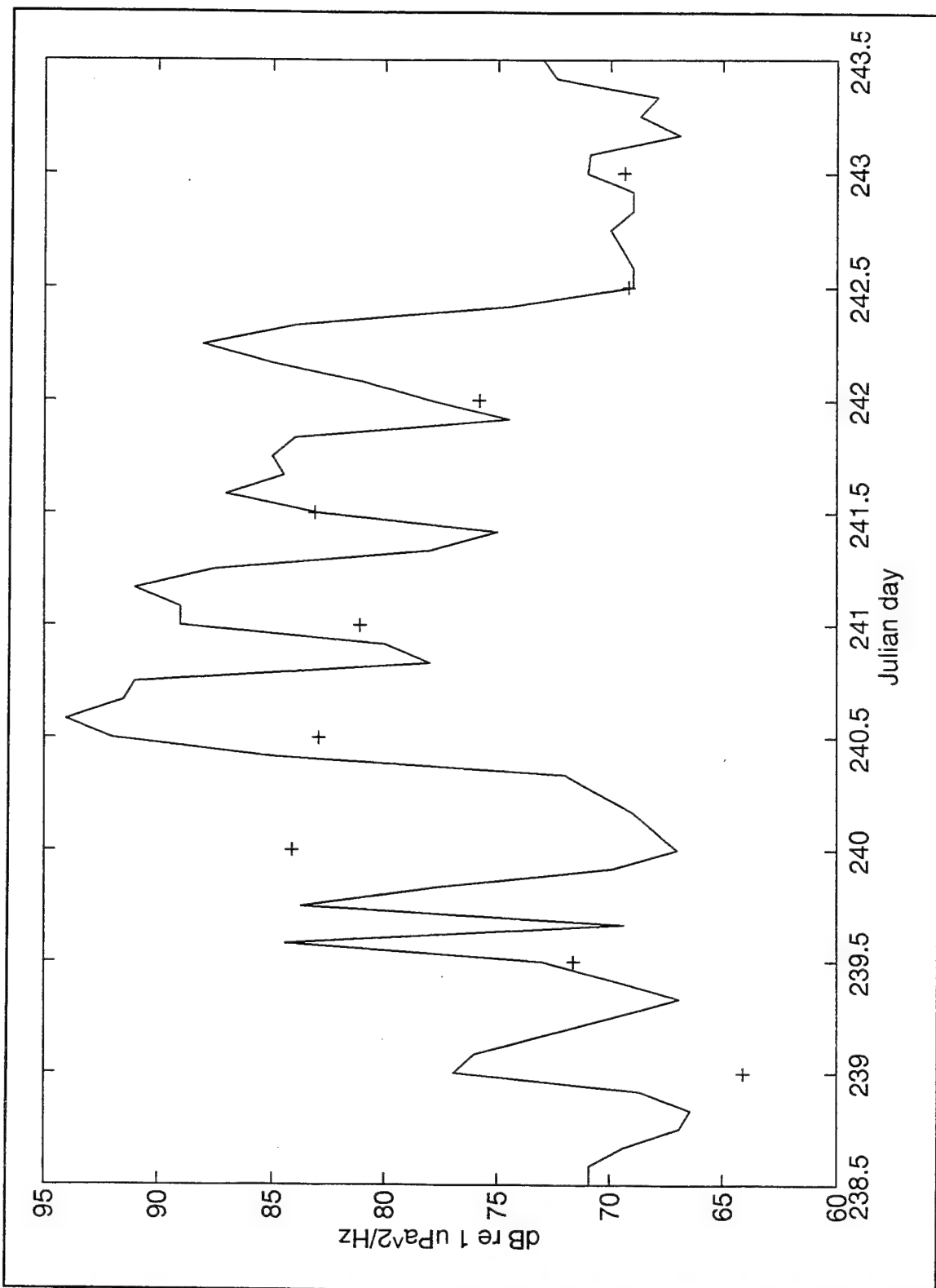
Figure 20   Time-series of measured AN levels (line) and ASNM predictions (crosses) for buoy 15 at 50 Hz, event II.
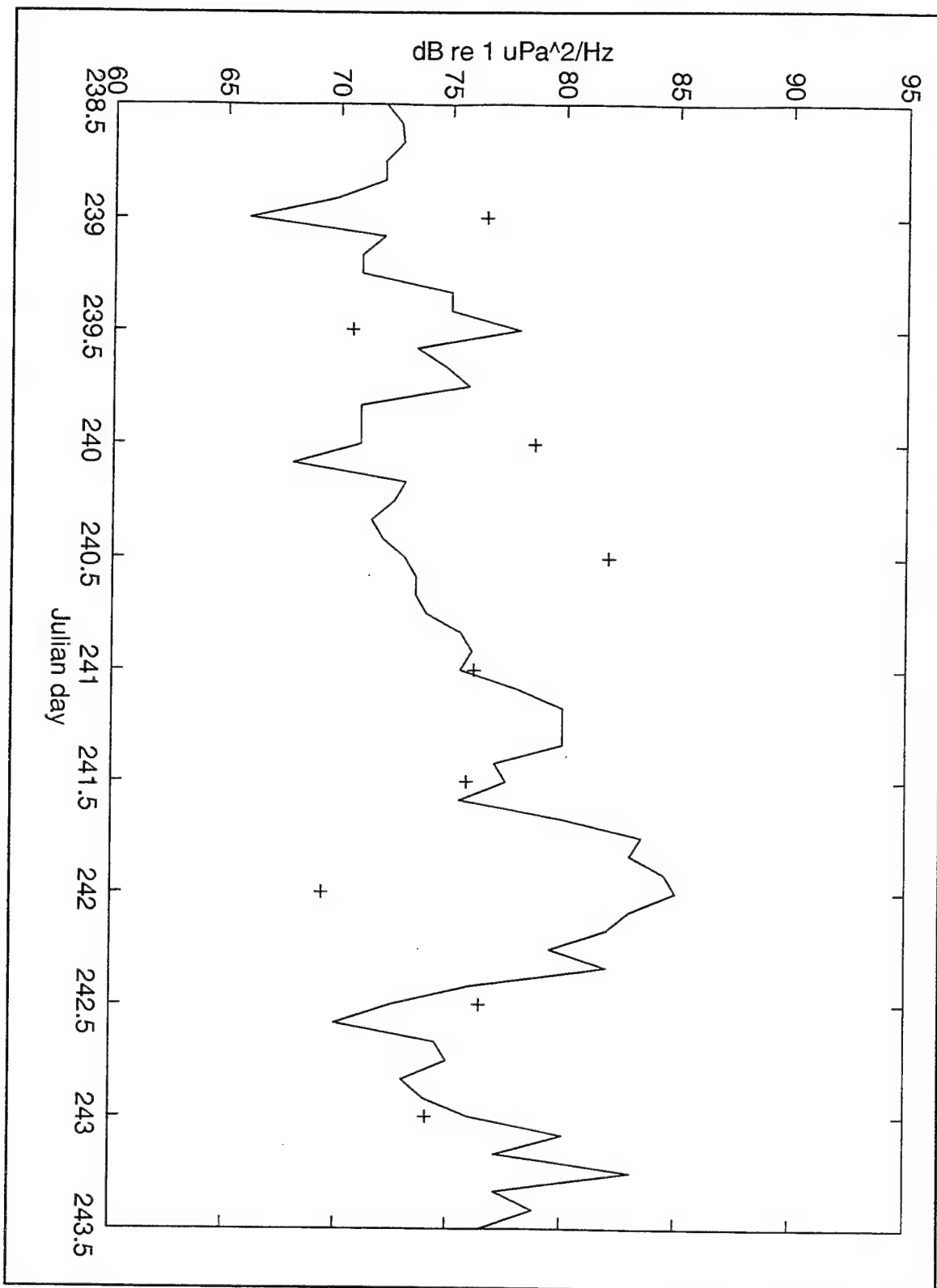
Figure 21 Time-series of measured AN levels (line) and ASNM predictions (crosses) for buoy 19 at 50 Hz, event II.

Table 9. Cross correlation coefficients between predicted and measured levels of AN for 50 Hz, event II. Negative time lags indicate predicted values lead the measured levels.

50 Hz	Cross	Correlation	Coefficient
Buoy	(Zero lag)	Max coeff	Lag (Hr)
13	0.073	0.65	-12
15	0.462	0.71	-12
19	-0.696	0.24	-12

anisotropic noise mechanism, such as randomly spaced active pressure ridging, dominating Arctic AN.

The locations of buoy 13 and 19 with respect to nearby land and the ice-edge reveal a possible explanation for this difference. The ice edge at this time (26 Aug) had retreated northwards and become more broken in nature (NPOC, 1992). Buoys 13 and 19 were to the north of the central Kara Plateau where areas of broken ice were present. An area of 6-8 tenths ice cover and a smaller area of 2-4 tenths existed to the west of the island of Ostrov Ushakova. Buoy 13's position was approximately 140 nm to the north of this area while buoy 19 was 40 nm farther north. This could account, in part, for the increase in the measured noise record at buoy 13 but clearly other factors are involved in the 6 dB difference in noise levels between these two buoys.

Buoy 13's correlation coefficient was low, 0.073. The correlation (Figure 19) can visually be seen to be deficient in forecasting the increase in AN and sustained peak values

73

after 27 Aug. From Table 10 it can be seen that the measured rise in AN during 27 Aug was 22.8 dB compared to only 10.6 dB forecast by the model. The correlation increased significantly to 0.65 when a lag of 12 hours was applied (Table 9).

The correlation coefficient for buoy 15 was 0.462, the highest for 50 Hz. This buoy also predicts the rise in AN more accurately, i.e., 24.8 dB compared to 20 dB forecast by the model. In this case the model forecast increase has been taken from midnight 26 Aug (Julian day 239) to midnight

Table 10. Summary of noise level increases from both measured and predicted values at 50 Hz. Increases in both values are calculated from before the event began to the first large peak in the noise level.

Buoys	Noise Increase (dB)	
	Measured	Predicted
13	22.8	10.6
15	24.8	20.0
19	12.0	11.4

27 Aug (Julian day 240) and is clearly 12-24 hours before the measured NL increase. A 12 hour lag between the data sets results in a maximum correlation coefficient of 0.71. Buoy 15 exhibits a series of large oscillations after midday on 27 Aug as opposed to most buoy frequencies which exhibit a peak plateau of higher AN during the stronger wind

periods. Feller (1994) discussed the possible cause of this periodicity, identifying tidal or inertial forcing. Both were discounted and the fluctuations remained unexplained.

Buoy 19 has a negative correlation coefficient of -0.696. Feller (1994) notes that this time-series is different in character than that for buoys 13 and 15 in that the increase in noise level associated with the onset of the stronger winds was a slow but steady rise in noise level extending over two days. The low correlation in the case of buoy 19 is due to the ASNM predictions and measured levels cycling from low to high levels out of phase (hence the strong negative correlation at zero lag). Due to this unexplained response in noise level associated with this time-series the model predictions lead the NL by 18-24 hours. This explains, to some degree, the negative correlation of this time-series. The rise in measured NL of this buoy is 12 dB over the 24 hour period of increasing winds from early on 27 Aug and the predicted level is 11 dB. The previously discussed time delay in the increase must be considered for the comparison.

b. 100 Hz

The 100 Hz time series of measured ambient noise versus the 12 hourly model predictions are shown for buoy 13 (Figure 22), buoy 15 (Figure 23) and buoy 19 (Figure 24). The 100 Hz noise records are very similar to their

respective 50 Hz noise records at all three frequencies.
Their correlation coefficients are shown in Table 11.

A detailed analysis of the measured and predicted noise
fields at this frequency is omitted because of the close
similarity of the results obtained at 50 Hz.

Table 11. Cross correlation coefficients between predicted
and measured levels of AN at 100 Hz, event II. Negative time
lags indicate predicted values lead the measured levels.

100 Hz	Coeff	Cross	Correlation
Buoy	(Zero lag)	Max coeff	Lag (Hr)
13	-0.18	0.59	-12
15	0.379	0.56	-12
19	-0.028	0.11	-12

Table 12. Summary of noise level increases from both
measured AN levels and predicted values at 100 Hz. Increases
in both values are calculated from before the event began to
the first large peak in the noise level.

Buoys	Noise Increase (dB)	
	Measured	Predicted
13	24.0	13.7
15	24.5	18.2
19	11.5	7.4
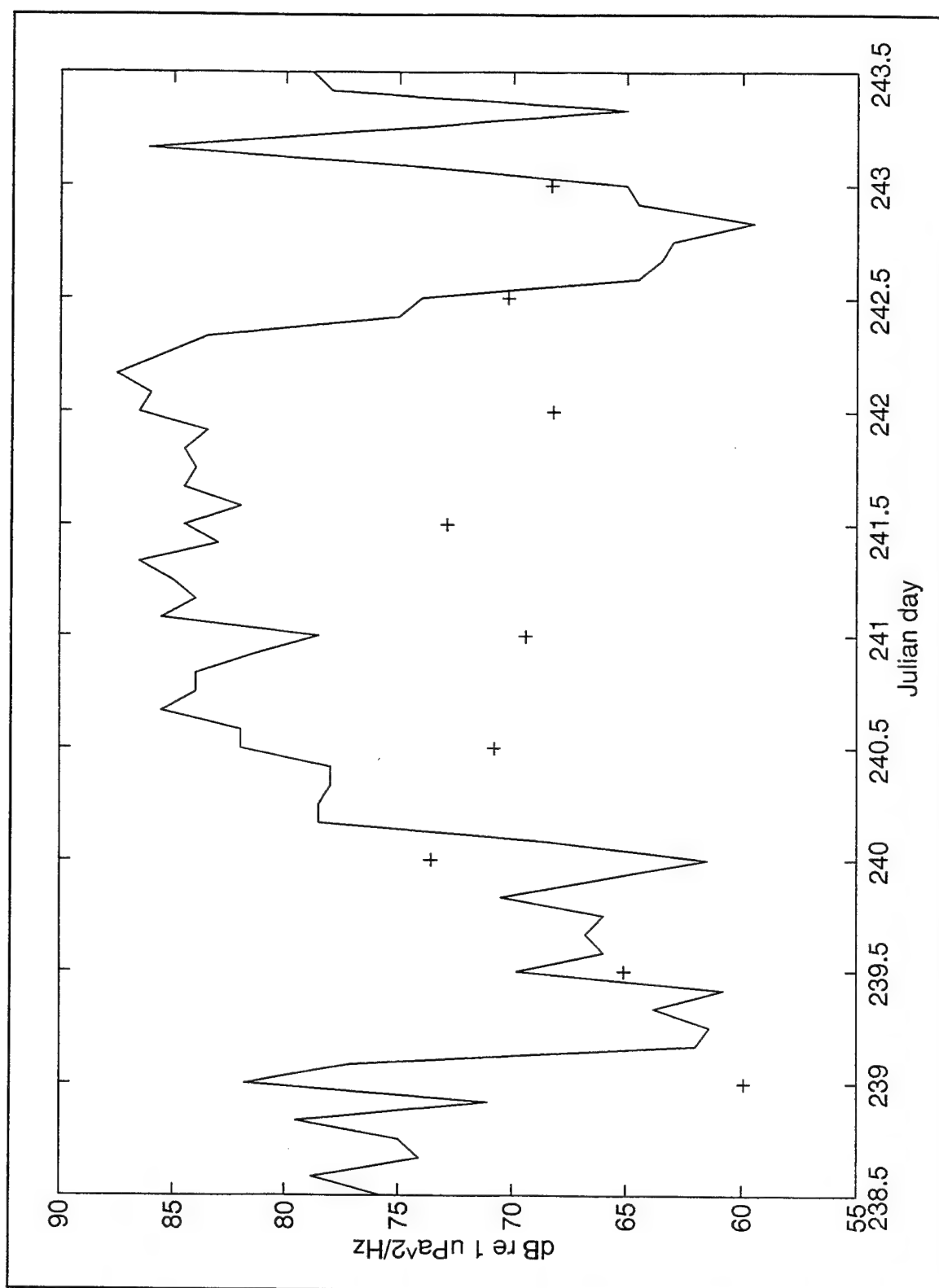
Figure 22   Time-series of measured AN levels (line) and ASNM
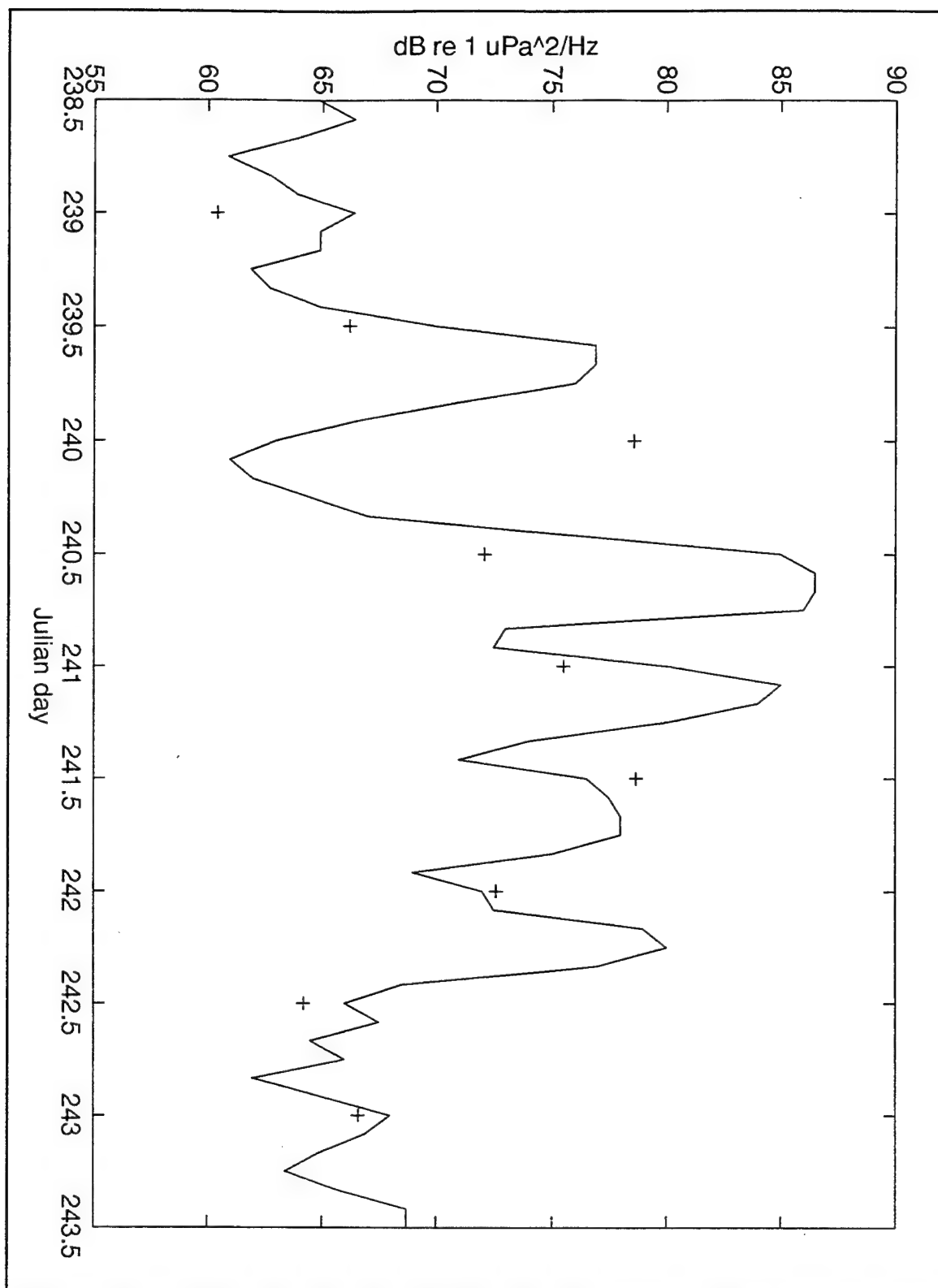predictions (crosses) for buoy 13 at 100 Hz, event II.

77

Figure 23   Time-series of measured AN levels (line) and ASNM
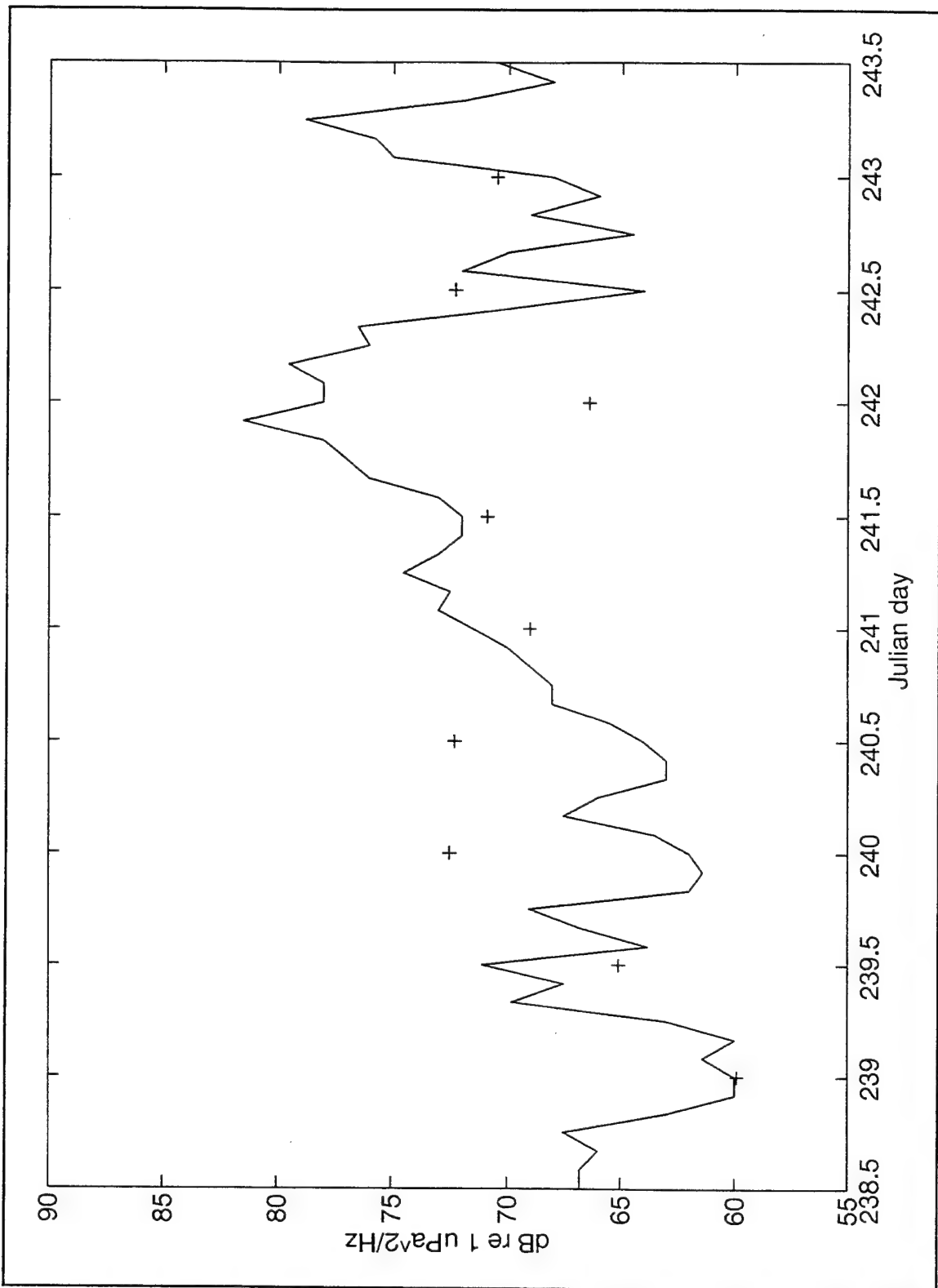predictions (crosses) for buoy 15 at 100 Hz, event II.

78

Figure 24 Time-series of measured AN levels (line) and ASNM
predictions (crosses) for buoy 19 at 100 Hz, event II

c.   500 Hz

The 500 Hz time series of measured ambient noise versus the 12 hourly model predictions are shown for buoy 13 (Figure 25), buoy 15 (Figure 26) and buoy 19 (Figure 27). The 500 Hz noise record, as previously discussed for event I, bears little similarity to the 50 and 100 Hz levels, as the 500 Hz record is dominated by local wind and ice/ice interactions. Table 13 shows the cross correlation coefficients for the 500 Hz times series.

Buoy 13 exhibits a relatively good correlation coefficient of 0.5 and quite accurately predicts the rise in measured noise level (Table 14). Likewise buoy 15 has a correlation coefficient of 0.53. The measured NL increase for buoy 15 is 9.5 dB during the 27 Aug. The model predicts an increase of 11.9 dB, although over a time period 12 hours earlier.

The correlation coefficient of buoy 19 is low, -0.025 and the predicted AN level increase of 4.3 dB does not compare well to the 10 dB measured AN level increase. Significantly for buoys 13 and 15 the correlation coefficients at zero lag (0.5 and 0.53, respectively) are much higher than those at -12 hour lag (0.45 and 0.14, respectively).

Overall at 500 Hz the comparison of measured versus predictions is reasonable. Therefore, for event II, where
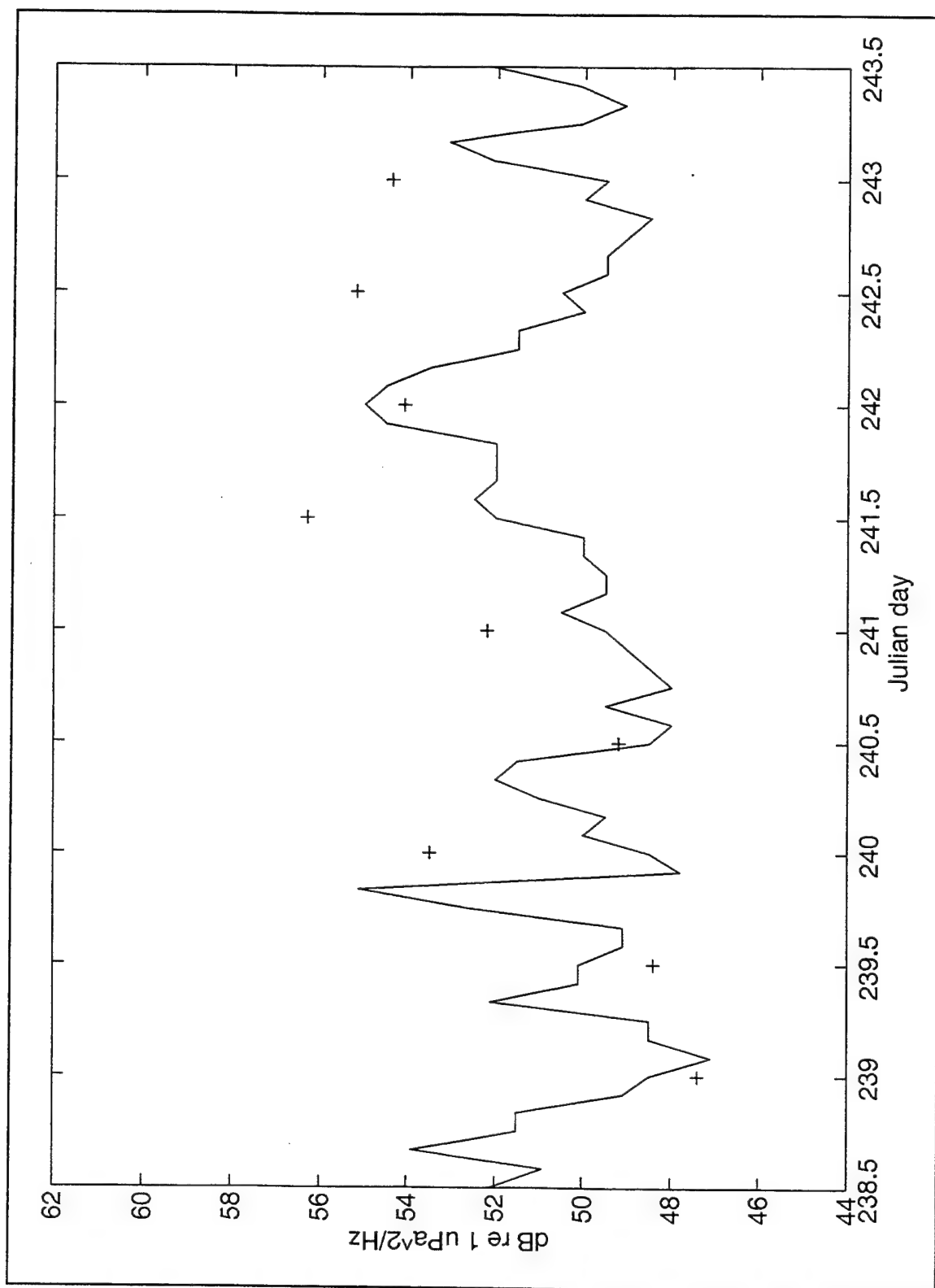
80

Figure 25   Time-series of measure AN levels (lines) and ASNM
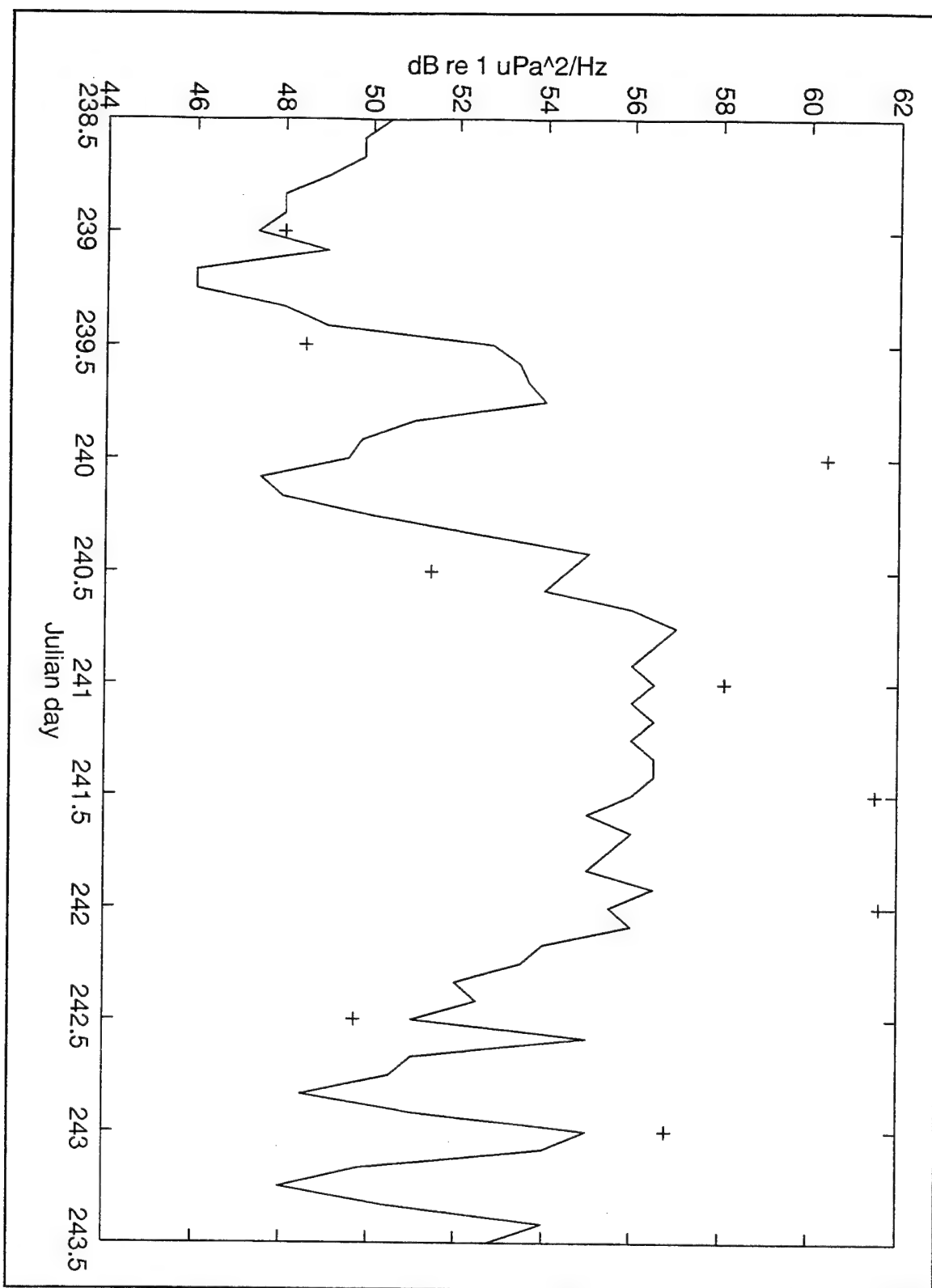predictions (crosses) for buoy 13 at 500 Hz, event II.

81

Figure 26   Time-series of measured AN levels (line) and ASNM
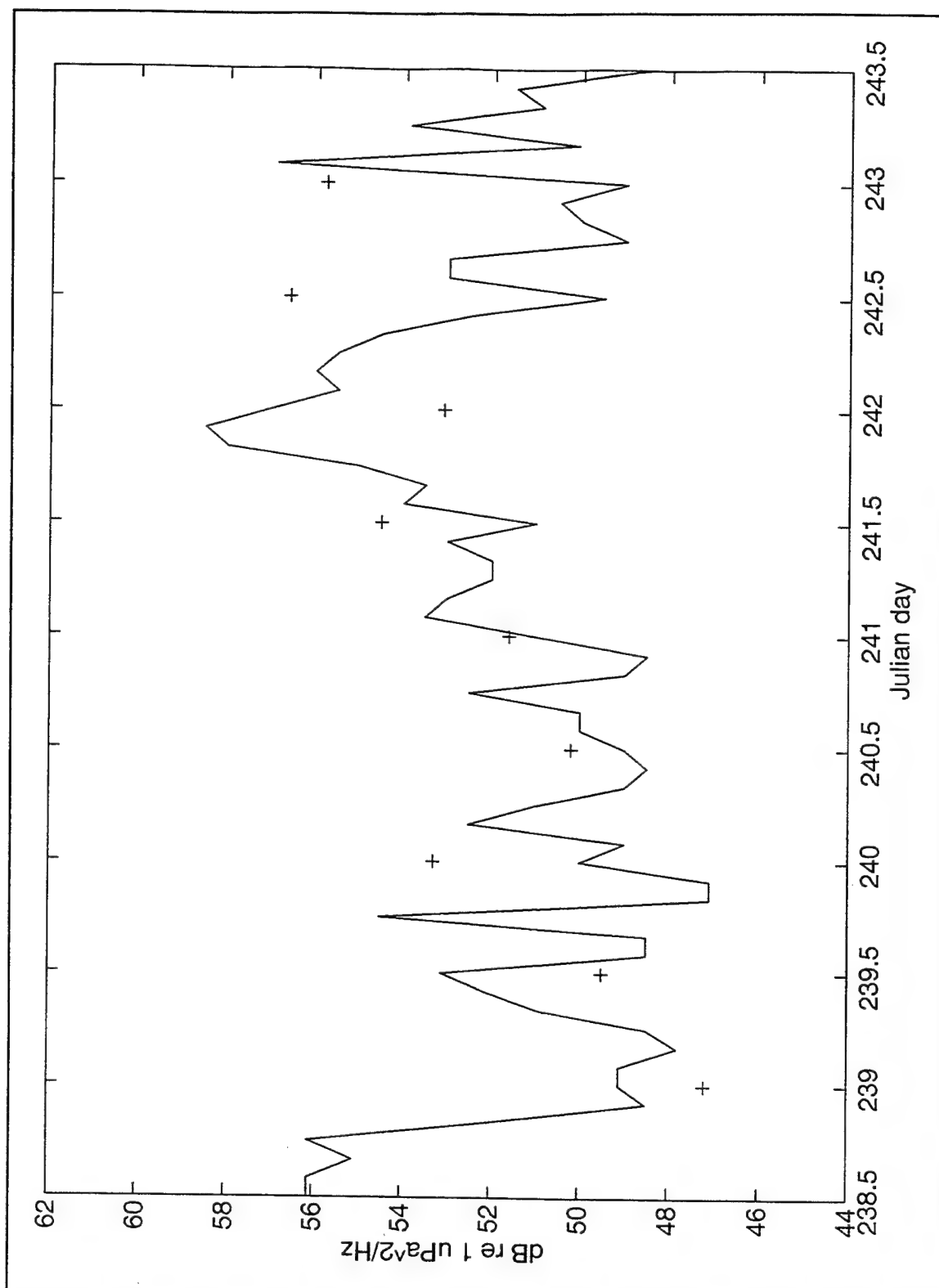predictions (crosses) for buoy 15 at 500 Hz, event II.

Figure 27   Time-series of measured AN levels (line) and ASNM
predictions (crosses) for buoy 19 at 500 Hz, event II

83

Table 13. Cross correlation coefficients between predicted and measured levels of AN at 500 Hz, event II. Negative time lags indicate predicted values lead the measured levels.

500 Hz	Cross	Correlation	Coefficient
Buoy	(Zero lag)	Max coeff	Lag (Hr)
13	0.50	0.5	0
15	0.53	0.53	0
19	-0.025	-0.025	0

Table 14. Summary of noise level increases from both measured and predicted values at 500 Hz. Increases in both values are calculated from before the event began to the first large peak in the noise level.

Buoys	Noise Increase	(dB)
	Measured	Predicted
13	7.0	7.1
15	9.5	11.9
19	10.0	4.3

moderate winds affect the buoys, at 500 Hz the model has generally performed well.

3.   Summary

The ASNM predicted values have compared moderately well with the measured levels in terms of correlation and predicting the rise in noise level, for the moderate (non-extreme) event modelled in this section. ASNM is designed to predict AN for extreme quiet and noisy events only because

84

in these extreme events the spatial distribution of active pressure ridges is nearly homogeneous (i.e., everywhere or nowhere). For moderate storms like event II, the distribution of active pressure ridges is most likely not spatially homogeneous.

Synoptic event I occurred during the Arctic winter season, and during very strong wind conditions where considerable active pressure ridging generation would occur. Hence, the model proved effective in forecasting AN levels. Synoptic event II, in comparison, produced moderate winds speeds of 15-30 knots. As discussed in Chapter III, Section F, it is at times of moderate synoptic activity when ASNM predictions are likely to be less accurate. This is because at moderate wind speeds, ASNM will accurately model the contributions of pressure ridges generated at comparatively distant locations, but nearby pressure ridging activity would affect the accuracy of the model's predicted values. It is at moderate wind speeds when more localized pressure ridging is likely to occur, as opposed to stronger or very much weaker wind speeds which would produce a more uniformly distributed pattern of pressure ridges, and is more accurately predicted by the model. This limitation probably causes the relatively low correlation coefficients at 50 and 100 Hz, where significant AN contributions from nearby pressure ridges dominate the AN contribution from more distant sources. At 500 Hz in moderate winds, mechanisms

85

other than active pressure ridging may contribute and little is known about the performance of ASNM in moderate wind conditions.

At 50 and 100 Hz, where AN is summed from close and distant sources, the maximum correlation coefficient values were often found at a -12 hour lag. The predicted values lead the measured levels and more significant correlations coefficients were obtained.

At the higher wind speeds the ice movement/ridging would react more quickly and generate noise with very little time lag. Moderate winds would cause slower build up in ice stress and consequently a slower development of pressure ridge activity. Therefore a longer time lag between the environmental forcing and noise generation is expected. In this case the identified time lag is 12 hours which is related to the resolution of the meteorological data. It is not possible with this data set to identify lags less than 12 hour which might produce higher maximum correlation coefficients. At very low wind speeds there is very little forcing and maximum correlation levels will probably be at zero lag during a quiet event. However, the decrease in AN level from very high to very low may be predicted by ASNM before it occurs, because there may be a lag between when the wind stops and when the ice momentum ceases.

The operational consequences of the existence of this 12 hour lag, if confirmed by further research, is highly

significant. A model prediction made at a time of moderate winds using an Arctic NOGAPS analysis field would be accurate in predicting the omnidirectional AN when used as a prognosis for 12 hours ahead.

C.   SYNOPTIC EVENT III

1.   Overview

Event III was selected for analysis because a cluster of five drifting AN buoys provided an opportunity to assess the variability of the noise field at a time when all the buoys were subject to weak wind forcing. The synoptic time period examined was from 19-24 Feb 1976 (Julian days 76050-76055). The five buoys were spread over a moderate area in the central Beaufort Sea, with a maximum separation of 580 km between the buoys. The measured buoy data for this time period has been analyzed by Fritsch (1995) and readers are referred to his study for a more in-depth analysis of the AN data.

The noise record for the five buoys can be seen in Figure 28. The synoptic event was chosen because it was a very quiet event, particularly during 21-23 Feb (Julian days 76051-3), when minimum levels of AN of between 56-63 dB were recorded at 32 Hz. The seasonal winter 5th percentile value, averaged over all five buoy records, was approximately 63 dB. Throughout the synoptic period the number of hours the

87
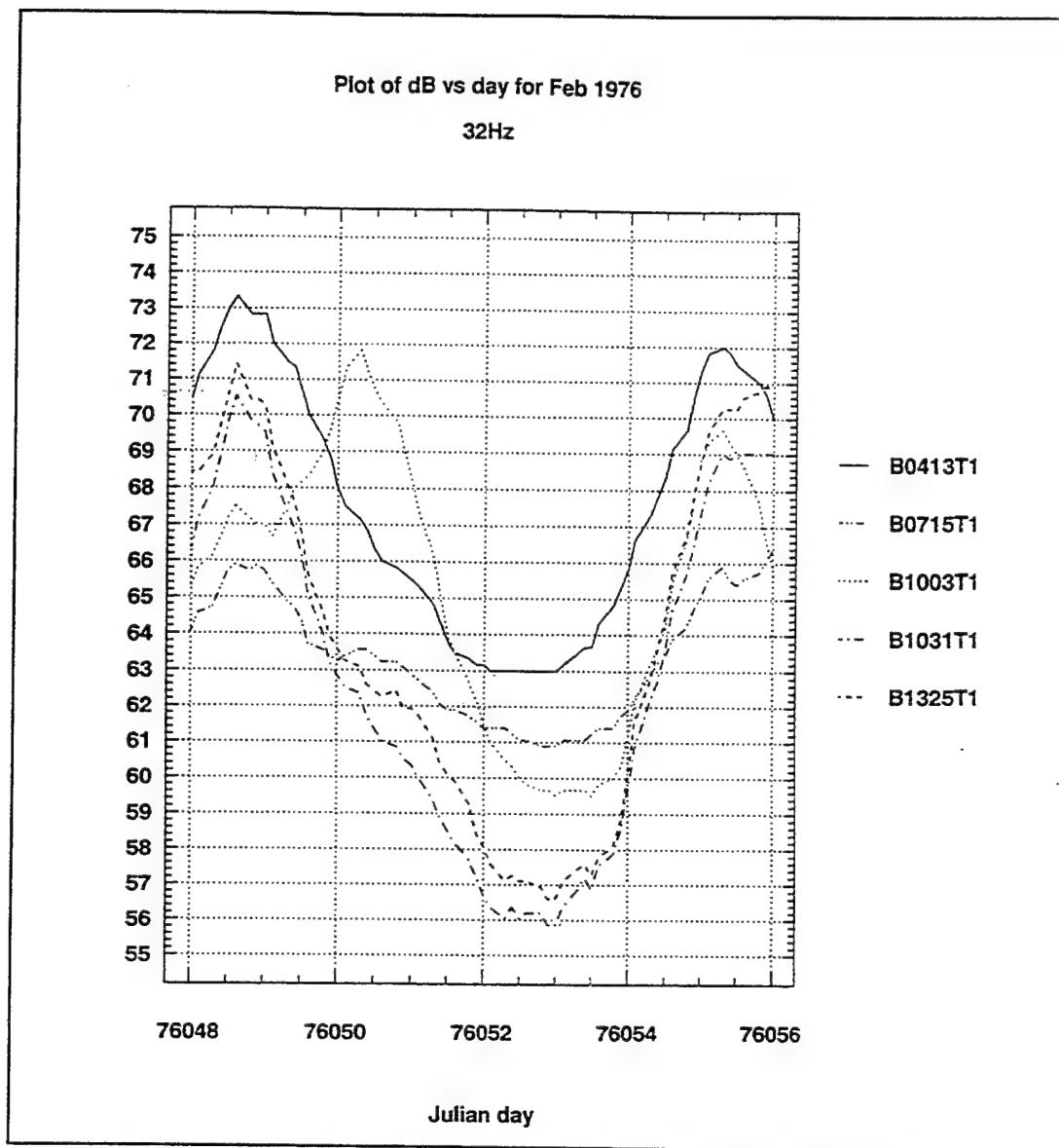
Figure 28   32 Hz time-series (quiet event) from 19-24
Feb 1976 (Julian days 76050-76055). 5th percentiles (dB
re uPa/√Hz): B0413T1, 67.0; B0715T1, 63.4; B1003T1,
63.0; B1031T1, 61.7; B1325T1, 63.1 (from Fritsch, 1995).

AN levels remained below the 5th percentile varied from 61.2
hours for buoy B100371 to 96 hours for buoys B071571 and
B132571. Therefore the noise record illustrates that it was
a particularly quiet and long lasting event.

88

For synoptic events I and II NOGAPS data was used as the forcing input to ASNM. Unfortunately the availability of stored NOGAPS data in a suitable format for input to the model was not available for dates prior to 1992. However, since the synoptic wind speeds were less than 6 knots over a large area surrounding the location of the buoys, it was possible to make a model prediction using an assumption of straight line propagation (Wilson, 1983).

2.   Results

Figure 29 shows the surface pressure field for 21 Feb 1976. A large area of light geostrophic winds, associated with the high pressure region, covered the Beaufort Sea area maintaining wind speeds of less than 6 kts (<3 m/s).

From Table 2 the source level density attributed to the lightest winds, 0-5 kts (<3 m/s) at 50 Hz is 53 dB. Despite the fact that a ASNM prediction cannot be made due to the lack of a gridded wind field, an estimation of the model's predictive capability can be made. Unlike the more recent buoys, the 1976 buoys recorded noise levels are at 32 Hz, not 50 Hz. Assuming a spectral noise distribution of -6 dB per octave, the 53 dB SLD at 50 Hz equates to approximately 56 dB at 32 Hz. As previously discussed in Chapter III, Section D1, the expression $AN = SLD + 10 \log \pi$ (where $10 \log \pi \sim 5$ dB) can be used in an area of uniformly light winds. Therefore, the predicted AN level would be 61 dB for
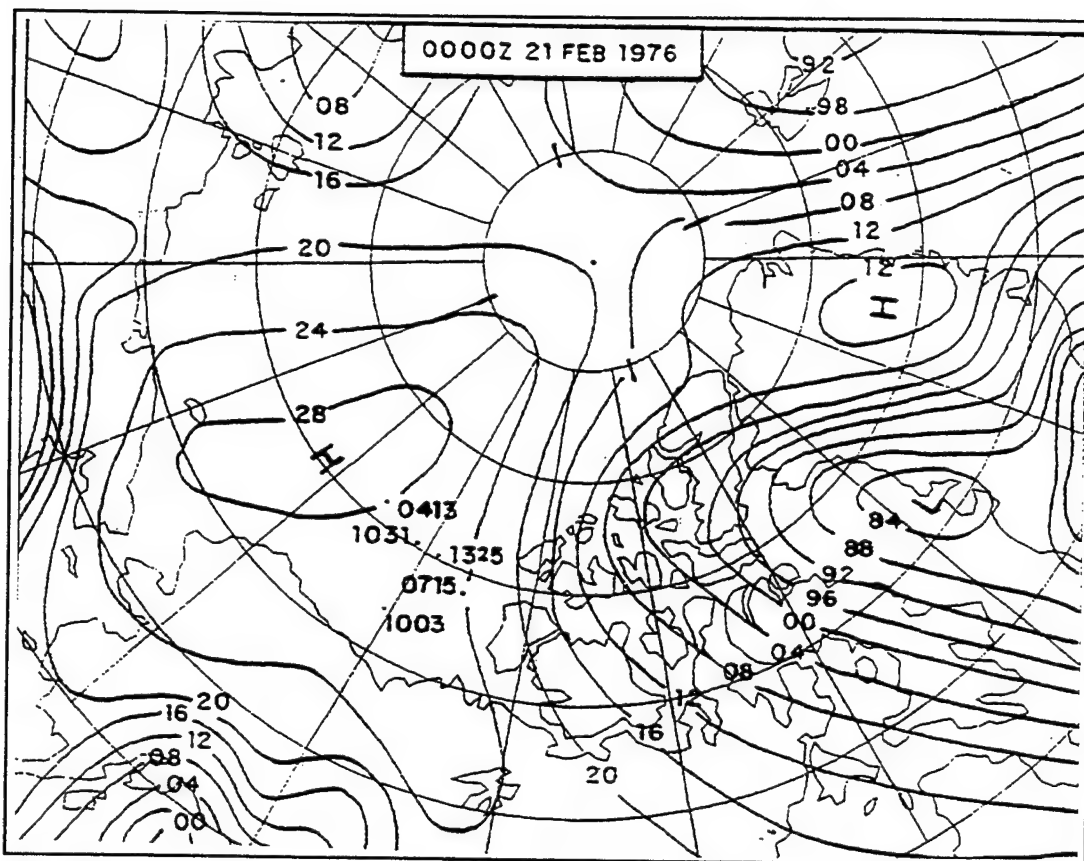
Figure 29   Surface pressure field and buoy locations for 0000Z 21 February 1976 (from Fritsch 1995).

any receiver located in the immediate vicinity of the low wind speed area. Comparing this to the measured levels of AN analyzed by Fritsch (Figure 28), it can be seen that a value of 61 dB is relatively central in the range of values measured by the five buoys (from 56 to 63 dB).

3.   Summary

Even though an in-depth quantitative comparison of model output and measured levels of AN is precluded due to unavailability of synoptic wind data, a qualitative

evaluation provides a useful ASNM/measured noise comparison. It illustrates that at very low wind speeds the model is likely to be accurate in predicting low levels (< 5th percentile) of AN. This is in agreement with the results in Section A of this chapter where the low AN values measured prior to the onset of stronger winds associated with the synoptic event were accurately predicted by the model. This is also an excellent case to validate the SLD's in Table 2, for the quiet noise extreme events.

V CONCLUSIONS AND RECOMMENDATIONS

A.   CONCLUSIONS

The objective of this research has been to develop and validate a model capable of predicting extreme noise events in the Arctic Ocean. Active pressure ridging is considered the primary noise generating mechanism at the low frequencies (<500 Hz) studied. The open-ocean ambient noise model, ANDES, was adapted for use in the ice-covered Arctic Ocean and designated the Arctic Storm Noise Model (ASNM). ASNM used NOGAPS gridded wind data as the forcing parameter and the resultant AN predictions were compared to recorded data obtained from ice-mounted drifting AN buoys in the central Arctic basin.

Three synoptic events were examined to test the robustness of the model. Event I exhibited strong wind forcing during a winter synoptic period. Moderate wind forcing during a summer synoptic period comprised event II and event III was a prolonged period of light wind forcing.

ASNM proved to be an accurate model in predicting extreme noise events. The model has been developed to predict large changes in AN levels related to extreme meteorological events affecting the Arctic region. The results from the analysis of synoptic event I illustrated ASNM's capability to predict a large increase in AN. The noise level rose nearly 30 dB from before the synoptic event

began to the first large noise peak, and this rise was accurately forecast by ASNM. Correlation coefficients between the time-series of the measured and predicted values were high (~ 0.8). Event III illustrated qualitatively that ASNM is accurate in predicting low noise extreme events.

The underlying hypothesis of the model, i.e., that the AN level recorded at a receiver receives contributions from both local and distant sources, as opposed to solely local sources, has proved to be a solid foundation upon which to build an AN model.

Results from event II, a moderate storm event, has shown that the model is limited in the accuracy of predictions made at times of moderate wind speeds, where extremely high or low AN levels are not achieved. This limitation is related to the nature of the spatial anisotropic distribution of the dominant noise sources - active pressure ridges. At low frequencies active pressure ridging behaves isotropically for high noise events where there are numerous active pressure ridges. During low noise or quiet events, there are very few active pressure ridges and the probability of having an active pressure ridge nearby is remote. However, for moderate wind speeds active pressure ridging can be highly anisotropic.

A spatially homogeneous noise distribution is assumed in every 1 degree lat/long cell in ASNM and, therefore, in its current form is limited when predicting AN for moderate

94

events. During extreme events affecting the Arctic basin, ASNM has proved accurate in predicting extreme levels of ambient noise.

B.   RECOMMENDATIONS

Further testing and development of the model should be conducted with the aim of producing an operational model for use by the submarine fleet. ASNM in its current form should only be used to predict AN for extreme events. A definition of extreme events should be determined, but currently can be defined by AN levels either < 10th percentile or > 90th percentile of the YEARLY noise record.

To extend the model to include accurate predictions made at moderate wind speeds, more information is necessary to quantify the distribution of active pressure ridging to AN generation. The potential of using remote sensing methods to identify active pressure ridges, possibly using SAR imagery, should be examined. Data gathering by units under the ice, from mobile platforms, directional arrays or vertical arrays is necessary to accurately determine the acoustic contribution of active pressure ridging and its spatial distribution. This data could then be used as an input to ASNM to develop the model.

A further step is to determine the internal ice stress from a a coupled ice-ocean model such as PIPS and relate the ice stress directly to the observed noise field.

APPENDIX A. DATA CHARTS FOR EVENT I
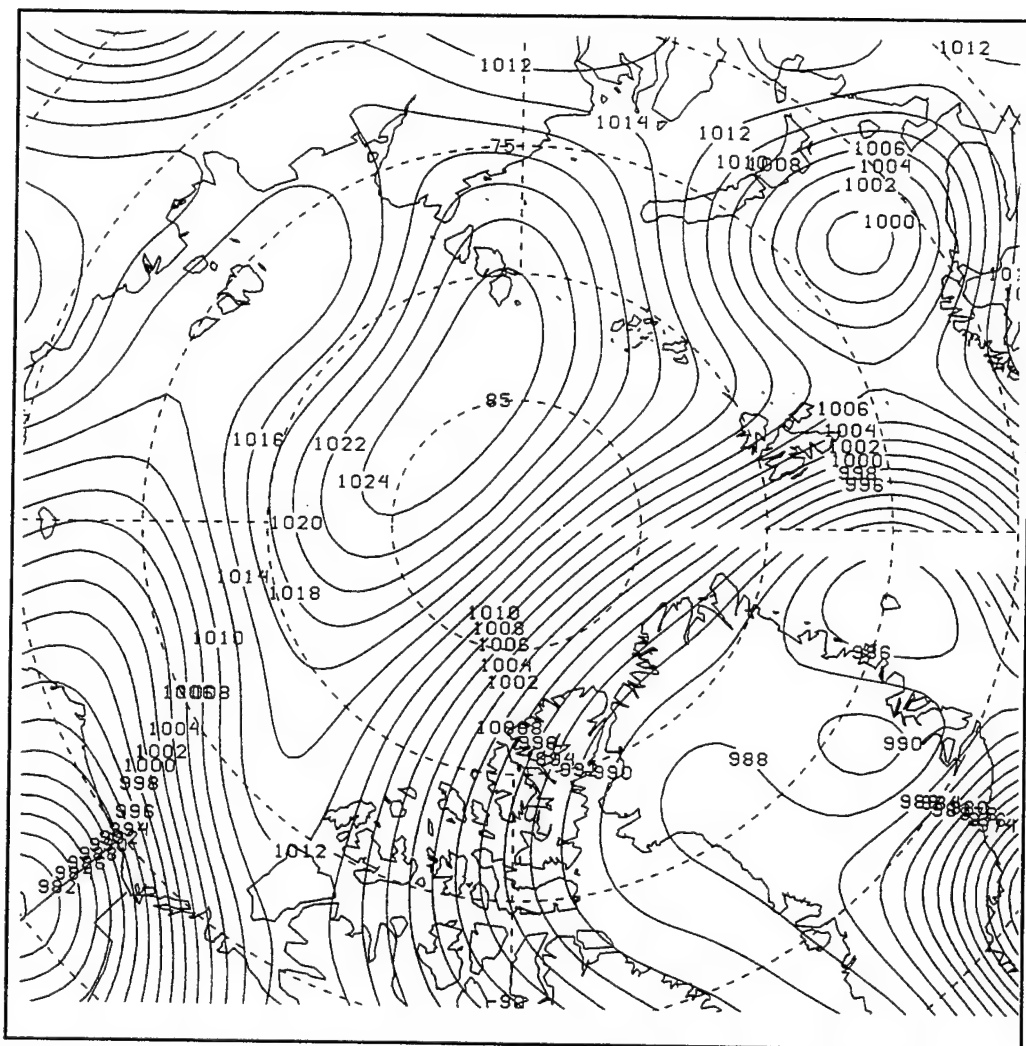
Figure 30   1000mb pressure field on 29 Jan 1993,
1200Z (Julian day 29) for the Arctic basin
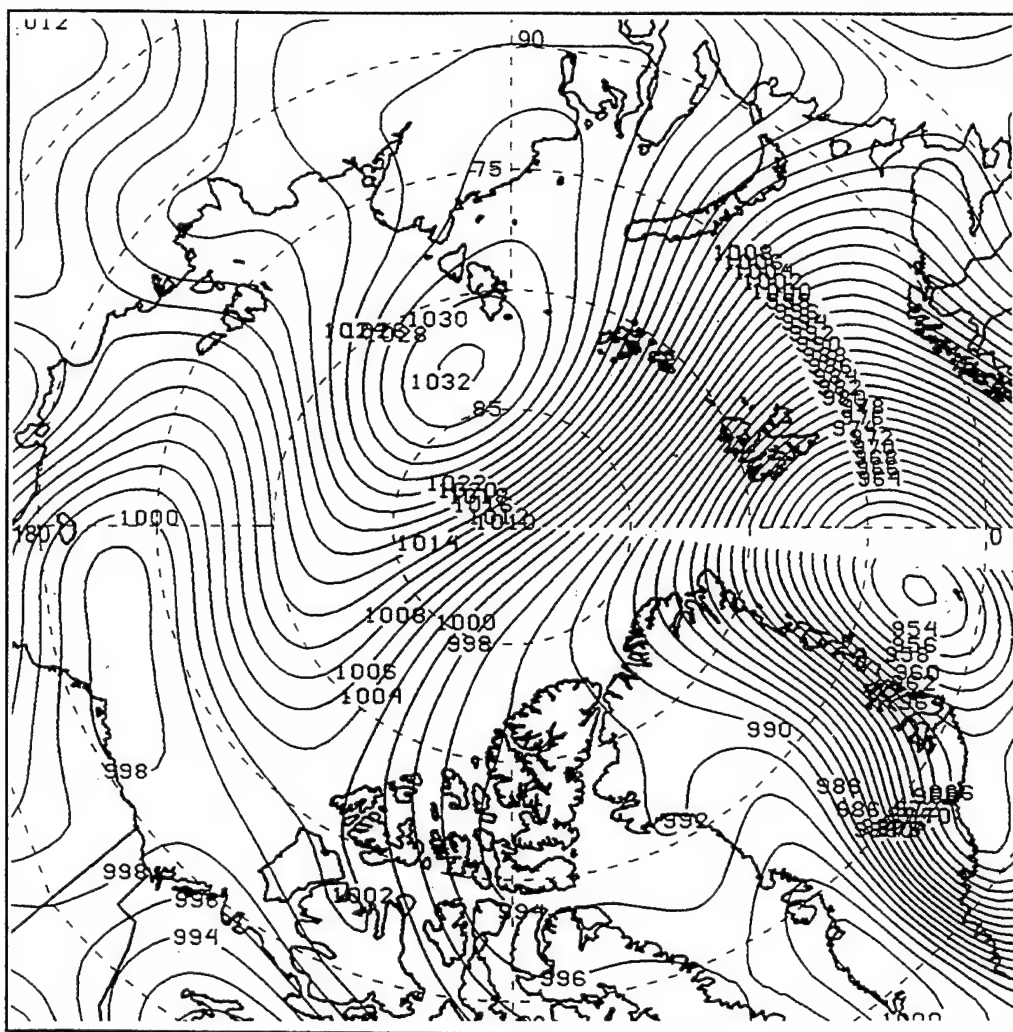
Figure 31   1000mb pressure field on 30 Jan 1993,
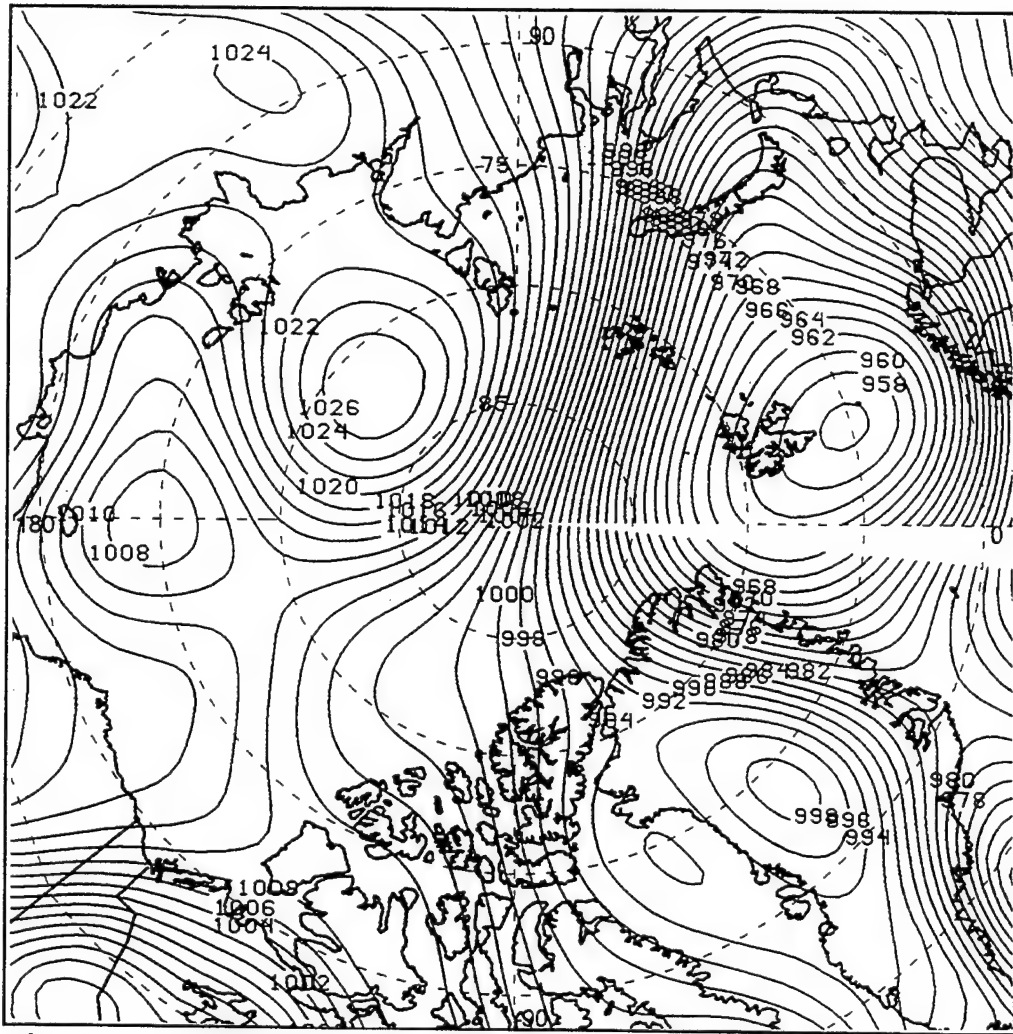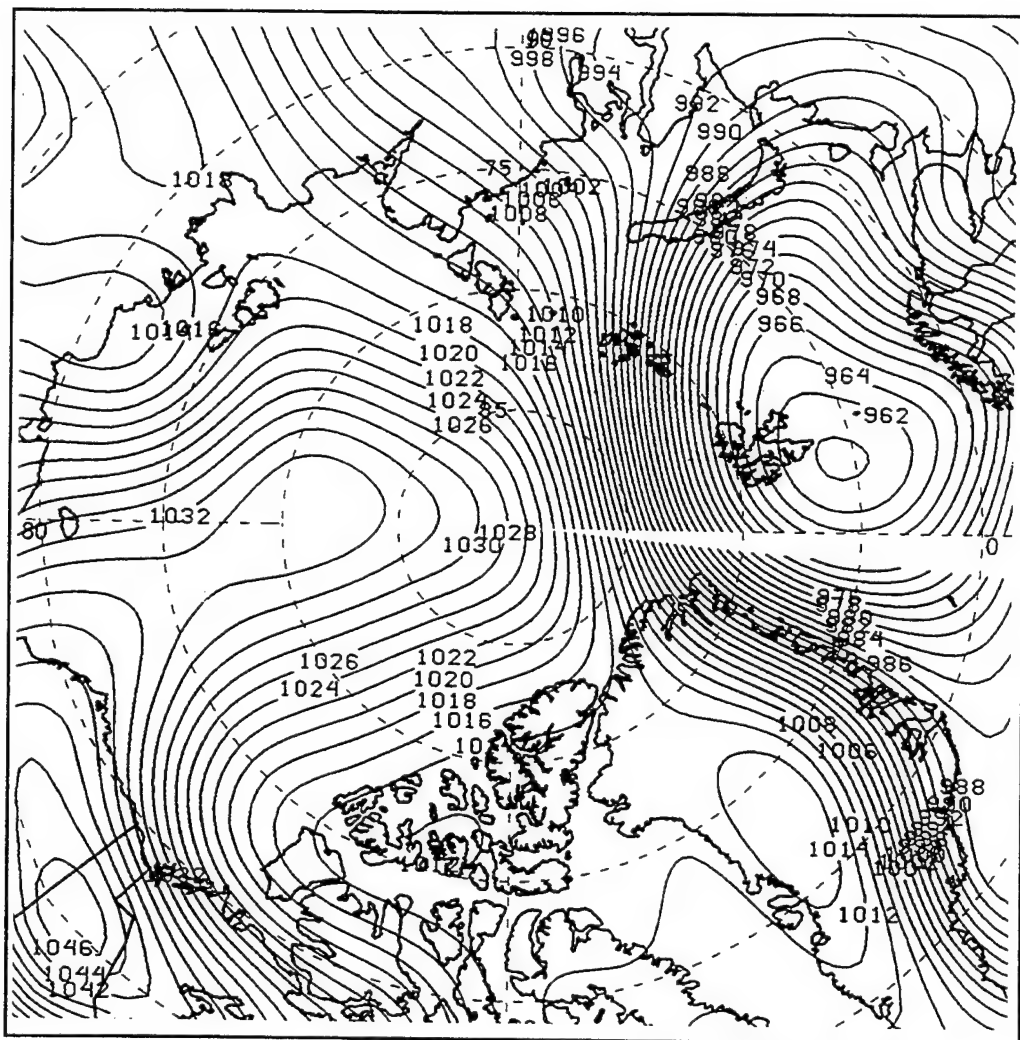1200Z (Julian day 30) for the Arctic basin (from
Feller, 1994).

Figure 32   1000mb pressure field on 31 Jan 1993,
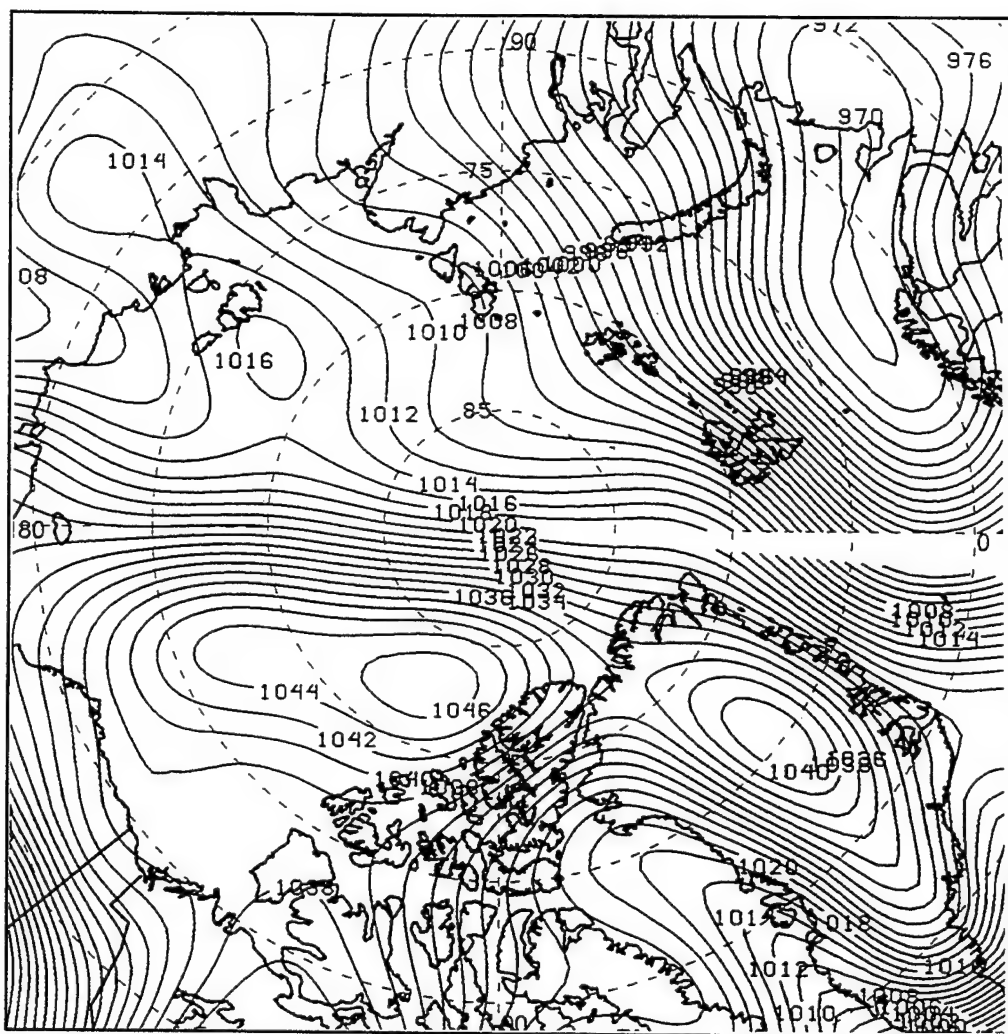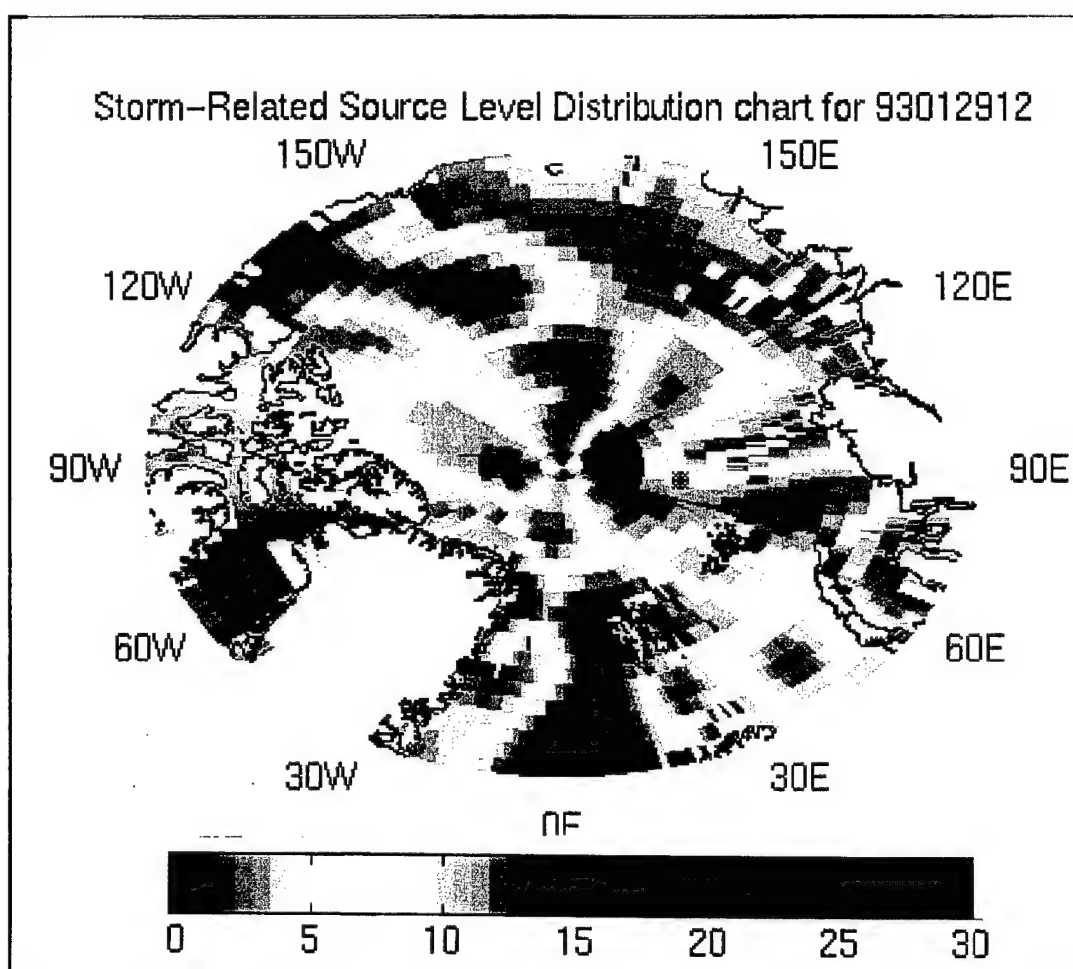1200Z (Julian day 31) for the Arctic basin

100
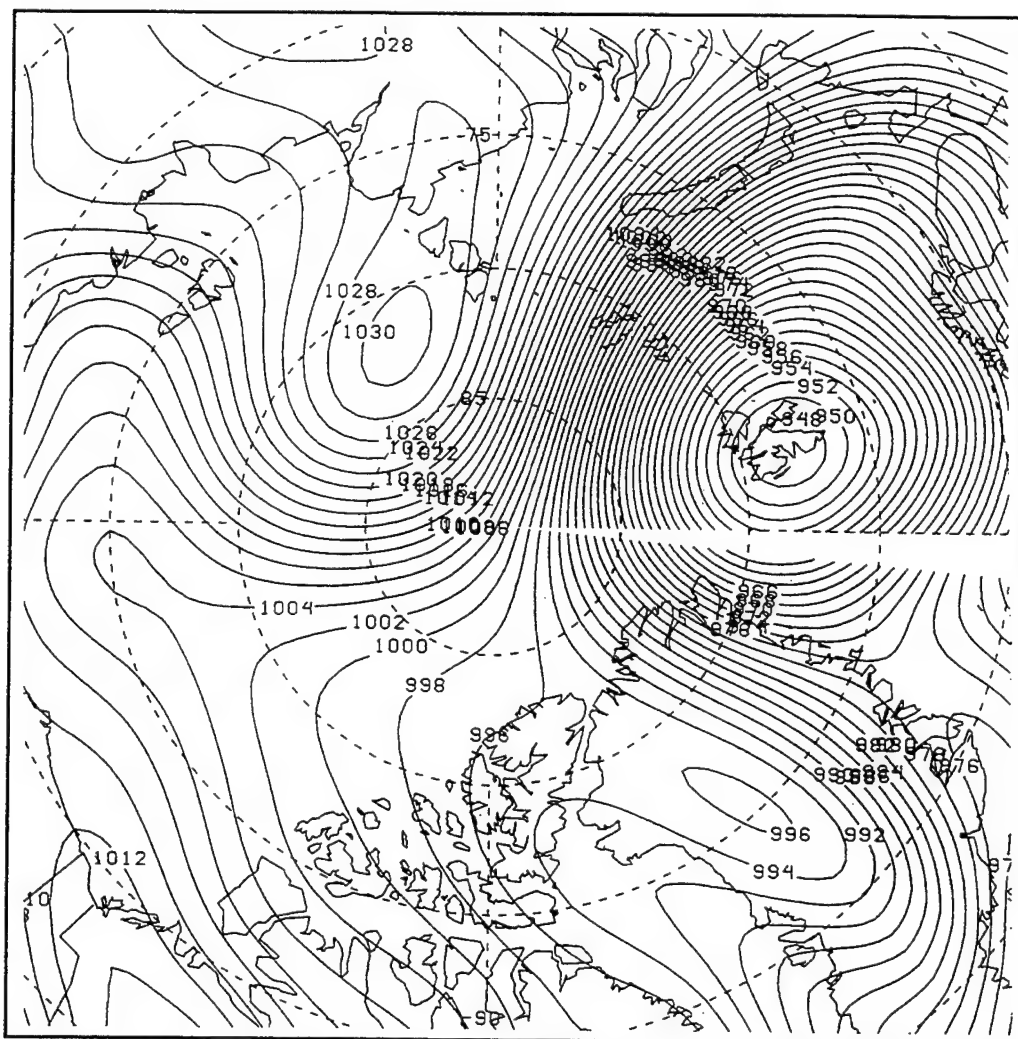
Figure 33   1000mb pressure fields on 01 Feb 1993,
1200Z (Julian day 32) for the Arctic basin (from
Feller, 1994).

101

Figure 34   1000mb pressure field on 03 Feb 1993,
1200Z (Julian day 34) for the Arctic basin (from
Feller, 1994).

Figure 35 1000mb pressure fields on 05 Feb 1993,
0000Z (Julian day 36) for the Arctic basin (from
Feller, 1994).

Figure 36   Source level density category chart for 29
Jan 1993, 1200Z, for the Arctic basin
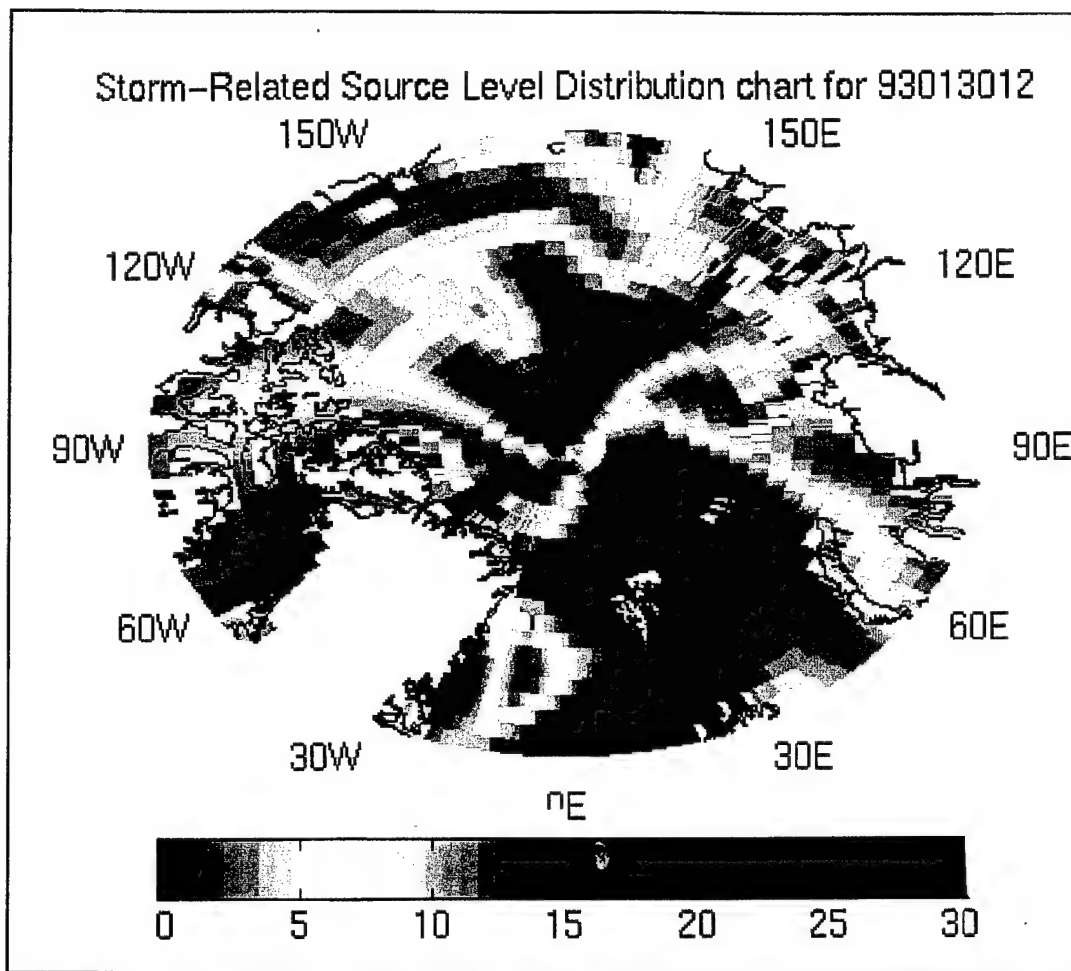
Figure 37   Source level density category chart for 30
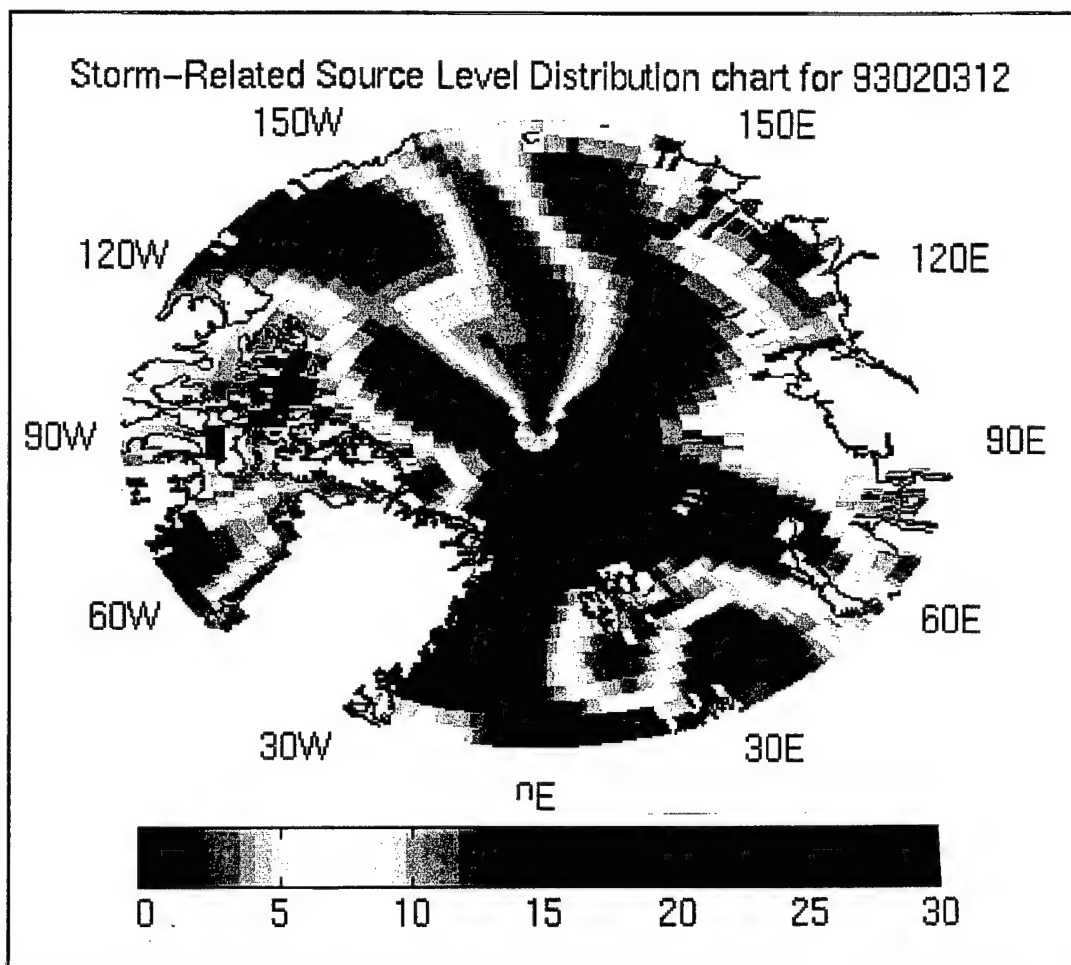Jan 1993, 1200Z, for the Arctic basin.
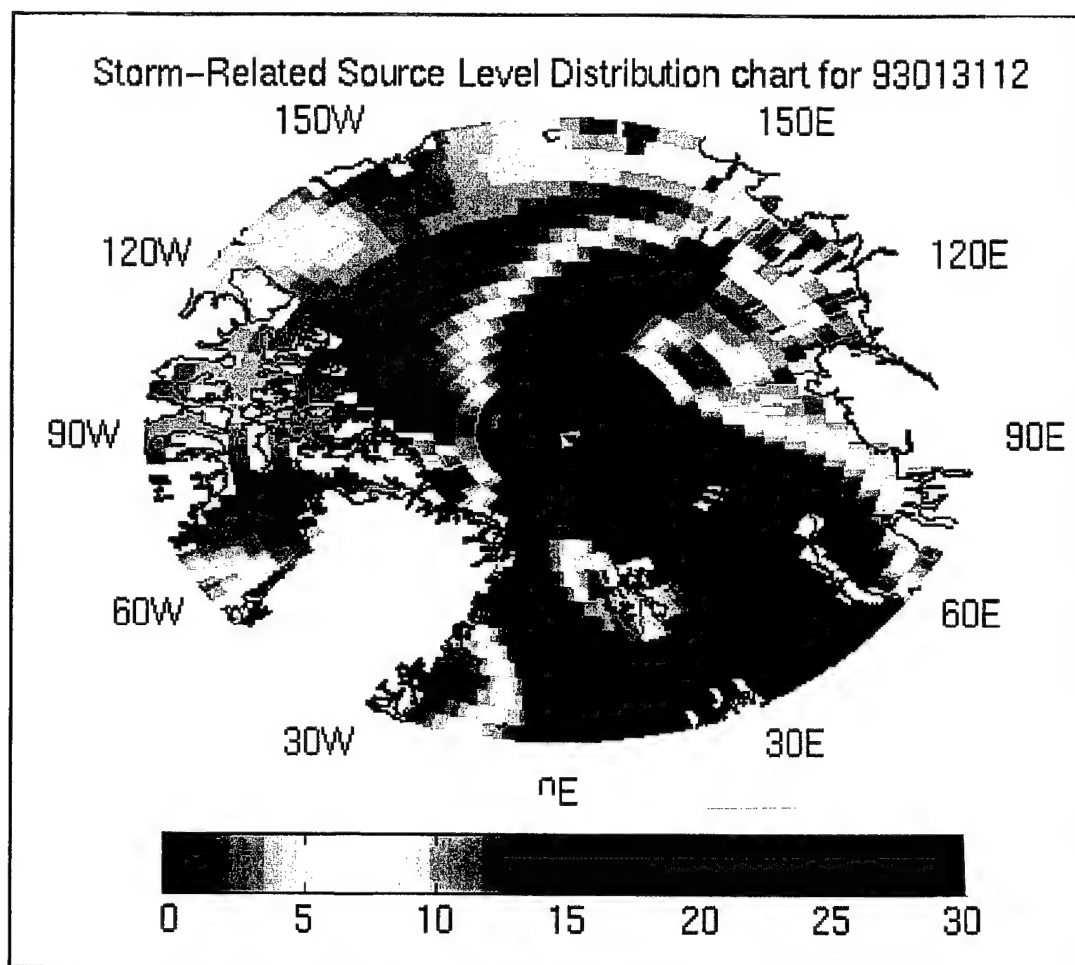
Figure 38   Source level density category chart for 31
Jan 1993, 1200Z, for the Arctic basin.
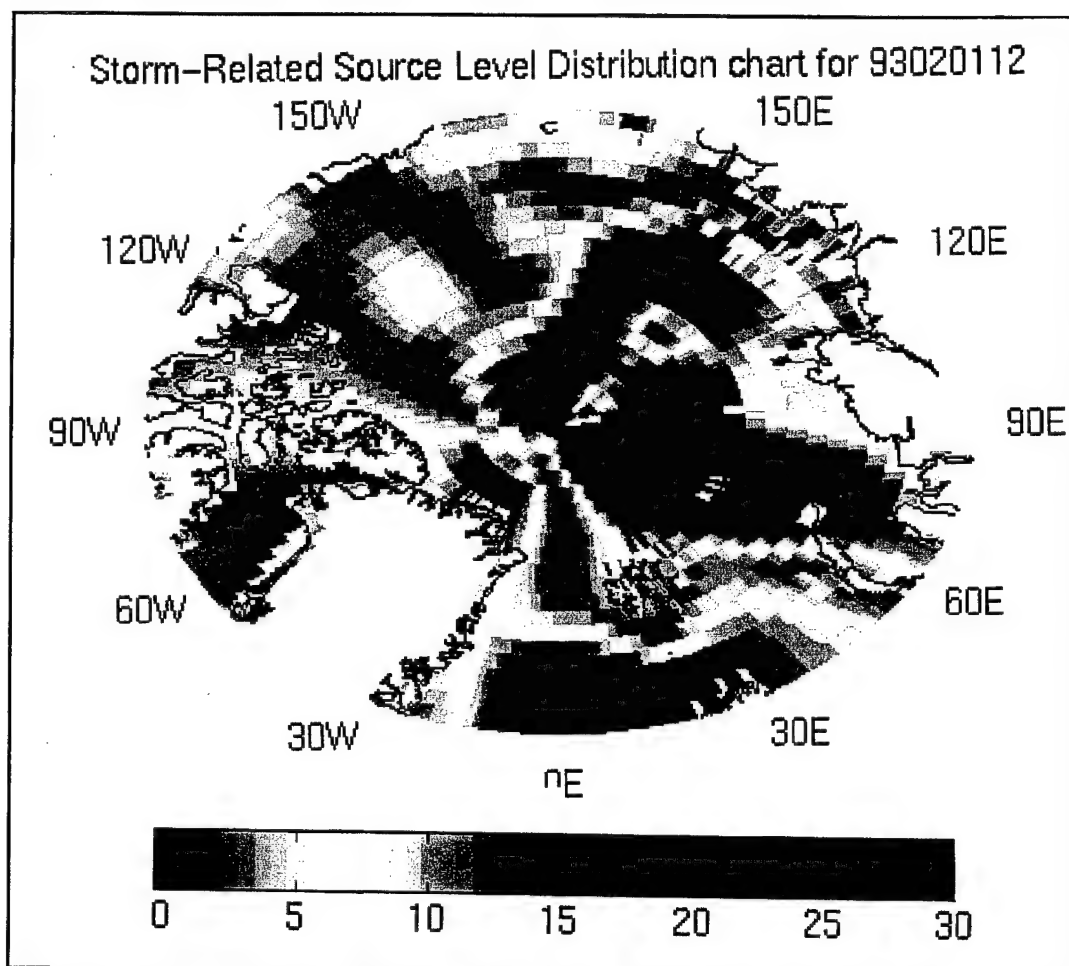
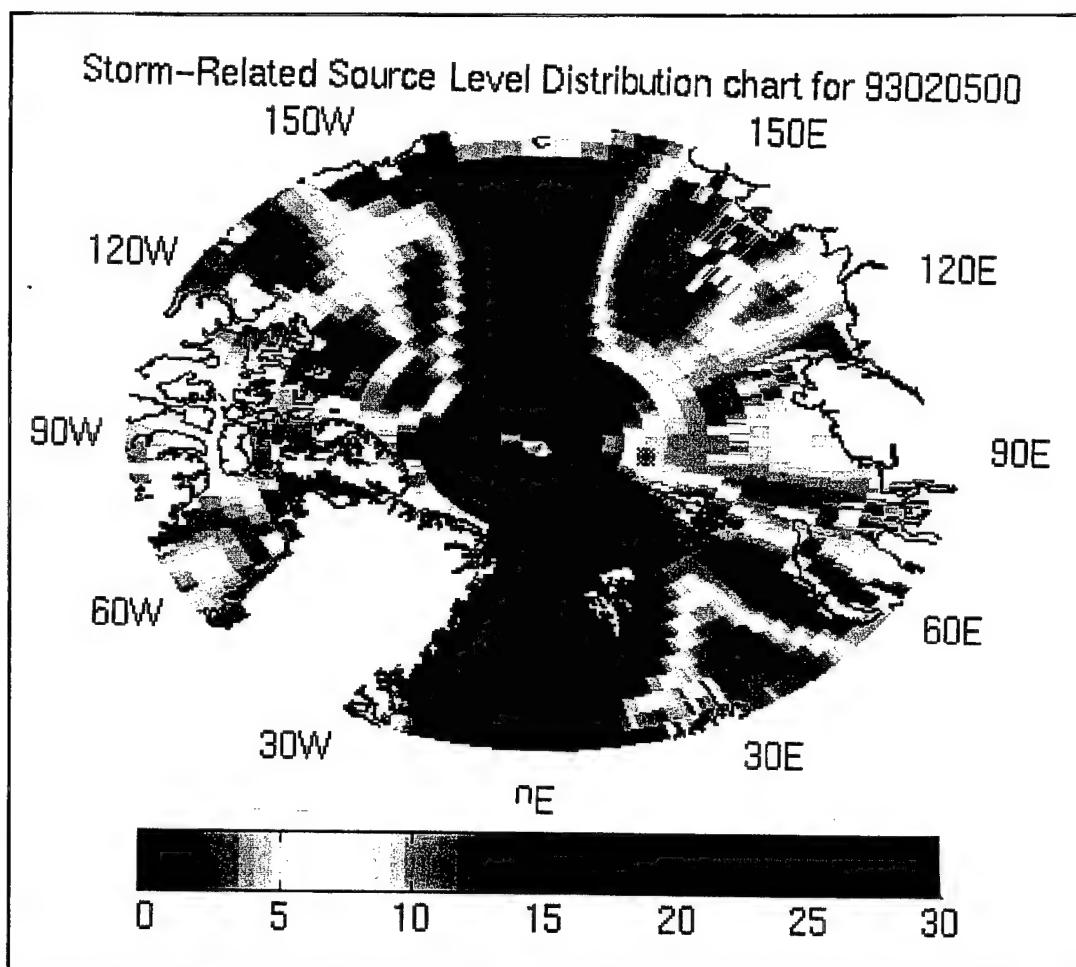Figure 39 Source level density category chart for 01 Feb 1993, 1200Z, for the Arctic basin.

Figure 40   Source level density category chart for 03
Feb 1993, 1200Z, for the Arctic basin.

Figure 41   Source level density category chart for 05
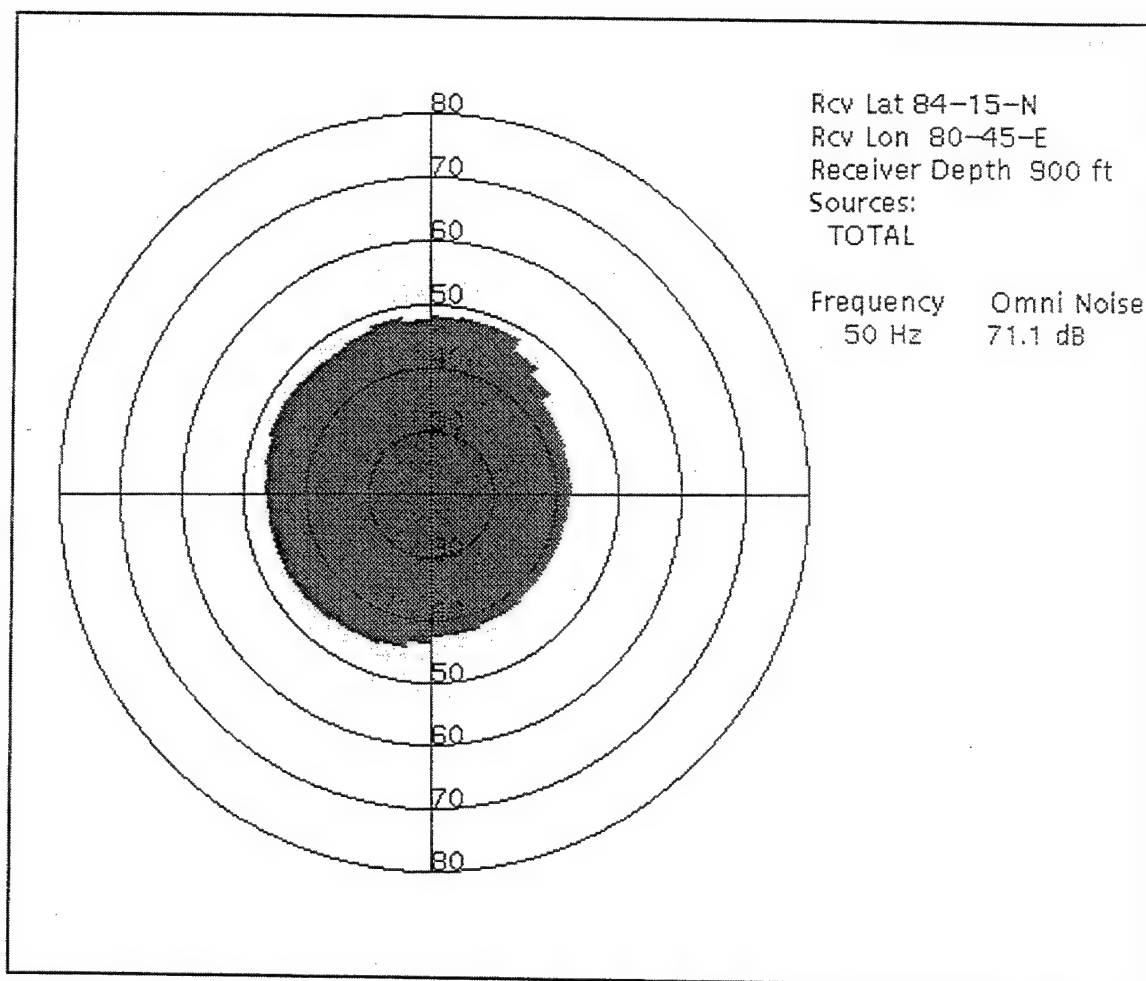Feb 1993, 0000Z, for the Arctic basin.

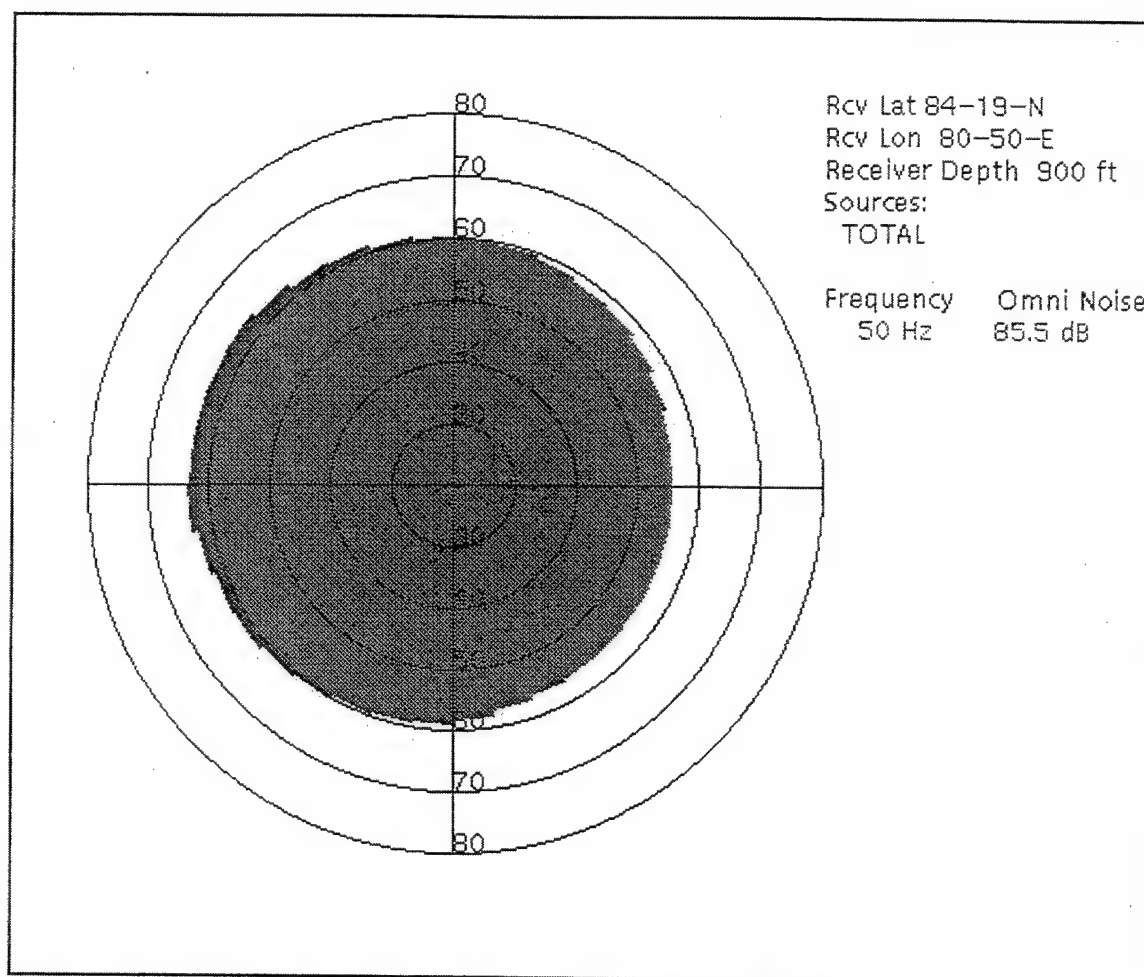Figure 42   ASNM predicted values of AN and directionality for buoy 13 on 29 Jan 1993, 1200Z.

Figure 43   ASNM predicted values of AN and directionality
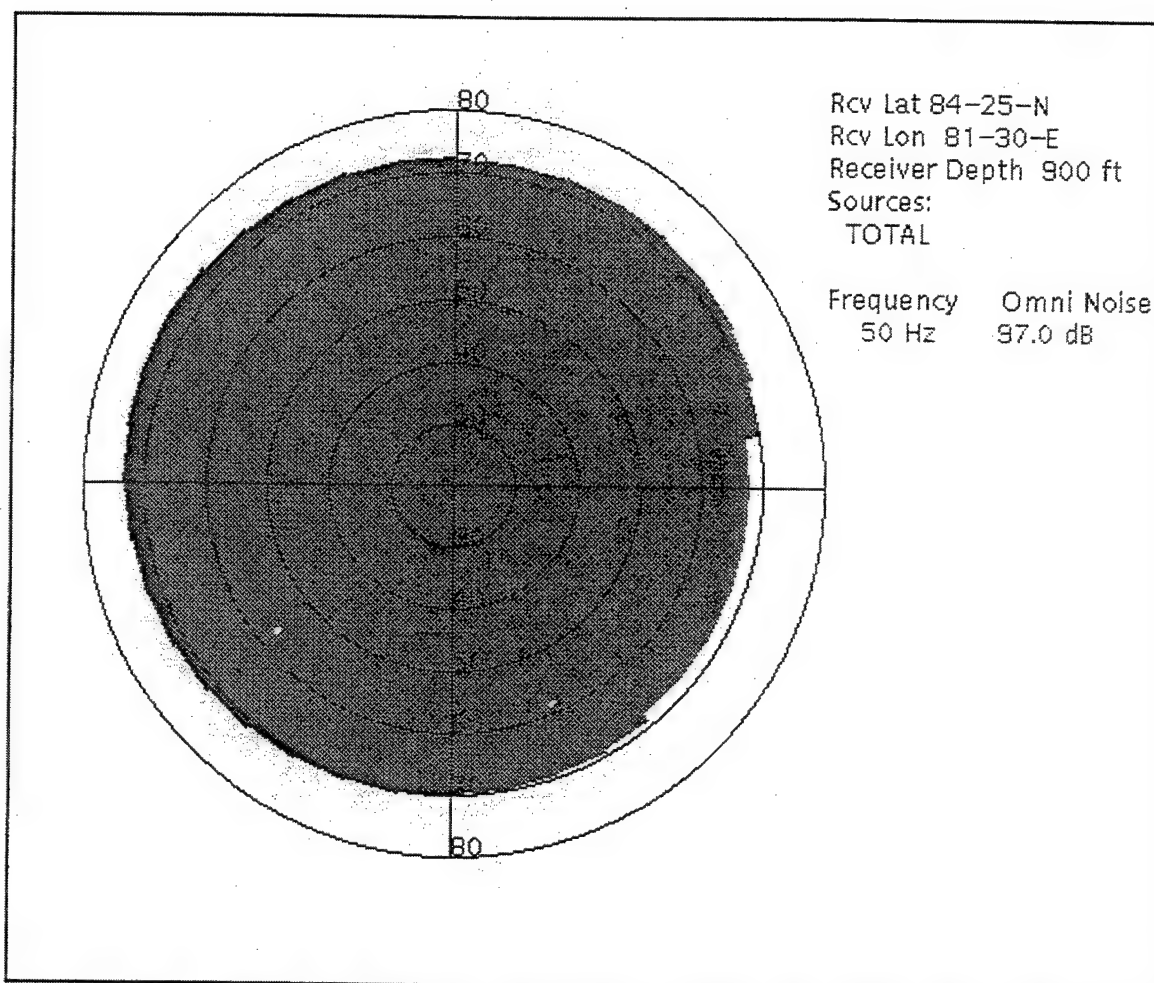for buoy 13 on 30 Jan 1993, 1200Z.

Rcv Lat 84-25-N
Rcv Lon 81-30-E
Receiver Depth 900 ft
Sources:
 TOTAL

Frequency   Omni Noise
 50 Hz   97.0 dB

Figure 44   ASNM predicted values of AN and directionality
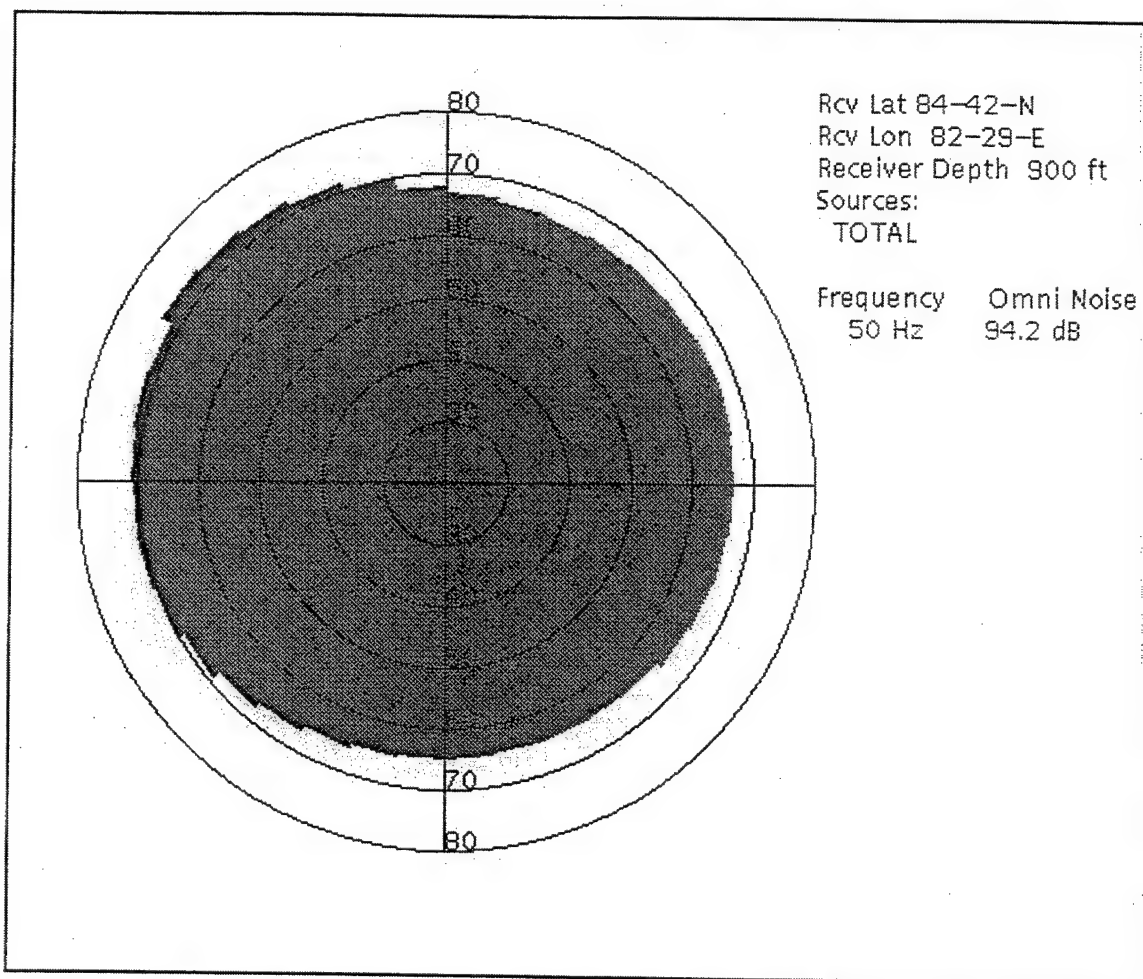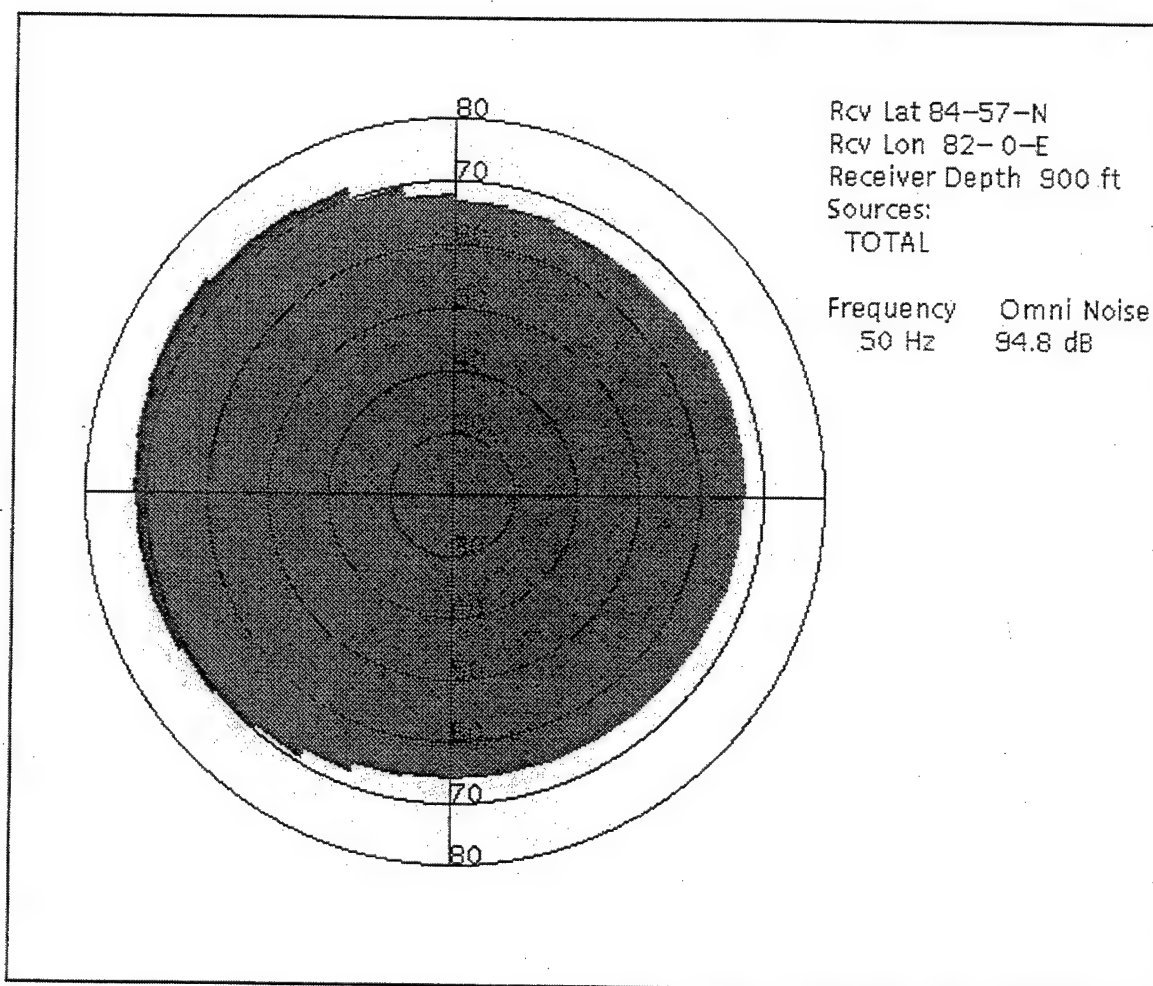for buoy 13 on 31 Jan 1993, 1200Z.

112

Figure 45 ASNM predicted values of AN and directionality for buoy 13 on 01 Feb 1993, 1200Z.

Figure 46   ASNM predicted values of AN and directionality
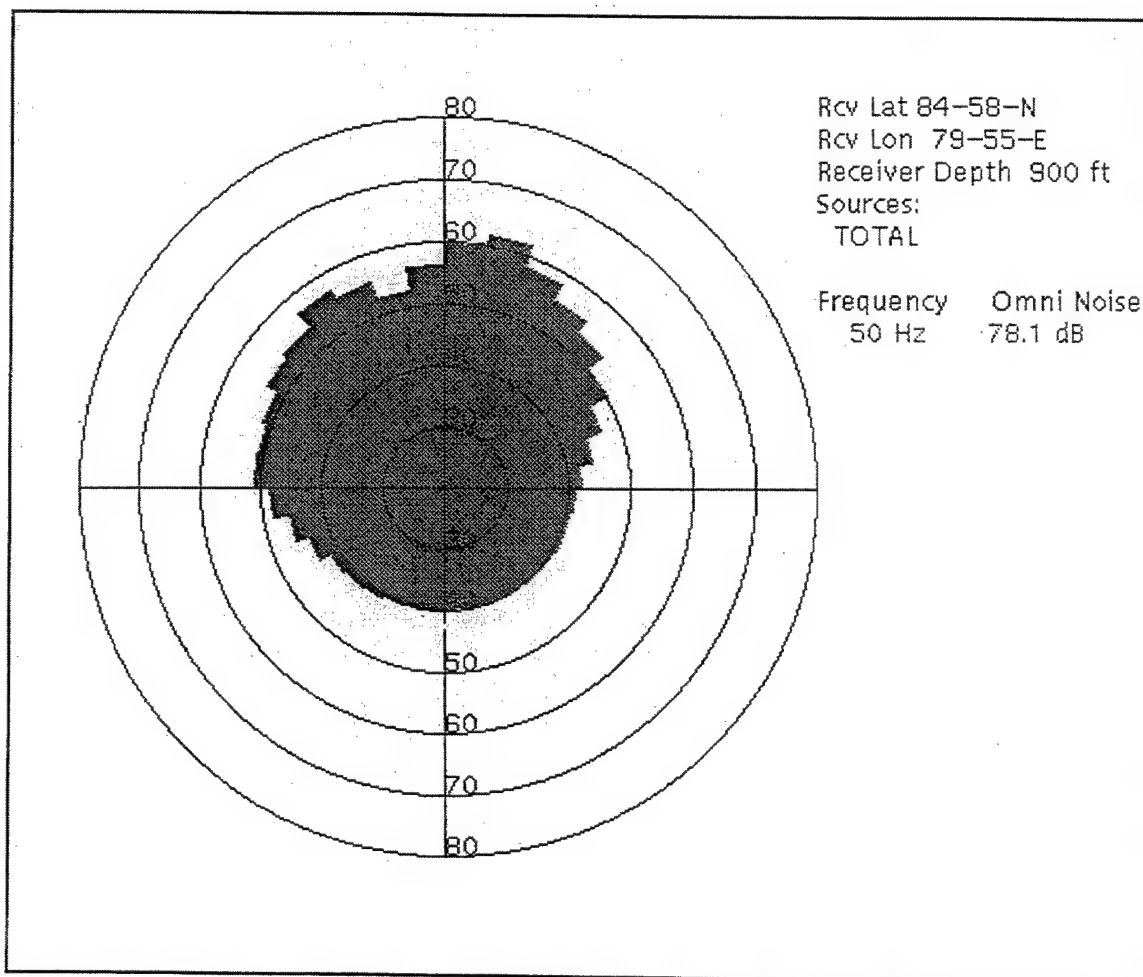for buoy 13 on 03 Feb 1993, 1200Z.

114

Figure 47   ASNM predicted values of AN and directionality for buoy 13 on 05 Feb 1993, 0000Z.

APPENDIX B. DATA CHARTS FOR EVENT II
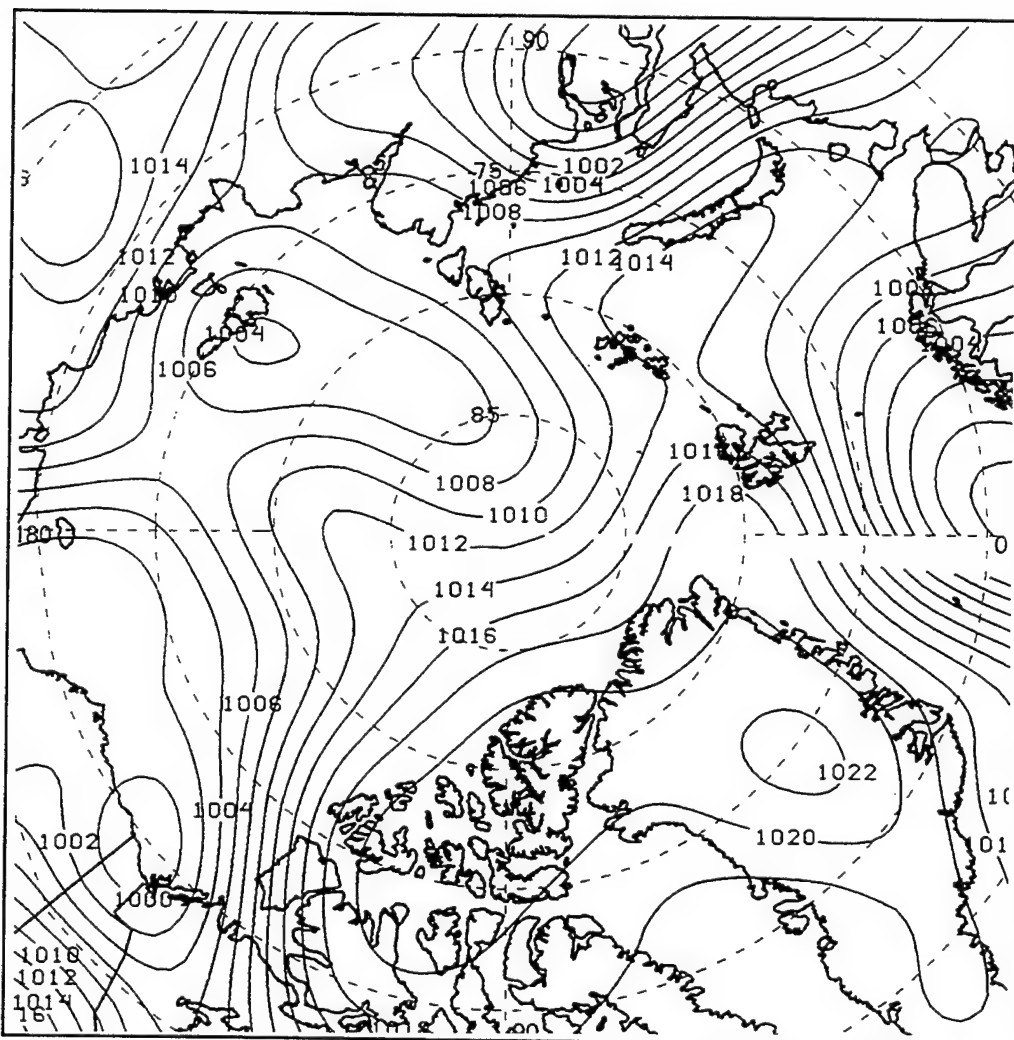
Figure 48 1000mb pressure fields on 26 Aug 1992, 0000Z (Julian day 239) for the Arctic basin (from Feller, 1994).

Figure 49   1000mb pressure fields on 27 Aug 1992,
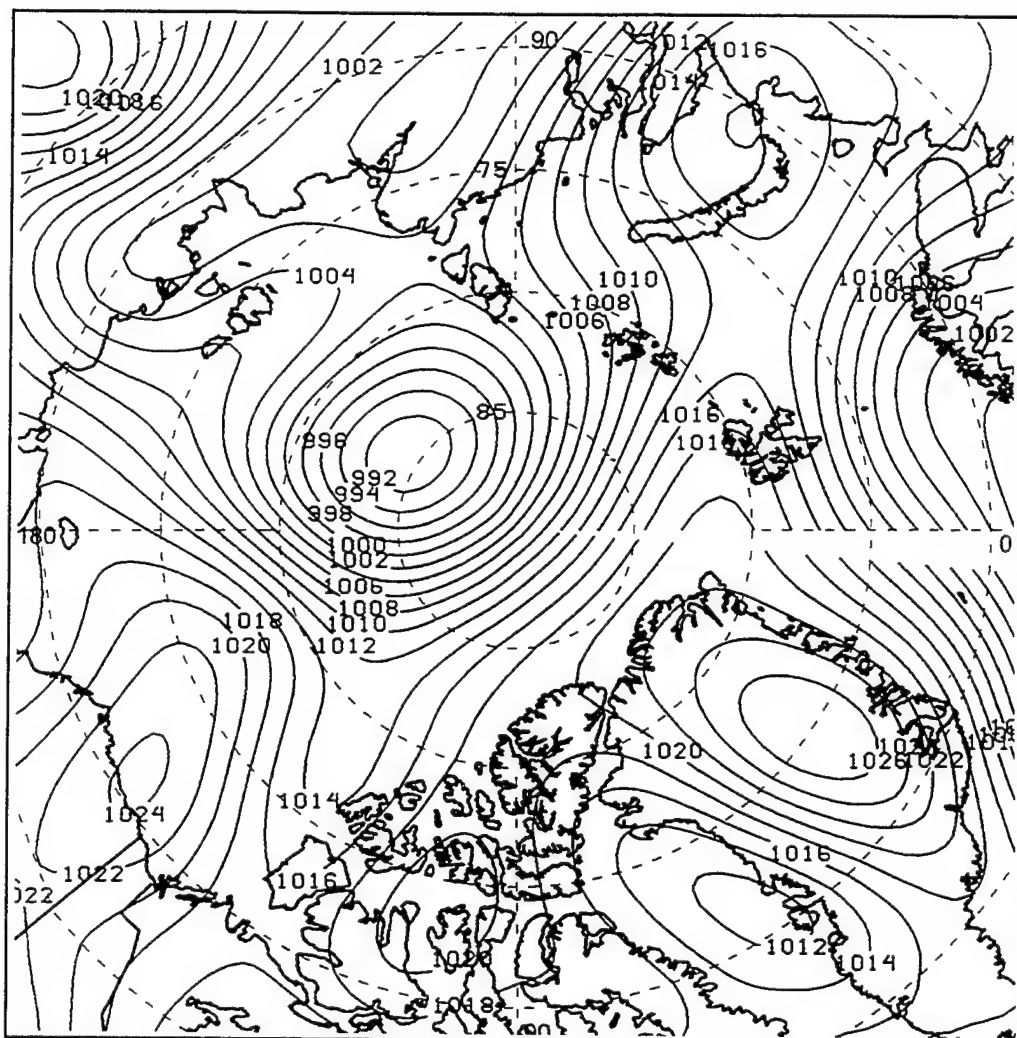0000Z (Julian day 240) for the Arctic basin (from
Feller, 1994).

Figure 50 1000mb pressure fields on 28 Aug 1992,
0000Z (Julian day 241) for the Arctic basin (from
Feller, 1994).

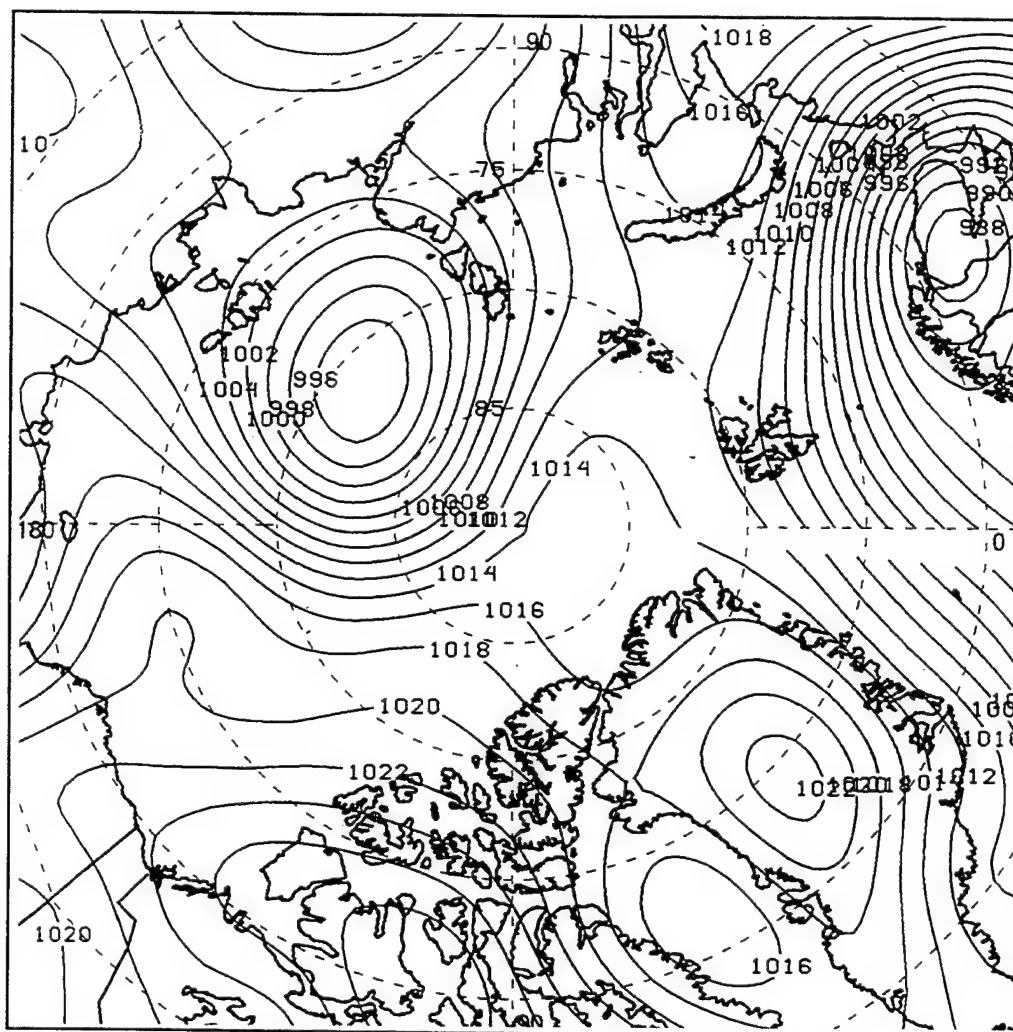Figure 51   1000mb pressure fields on 29 Aug 1992,
1200Z (Julian day 242) for the Arctic basin (from
Feller, 1994).

Figure 52   Source level density category chart on 26 Aug 1992, 0000Z, for the Arctic basin.
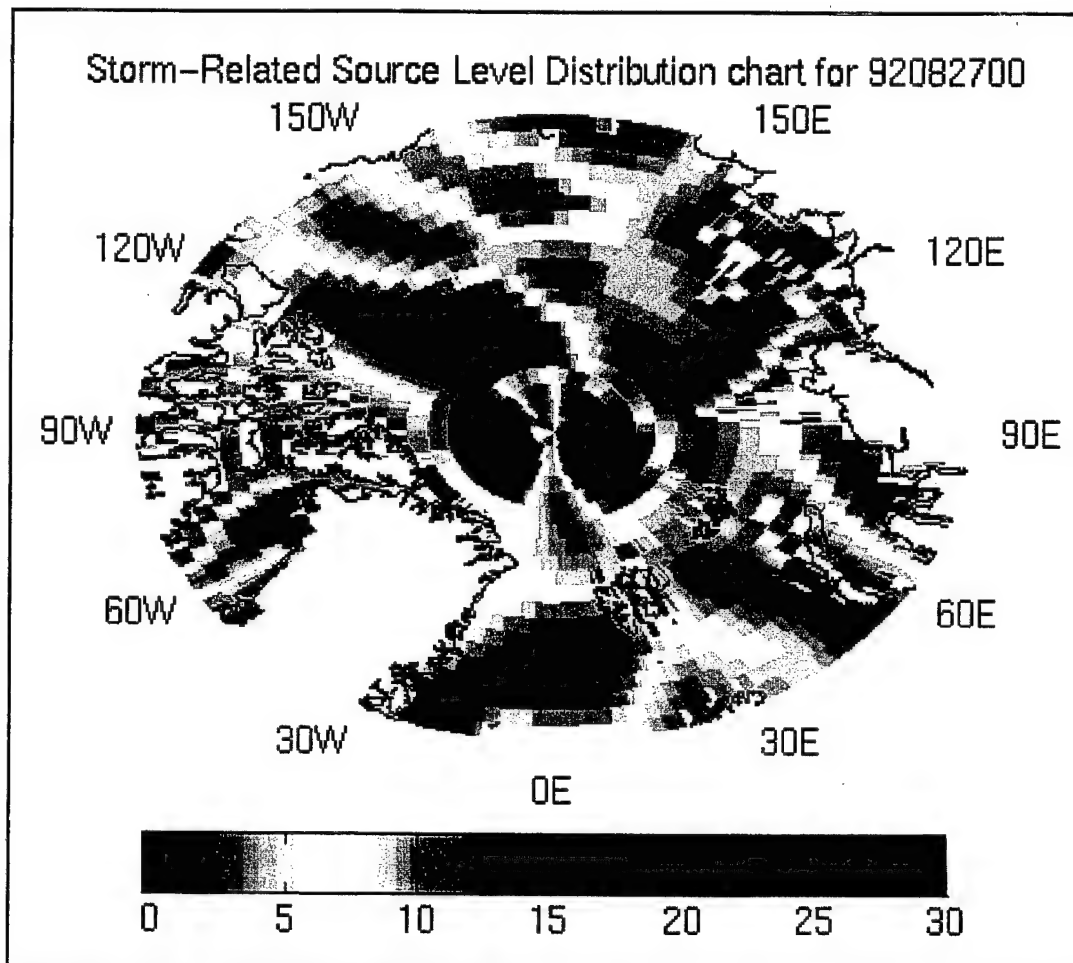
Figure 53   Source level density category chart on 27 Aug
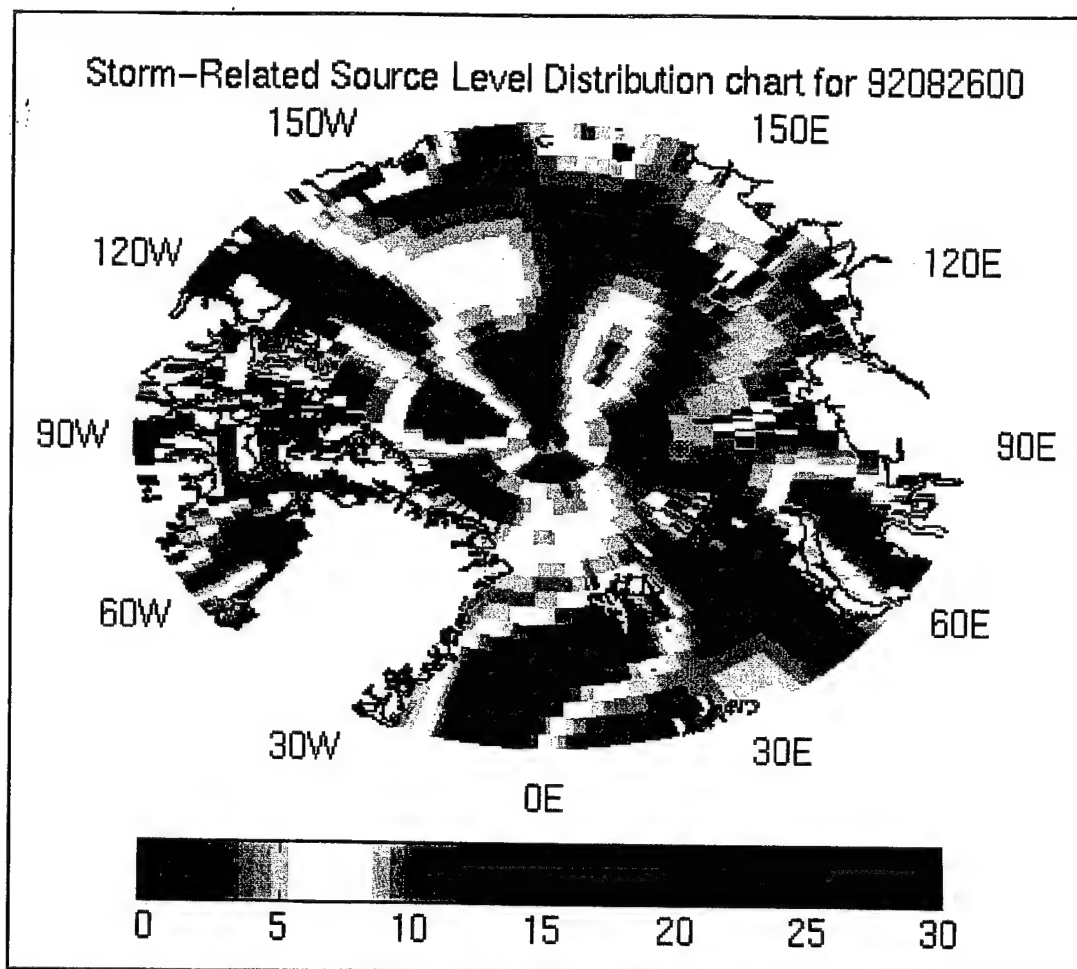1992, 0000Z, for the Arctic basin.
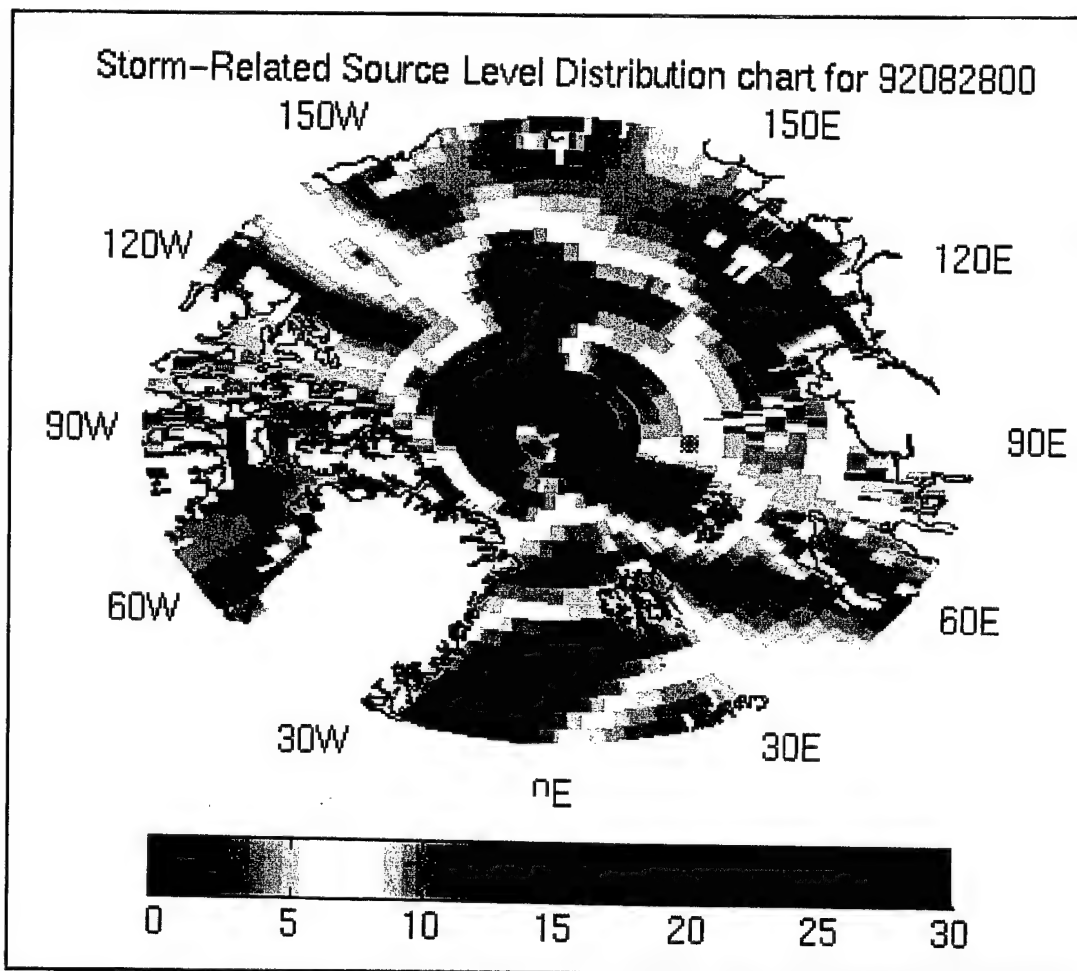
Figure 54 Source level density category chart on 28 Aug
1992, 0000Z, for the Arctic basin.
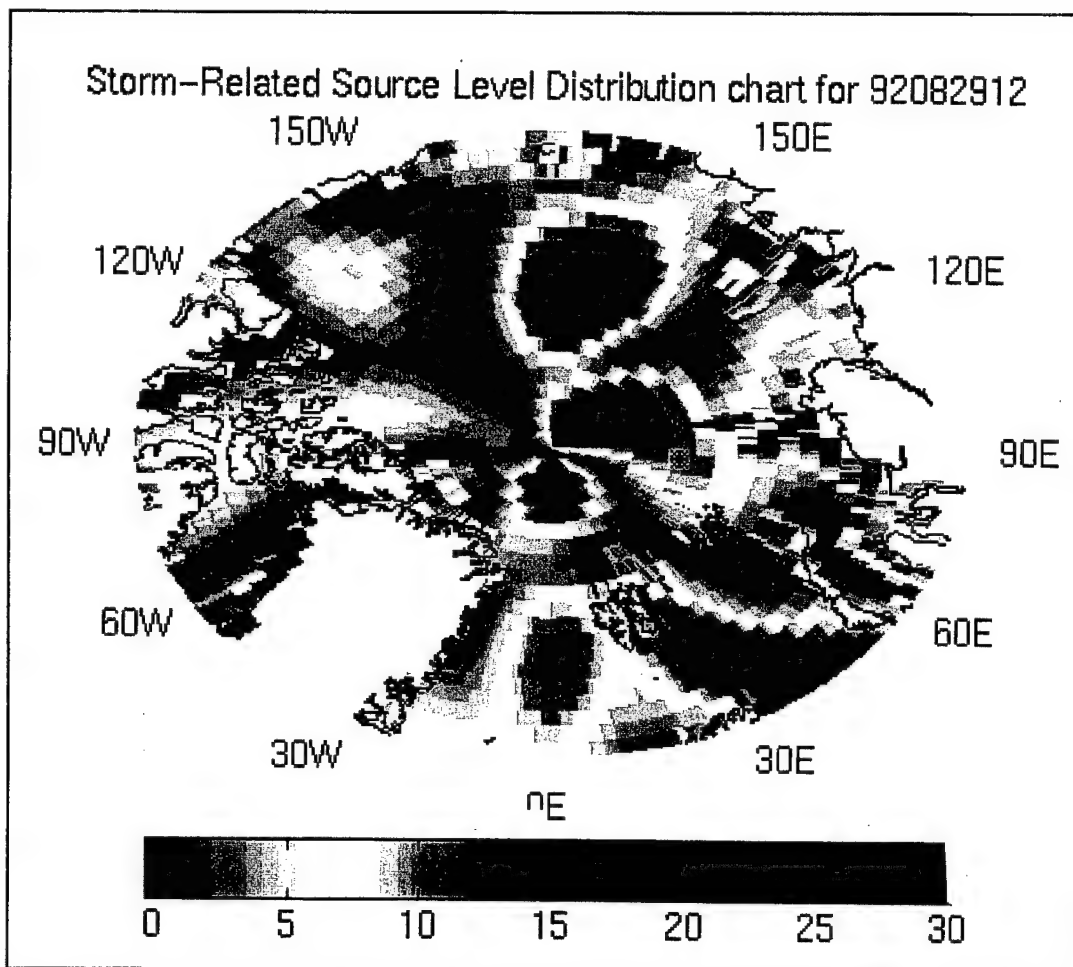
Figure 55   Source level density category chart on 29 Aug
1992, 1200Z, for the Arctic basin.
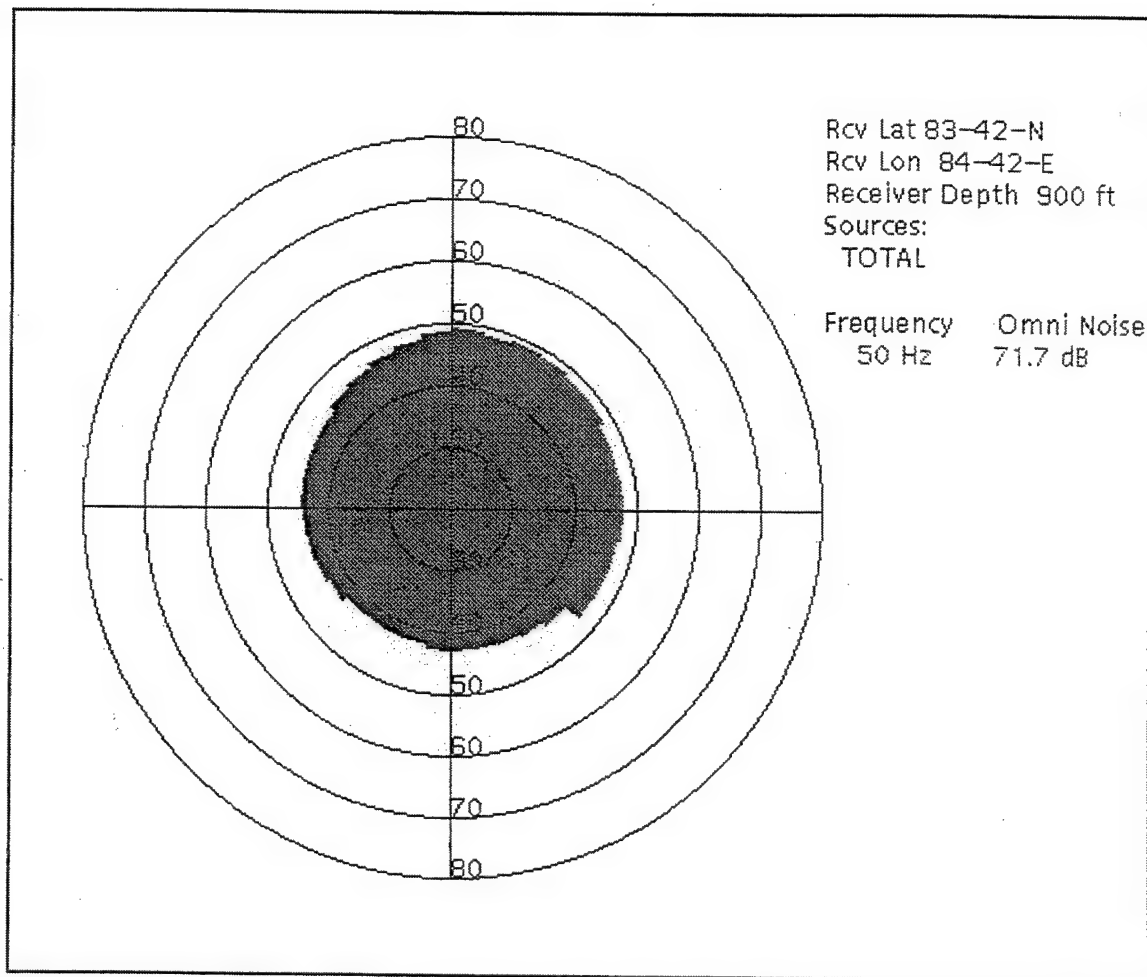
Figure 56 ASNM predicted value of AN and directionality for buoy 13 on 26 Aug 1992, 0000Z.

Figure 57 ASNM predicted values of AN and directionality for
buoy 13 on 27 Aug 1992, 0000Z.

Figure 58 ASNM predicted values of AN and directionality for
buoy 13 on 28 Aug 1992, 0000Z.

Figure 59 ASNM predicted values of AN and directionality for buoy 13 on 29 Aug 1992, 1200Z.

LIST OF REFERENCES

Buck, B. M. and J.H. Wilson, "The Semi-Empirical Buck Wilson Arctic Transmission Loss Model," submitted for publication to J. Acoust. Soc. Am.

Bourke, R.H. and A.S. McLaren, "Contour Mapping of Arctic Basin Ice Draft and Roughness Parameters," J. Geophys. Res., 97, (C11), 715-728 (1992).
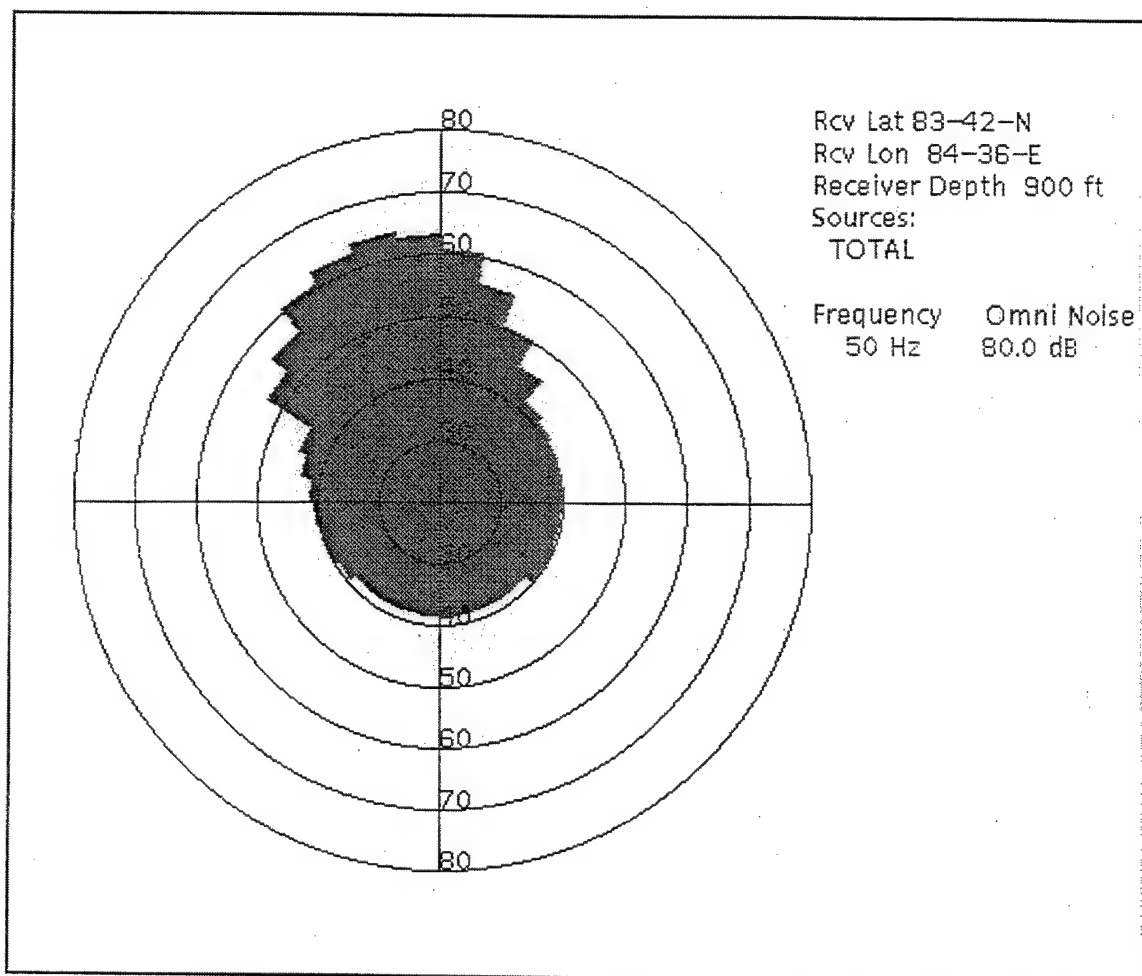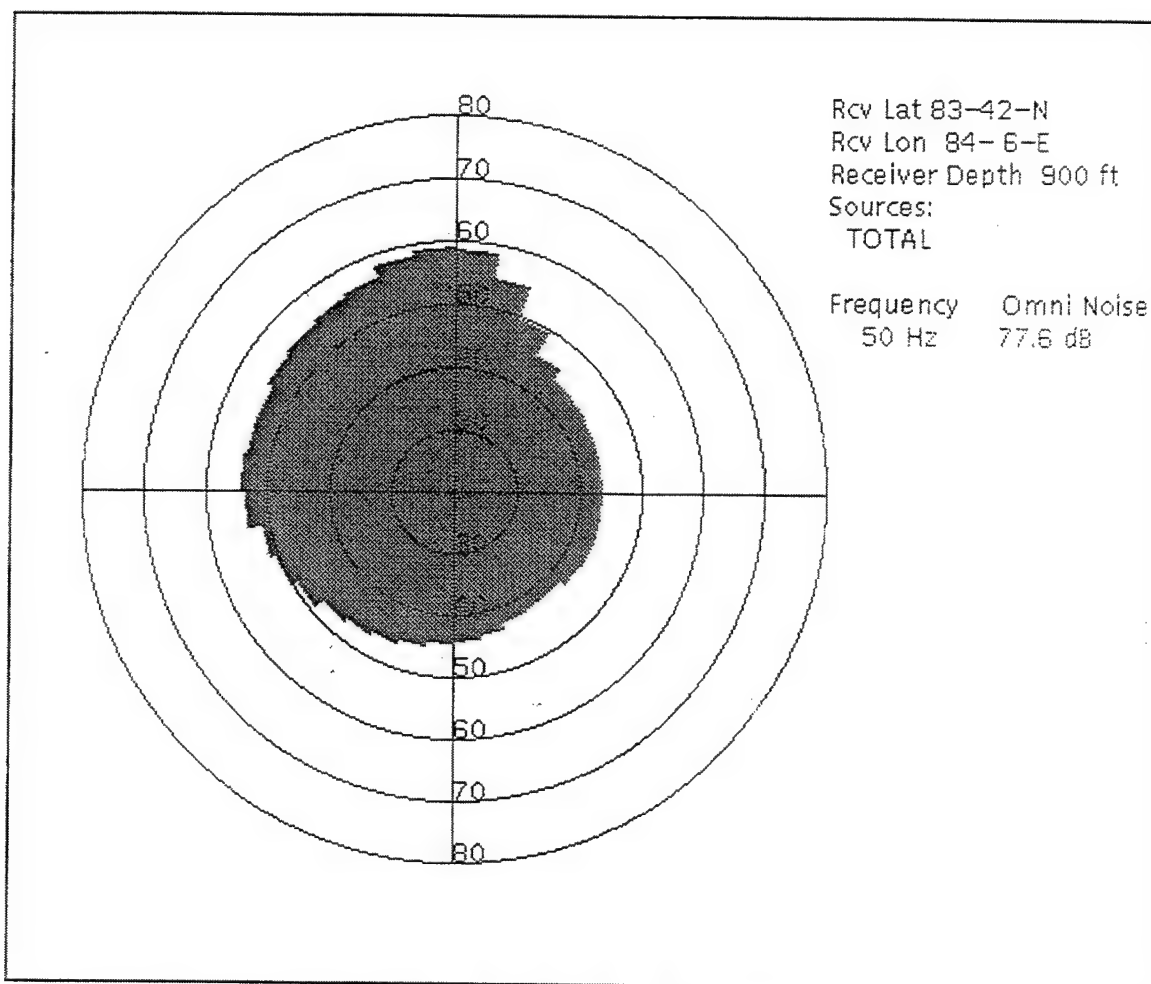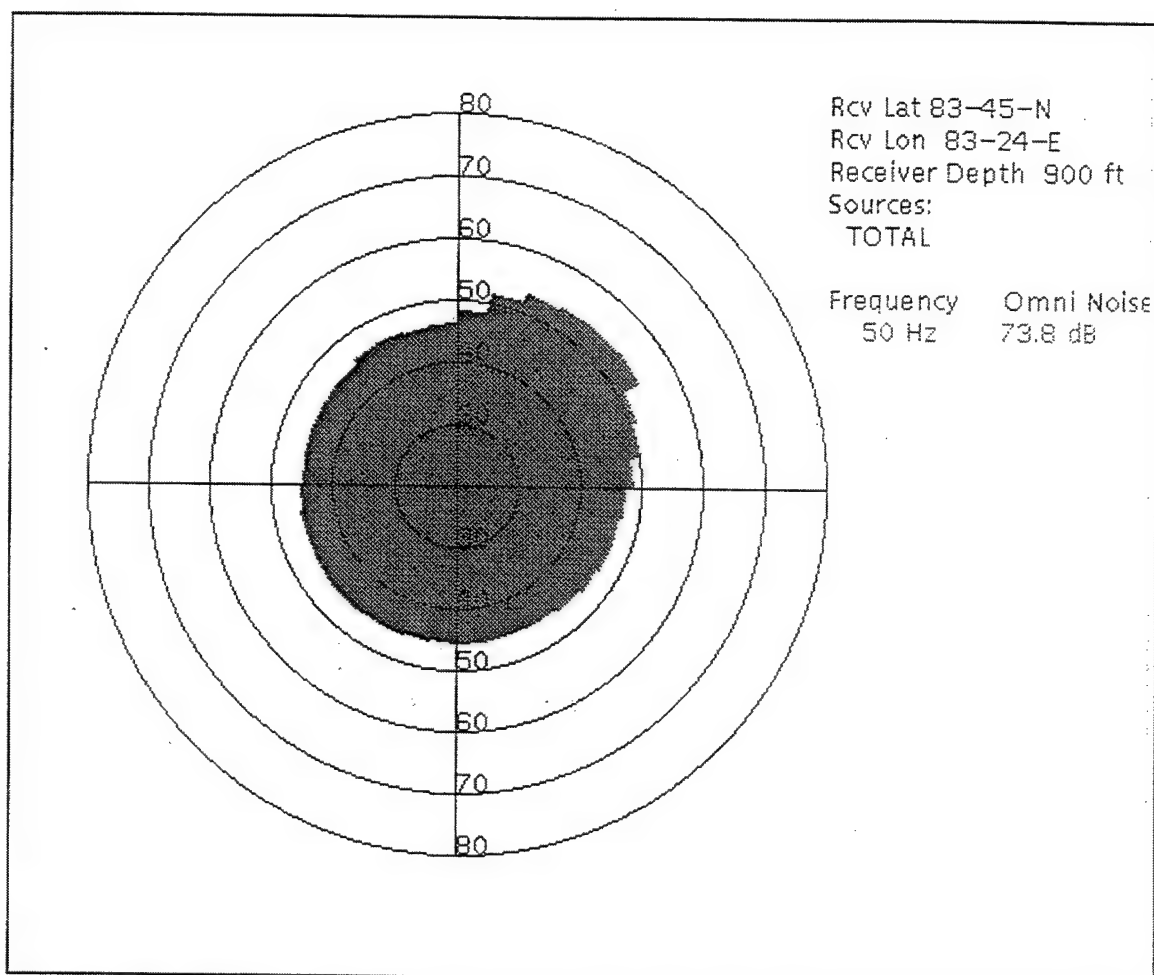
Bourke, R.H. and A.R. Parsons, "Ambient Noise Characteristics of the Northwestern Barents Sea," J. Acoust. Soc. Am., 94, 2799-2808 (1993).

Buck, B.M. and J.H. Wilson, "Nearfield Noise Measurements from an Arctic Pressure Ridge," J. Acoust. Soc. Am., 80, 256-264 (1986).

Bucker, H.P. and B.F. Gordon, "Arctic Acoustic Propagation Model with Ice Scattering," NOSC TR 985, (September 1984).

Diachok, O.I. and R.S. Winokur, "Spatial Variability of Under-Water Ambient Noise at the Ice-Water Boundary," J. Acoust. Soc. Am., 55, 750-753 (1974).

Feller, D., "Environmental Forcing of Ambient Noise in the Nansen and Amudsen Basins of the Arctic Ocean" Master's Thesis, Naval Postgraduate School, Monterey, California, (September 1994).

Fritsch, F., "Synoptic Atmospheric Forcing of Arctic Underice Ambient Noise," Master's Thesis, Naval Postgraduate School, Monterey, California, (December 1995).

Hogan, T.F. and T.E. Rosmond, "The Description of the Navy Operational Global Atmospheric Prediction System's Spectral Forecast Model," Monthly Weather Review, 119, 1786-1815 (1991).

Lewis, J.K. and W.W. Denner, "Arctic Ambient Noise in the Beaufort Sea: Seasonal Relationships to Sea Ice Kinematics," J. Acoust. Soc. Am., 83, 549-565 (1988).

Makris, N.C. and I. Dyer, "Environmental Correlates of Pack Ice Noise," J. Acoust. Soc. Am., 79, 1434-1440 (1986).

Makris, N.C. and I. Dyer, "Environmental Correlates of Arctic Ice-Edge Noise," J. Acoust. Soc. Am., 90, 3288-3298 (1991)

Newton, Personal Communication, 1990.

Oard, V.T., "Characteristic Spectral Signatures of Arctic Noise Generating Mechanisms," Master's Thesis, Naval Postgraduate School, Monterey, California, (June 1987).

Parsons, A.R., "Environmental Forcing of Ambient Noise in the Barents Sea," Master's Thesis, Naval Postgraduate School, Monterey, California, (June 1992).

Pritchard, R.S., "Arctic Ocean Background Noise Caused by Ridging of Sea Ice", J. Acoust. Soc. Am., 75, 419-427 (1984).

Renner, W., "User's Guide for the ANDES Model," SAIC publication, (October 1993).

Rosmond, T.E., "The Design and testing of the Navy Operational Global Atmospheric Prediction System," Weather and Forecasting, 7, 262-272 (1992).

Urick, R.J., "Principles of Underwater Sound," 3rd Edition (McGraw-Hill, New York, 1983)

Wilson, J.H., "Wind-Generated Noise Modeling," J. Acoust. Soc. Am., 73, 211-216 (1983).

INITIAL DISTRIBUTION LIST

No. Copies

1. Defense Technical Information Center   2
   8725 John J. Kingman Road., Ste 0944
   Ft. Belvoir, VA 22060-6218

2. Dudley Knox Library   2
   Naval Postgraduate School
   411 Dyer Rd.
   Monterey, CA 93943-5101

3. Chairman (Code OC/BF)   3
   Department of Oceanography
   Naval Postgraduate School
   Monterey, CA 93943-5000

4. Ms Laura Ehret (Code EC/EH)   1
   Department of Oceanography
   Naval Postgraduate School
   Monterey, CA 93943-5000

5. Dr. James H.Wilson   2
   Neptune Sciences, Inc.
   3834 Vista Azul
   San Clemente, CA 92674

6. Lt Cdr David A. Collins RN   2
   P.O. Box 5161
   Carmel-by-the-Sea, CA 93921-5161

7. Lt David Feller   1
   1396 Liberty Ave
   North Bellmore, NY 11710

8. Commander   3
   Naval Oceanography Command
   Code 7170
   Stennis Space Ctr, MS 39529-5000
   Attn: Mr. Jack McDermid
         Dr. Dan Ramsdale
         Dr Ron Wagstaff

9. Commanding Officer   1
   Naval Polar Oceanography Center, Suitland
   Washington, DC 20373

10. Dr. Robert S. Pritchard
    Ice Casting Inc.
    11042 Sand Point Way NE
    Seattle, WA 98125   1

11. Dr. Warren W. Denner
    Earth Ocean Science
    P.O. Box 1378
    Carmel Valley, CA 93924   1

12. Dr James K. Lewis
    207 South Seashore Ave.
    Long Beach, MS 39560   1

13. Mr. Beaumont M. Buck
    Polar Associates, Inc.
    1828 State St.
    Santa Barbara, CA 93101   1

14. Mr. Jim Donald
    Naval Undersea Warfare Center
    New London Lab
    Code 019
    New London, CT 06320   1

15. Commanding Officer
    Naval Research Laboratory
    Code 5100/5123/5160
    Washington, DC 230375-5000
    Attn: Dr. T.C. Yang
          Dr. R. Heitmeyer   2

16. Commanding Officer
    NCCOSC RDTE DIV
    53560 Hull St.
    San Diego, CA 92152-5100
    Attn: Capt A.W. Lengerich
          Capt Williams
          Dr. B. Soterin
          Dr. H. Bucker
          Dr. F. Ryan   5

17. Office of Naval Research
    800 n. Quicy St.
    Arlington, VA 22217-5660
    Attn: Mr. Ken Dial Code 322
          Dr. Mike Van Woert Code 322
          Mr. Barry Blumenthal Code C124 A
          Dr. Tom Curtain Code 322 HL   4

18. Advanced Environmental Acoustic Support Program   3
    Code ONR-DET
    Building 1020 Rm. 184
    Stennis Space Center, MS 39529-5000
    Attn: Mr. Ed Chaika
          Mr. Dave Small
          Mr. Bobby Wheatley

19. Advanced Environmental Acoustic Support Program   2
    Office of Naval Research
    Arlington, VA 22217-5360
    Attn: Dr. Eigo Hashimoto
          Dr. Ed Estalote

20. Commander, Submarine Development Squadron 12   1
    NAVSUBASE New London
    Groton, CT 06349-5200
    Attn: Master Chief Sonarman Stuckard

21. Commander, Submarine Development Group 1   1
    139 Sylvester Road
    San Diego, CA 92106-3597

22. Commander, Submarine Group 5   1
    137 Sylvester Road
    San Diego, CA 92106-3521

23. Commander, Submarine Force U.S. Atlantic Fleet   1
    7958 Blandy Road
    Norfolk, VA 23551-2492
    Attn: N-2

24. Commander, Submarine Force U.S. Pacific Fleet   1
    Pearl Harbor, HI 96860-6650
    Attn: N-2

25. Ms. Josie Paquin-Fabre   1
    Neptune Sciences, Inc.
    150 Cleveland Ave.
    Slidell, LA 70458

26. DNSOM   1
    Lacon House,
    Theobalds Rd.
    London WC1X 8RY
    England
    Attn: Cdr A R Trevithick RN

27. DACOS (METOC)   1
    CINCFLEET
    Northwood,
    Middlesex,
    London,
    England

28. Cdr R PEGG RN   1
    British Navy Staff
    3100 Massachusetts Avenue, NW
    Washington,
    D.C. 20008